Journal of Rock Mechanics and Geotechnical Engineering

Successful Mechanical Earth Model Construction with Numerical and Analytical Solutions for Wellbore Stability Analysis, A Case Study

--Manuscript Draft--

Manuscript Number:	
Article Type:	Review Article
Keywords:	Wellbore stability analysis; Mechanical Earth Model (MEM); Linear elastic model; elatoplastic model; Rock failure criteria; Mud weight window; Normalized Yielded Zone Area (NYZA)
Corresponding Author:	Abdolnabi Hashemi, Ph.D. Petroleum University of Technology Ahwaz, Khuzestan IRAN (ISLAMIC REPUBLIC OF)
First Author:	Meysam Motahari, Master Degree
Order of Authors:	Meysam Motahari, Master Degree
	Abdolnabi Hashemi, Ph.D.
	Abdollah Molaghab
Abstract:	Wellbore stability is one of the essential parts of the drilling operation, and if it is not noted, the possible wellbore instability can lead to many drilling difficulties. Many parameters such as mud weight, well trajectory, mechanical properties, in-situ stresses, etc. could affect the wellbore instability. The mud weight is the most prevalent parameter in performing wellbore stability studies to prevent wellbore instability if designed and controlled precisely. Furthermore, wellbore stability analysis can be implemented using an analytical solution or a numerical solution. This paper uses both analytical and numerical solutions to perform wellbore stability analysis for four-hole sections of a well, named Well-A, in an Iranian southwest oil field. First, a mechanical earth model (MEM) was established and calibrated through the required information. Then, for the analytical solution, four rock failure criteria, including Mohr-Coulomb, Mogi-Coulomb, Hoek-Brown, and Modified Lade, were employed to predict the safe mud weight windows and to figure out the optimum trajectories based on a linear elastic model. Finally, based on an elastoplastic model, a numerical solution using a finite-difference code was conducted to evaluate the results of the analytical solution as well as to determine the optimum mud weights. From the results of this study, it was found that the Mogi-Coulomb provides the most realistic safe mud weight window due to having the most appropriate agreement with the real operation evidence observed from caliper/bit size and image logs. Numerical solution results demonstrate good accordance with the real observations as well as these results successfully confirmed the authenticity of analytical solution results or the mud weight window determined by the Mogi-Coulomb failure criterion. Consequently, an elastoplastic model would be competent and beneficial for carrying out geomechanics and wellbore stability analysis for Well-A or the next similar wells in this Iranian field.
Suggested Reviewers:	Raoof Gholami Raoof.Gholami@gmail.com

Cover Letter

Abdolnabi Hashemi

Associate Professor at Petroleum University of Technology

Department of Petroleum Engineering, Ahwaz Faculty of Petroleum,

Petroleum University of Technology, Ahwaz, Iran

7/ 02/ 2021

Dear Dr. Xia-Ting Feng,

I would like to request you to consider the attached manuscript entitled "**Successful Mechanical Earth Model Construction with Numerical and Analytical Solutions for Wellbore Stability Analysis, A Case Study**" for publication in **Journal of Rock Mechanics and Geotechnical Engineering** as an original article.

We confirm that this work is original and has not been published elsewhere, nor is it currently under consideration for publication elsewhere.

In this paper, we indicate that using numerical modeling and elastoplastic model could be a qualified approach for conducting wellbore stability or geomechanics studies in a case study well in a southwest Iranian oil field, and also they can confirm the accuracy of the elastic model or analytical solution results appropriately. Also, we establish a comprehensive mechanical earth model. This is significant because this field is one of the most noticeable oil fields in Iran, and severe wellbore instabilities have already been reported. However, wellbore stability studies have not been performed extensively, primarily based on both elastic and elastoplastic models. Therefore, in this study, we employed both numerical and analytical solutions, based on both elastic and elastoplastic models, to carry out a plenary wellbore stability analysis in the entire depth of the case study well. We believe that the findings of this study are relevant to the scope of your journal and will be of interest to its readership.

There are no conflicts of interest to declare. All authors have approved the manuscript and agree with its submission to Journal of Rock Mechanics and Geotechnical Engineering.

Please address all correspondence concerning this manuscript to me at **a.hashemi@put.ac.ir**

I look forward to hearing from you.

Sincerely,

Dr. Abdolnabi Hashemi (Corresponding Author)

- First stability analysis in a case study using elastoplastic and elastic models
- Successful mechanical earth model establishment in the current case study
- Safe mud weight window determination for preventing instabilities and fractures
- Triumphant validation of the elastic model results via the numerical simulation
- Presenting the optimum mud weight and safest trajectory for the case study

Successful Mechanical Earth Model Construction with Numerical and Analytical Solutions for Wellbore Stability Analysis, A Case Study

Meysam Motahari[1], Abdolnabi Hashemi[1*], Abdollah Molaghab[2],

1 Department of Petroleum Engineering, Ahwaz Faculty of Petroleum, Petroleum University of Technology (PUT), Ahwaz, Iran

2 Geology Division, National Iranian South Oil Company, Ahwaz, Iran

Abstract

Wellbore stability is one of the essential parts of the drilling operation, and if it is not noted, the possible wellbore instability can lead to many drilling difficulties. Many parameters such as mud weight, well trajectory, mechanical properties, in-situ stresses, etc. could affect the wellbore instability. The mud weight is the most prevalent parameter in performing wellbore stability studies to prevent wellbore instability if designed and controlled precisely. Furthermore, wellbore stability analysis can be implemented using an analytical solution or a numerical solution. This paper uses both analytical and numerical solutions to perform wellbore stability analysis for four-hole sections of a well, named Well-A, in an Iranian southwest oil field. First, a mechanical earth model (MEM) was established and calibrated

* Corresponding Author. Currently Visiting Professor at Montan Universitat Leoben, Austria, Home page: https://dpe.ac.at/people/abdolnabi-hashemi/.

E-mail addresses: a.hashemi@put.ac.ir (A. Hashemi), meysam.motahari92@gmail.com (M. Motahari)

through the required information. Then, for the analytical solution, four rock failure criteria, including Mohr-Coulomb, Mogi-Coulomb, Hoek-Brown, and Modified Lade, were employed to predict the safe mud weight windows and to figure out the optimum trajectories based on a linear elastic model. Finally, based on an elastoplastic model, a numerical solution using a finite-difference code was conducted to evaluate the results of the analytical solution as well as to determine the optimum mud weights. From the results of this study, it was found that the Mogi-Coulomb provides the most realistic safe mud weight window due to having the most appropriate agreement with the real operation evidence observed from caliper/bit size and image logs. Numerical solution results demonstrate good accordance with the real observations as well as these results successfully confirmed the authenticity of analytical solution results or the mud weight window determined by the Mogi-Coulomb failure criterion. Consequently, an elastoplastic model would be competent and beneficial for carrying out geomechanics and wellbore stability analysis for Well-A or the next similar wells in this Iranian field.

Keywords

Wellbore stability analysis, Mechanical Earth Model (MEM), Linear elastic and elastoplastic models, Rock failure criteria, Mud weight window, Normalized Yielded Zone Area (NYZA).

1. Introduction

Wellbore stability is defined as the prevention of brittle failure or plastic deformation of the rock surrounding the wellbore because of mechanical stresses or chemical interaction between drilling fluid and wellbore rocks (Zoback, 2007). Wellbore instability is one of the main reasons for drilling hardships because it can cause many hazards in drilling operations such as pipe stuck, tight spots, sidetrack, wellbore enlargement, under-gage borehole, etc. (Hossain and Islam, 2018). These hazards can lead to the increment of drilling costs, stopping the production operation, and finally losing the well (Dusseault, 1994). Thus, wellbore stability is a critical point in drilling operations. The most widespread failures that occur around the borehole and cause wellbore instability are the shear failure and the tensile failure, known as breakout and breakdown, respectively (Maleki et al., 2014). Hence, proper maintenance techniques are required to prevent wellbore instability. The maintenance technique has a lot of steps to perform. Numerous parameters affect wellbore stability maintenance techniques, including mud weight (MW), drilling fluid type, well azimuth and inclination (i.e., well trajectory), in-situ stresses, rock mechanical properties, etc. (Zhang, 2019). The most crucial step is wellbore stability investigation by determining MW, mud type, and wellbore trajectory (Mansourizadeh et al., 2016). The MW window determination using direct methods is the most common procedure to perform wellbore stability analysis. In the direct methods, an analytical solution using rock failure criteria based on the linear elastic model is carried out to deliver wellbore stability (Huang, 2014).

The conventional linear elastic model is very conservative in estimating the MW window. Also, rock property or behavior is not mostly near the elastic model. The nonlinear plastic model or elastoplastic behavior of rocks has commonly been accepted due to demonstrating the rock behavior more really (Chen and Abousleiman, 2017). The numerical models can tackle a more domain of materials behavior or models considering the effect of

variables on the stress distribution or failures. Therefore, numerical methods, such as finite-difference code (FLAC[†]), finite element code, etc., will be more useful for performing wellbore stability analysis (Salehi et al., 2010). These numerical codes can present more realistic and precise results in investigating wellbore stability by providing many linear and nonlinear models.

This paper aims to perform wellbore stability analysis for a case study well, called Well-A, in a southwest Iranian oil field based on both elastic and elastoplastic models. This field is one of the most significant oil fields in Iran due to the high reserve of hydrocarbon fluids. In this field, severe wellbore instabilities have already been reported. Nonetheless, geomechanics or wellbore stability studies have not been performed comprehensively, primarily based on both elastic and elastoplastic models. Therefore, in this research, both elastic and elastoplastic models using numerical and analytical solutions are employed to conduct a comprehensive stability analysis in the entire depth of the current well. Besides, the National Iranian South Oil Company has supported this research and provided all the vital data of this study.

2. Case Study

The current Iranian oilfield is one of the largest and most complex sedimentary basins in the southwest of Iran. The field is situated in the Iranian section of the Zagros fold-thrust belt, located in Dezful embayment. This belt stretches from the Anatolian fault in eastern Turkey to the Minab fault near the Makran region in the southeast of Iran. This domain is owned by the National Iranian Oil Company (NIOC) and operated via the National Iranian South Oil Company (NISOC).

[†] Fast Lagrangian Analysis of Continua

Well-A has been drilled in this Iranian field to develop oil production. The well is located in the North Limb of the current geotectonic field, shown in Fig.1. Well-A involves four main hole sections with different diameters, which are explained as follow:

- *17.5-inch Hole:*

The first hole was drilled from 985 m to 1504 m MD (Measured Depth) with a 17.5-inch bit. It contains Gachsaran (GS) formation as a seal /cap rock. The lithology of this formation mainly consists of anhydrite, salt, marl, and the extent of shale.

- *12.25-inch* Hole:

The second hole has a diameter of 12.25-inch and has been drilled from a depth of 1518 m to 2430 m MD, including three Asmari (AS), Pubdeh (Pd), and Gurpi (Gu) formations. In terms of lithology, the Asmari, which is a reservoir formation, is primarily composed of limestone, and the other two are mainly composed of shale.

- *8.375-inch* Hole:

This section has been drilled between 2436 m and 3536 m MD depths by a bit with an 8.375-inch size. This hole includes three main formations namely; Ilam (IL), Sarvak (SV), and Kazhdomi (KZ). Also, a small part of the Dariyan (DR) formation exists at the bottom of this hole. Ilam and Sarvak, which are a reservoir formation, are mainly limestones. Moreover, Kazhdomi is mostly shales with a negligible amount of lime.

- *6.125-inch* Hole:

The fourth and last hole has a 6.125-inch size with a depth from 3540 m to 4130 m MD, which includes three DR, Gadvan (GA), and Fahlian (FA) formations. In terms of lithology, Dariyan and Gadvan are primarily shale formations with some amount of lime. Fahlian is a reservoir formation, and it is composed chiefly of limestone.

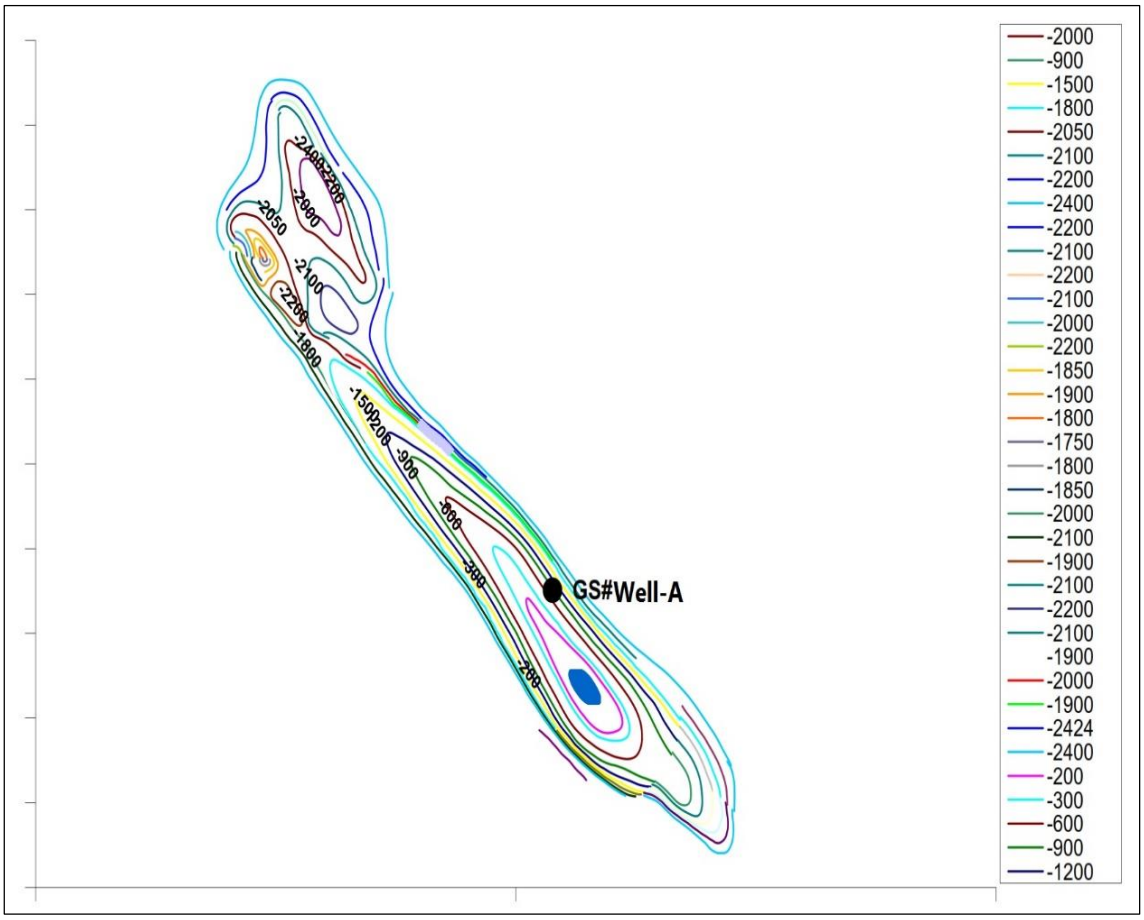

Fig. 1. Location of Well-A in the current oilfield

From the drilling data such as DDR, Well-A was drilled vertically from the 17.5-inch hole to the top of Gurpi formation. Then it has deviated at a depth of 2263 m MD, which is known as a kick-off point (KOP). Finally, this well was drilled directionally in both 8.375 and 6.125-inch holes. Fig. 2 shows a cross-section plot of Well-A drilled in the current field.

Complete petrophysical logs data, including dipole sonic logs (i.e., compressive and shear waves), neutron porosity, density, and gamma-ray together with four-armed caliper and image logs were run into the whole four holes of Well-A. The relevant datasets of these logs were acquired during the drilling operation. This study used the well-logs data to build a thorough mechanical earth model (MEM) and perform appropriate stability analysis for this well. Fig.3 represents the petrophysical logs of this well acquired from the NISOC database. In this figure, the first track indicates the drilled depth. The second and third tracks subtend

compression (DTC) and shear (DTS) transit time. Gamma-ray (GR), neutron porosity (NPHI), and density (RHOB) logs are shown in the next three tracks, respectively.

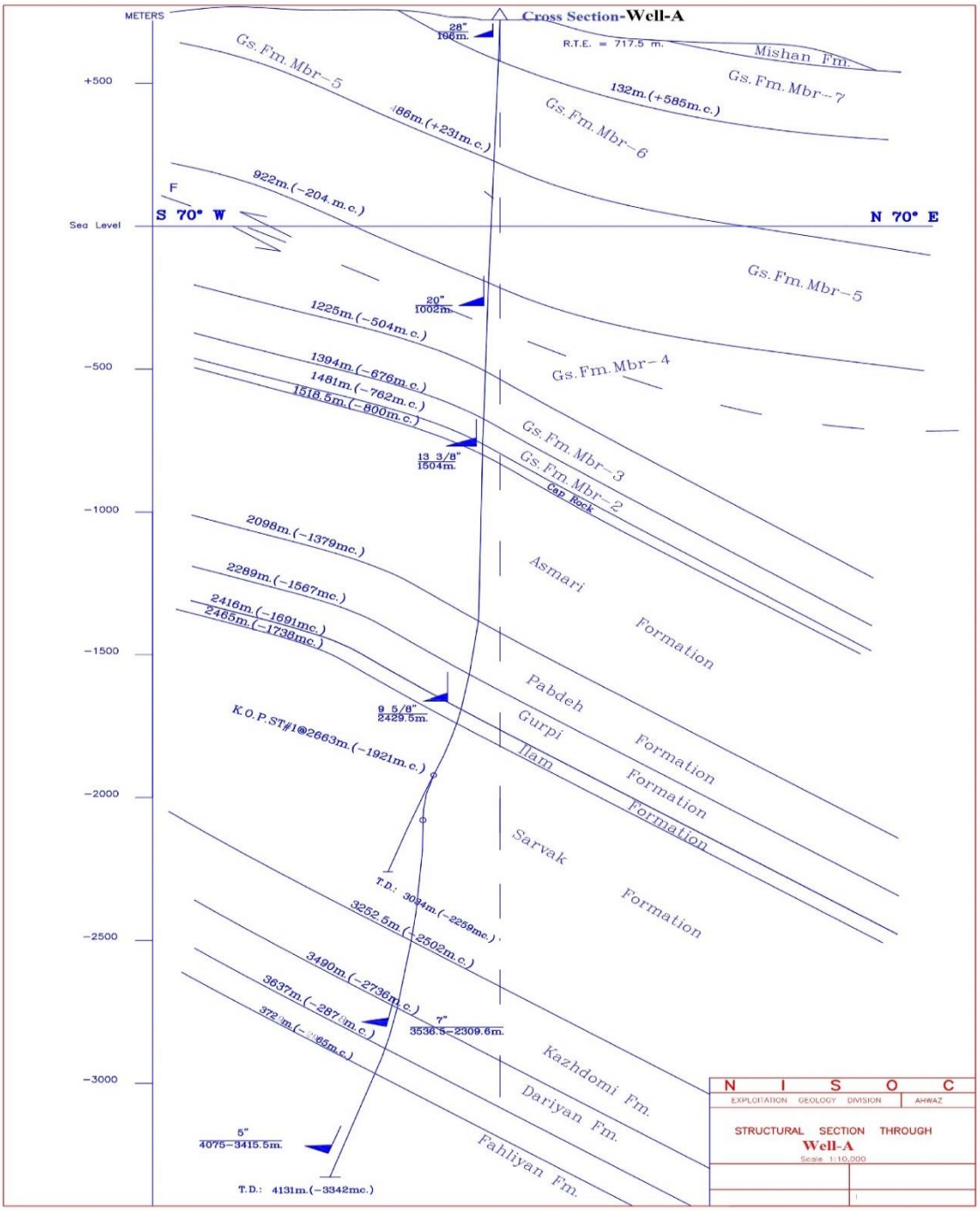

Fig. 2. Cross-section plot of Well-A

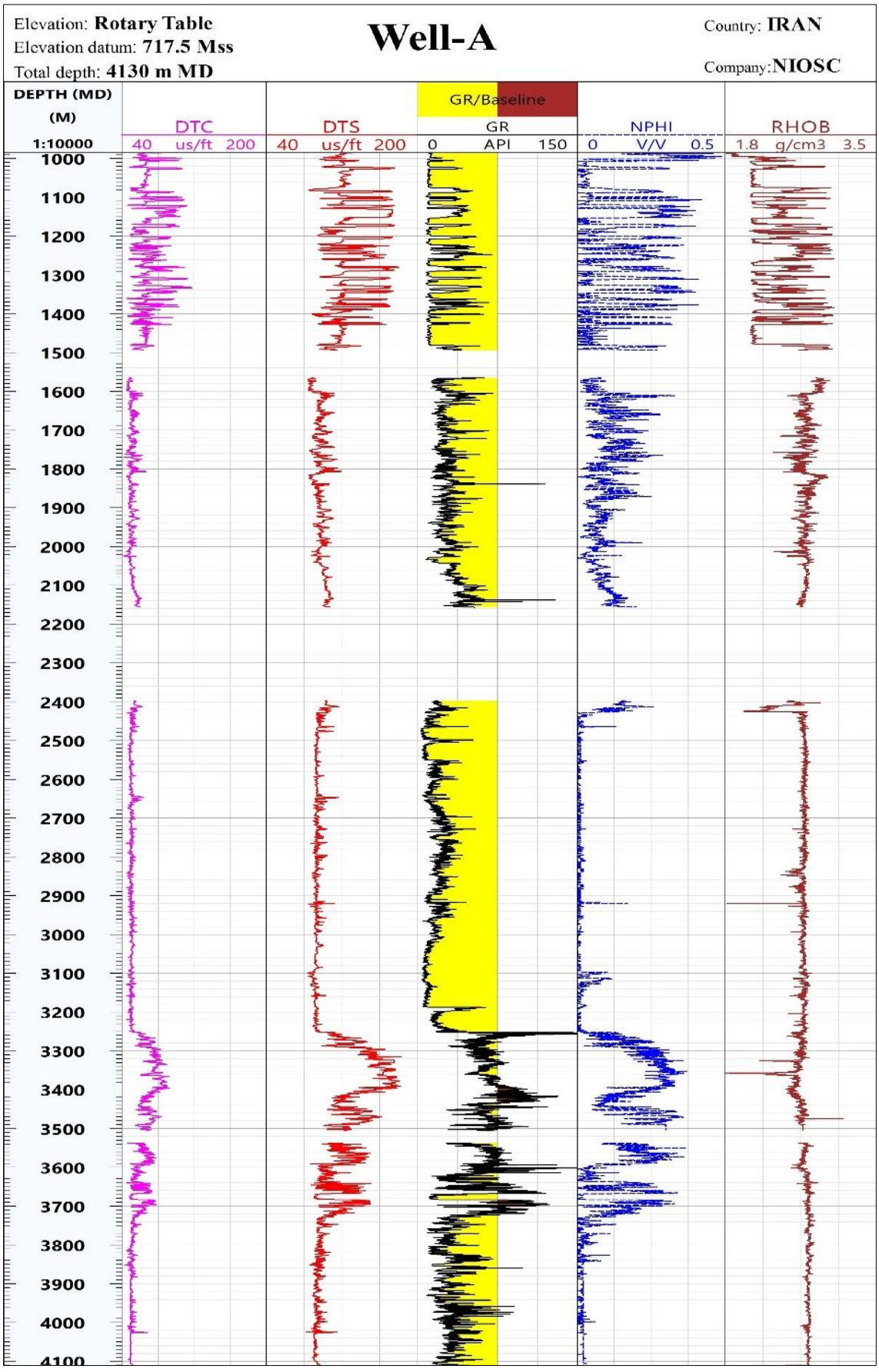

Fig. 3. Petrophysical logs data of Well-A in the Iranian southwest field

3. MEM Construction for Well-A

Mechanical Earth Model (MEM) is the modeling of the mechanical properties coupled with the in-situ stresses and pore pressure as a function of depth (Rasouli et al., 2011). MEM unifies all mechanical information of a field or basin into one database. Hence, constructing a correct MEM would play a remarkable role in the well-planning and development of drilling operations since the model can be highly useful for comprehending the earth's response when exposed to the drilling process. The basic process of building MEM for Well-A contains (1) the profile construction of mechanical properties from the petrophysical logs, (2) calculating the magnitude of three in-situ stresses and pore pressure, and (3) specifying the direction of in-situ stresses from image logs such as XRMI (Gholami et al., 2014). The following subsections review the process of a MEM construction.

3.1. Elastic Properties

Elastic properties are classified into two dynamic and static elastic properties (Weijermars, 1997). Dynamic elastic properties can be calculated from acoustic measurement, and static properties can be determined from the laboratory uniaxial or triaxial tests. Also, elastic properties are primary inputs for computing the rock strengths and in-situ stresses (Salehi et al., 2010; Rasouli et al., 2011; Maleki et al., 2014). The typical procedure for determining them is calculating dynamic properties using well-logging data and then converting the dynamic elastic to static elastic properties by empirical correlations (Najibi et al., 2015). In this study, NISOC provided the required empirical correlations derived from the results of numerous laboratory tests applied on various core specimens of this field. Young's modulus and Poisson's ratio are two common elastic properties. Young's modulus is the slope of the stress-strain curve in the elastic limitation (Hsieh, 2009). Dynamic Young's modulus (E_d) can be calculated using the below equation (Fjaer et al., 1992).

$$E_d = 1.82 \times 10^{-5} \rho_b \frac{\frac{1}{(DTS)^2}(3(DTS)^2 - 4(DTC)^2)}{(DTS)^2 - (DTC)^2} \quad (1)$$

Also, this research uses the below relation for estimating static Young's modulus:

$$E_{static} = 0.7 \times E_d \quad (2)$$

Poisson's ratio is a measure of the Poisson effect describing the expansion or contraction of material in directions perpendicular to the loading (Hsieh, 2009). The equation to calculate dynamic Poisson's ratio (ϑ) is formulated as following (Fjaer et al., 1992).

$$\vartheta = \frac{\frac{1}{2}(DTS/DTC)^2 - 1}{(DTS/DTC)^2 - 1} \quad (3)$$

It is assumed that the static and dynamic Poisson's ratios are equal in this project.

Bulk and shear modules are two elastic properties of rock, which must be determined in this research, especially in the numerical simulation. Both static bulk and shear moduli are related to static Young's modulus and Poisson's ratio, which can be obtained from the equations of $K = \frac{E_{static}}{(3(1-2\vartheta))}$ and $G = \frac{E_{static}}{(2+2\vartheta)}$ (Fjaer et al., 1992).

3.2. Rock Strengths

Uniaxial compressive strength (UCS) is one of the most commonly used rock strength parameters and needs to be obtained for MEM construction. UCS is the maximum stress that a specimen can endure in a uniaxial test (Hsieh, 2009). In this paper, the below correlation has been employed to estimate UCS.

$$\text{UCS (MPa)} = 2.27\text{E}_{\text{static}} + 4.7 \quad (4)$$

Tensile strength is another rock strength, and it is the maximum stress that a material can withstand while being stretched (Hsieh, 2009). TS usually is considered as a percentage of UCS, and it has been utilized in the form of TS=0.1UCS in this study.

3.3. Friction Angle and Cohesion

The internal friction angle (φ) is defined based on the Mohr-Columbus failure criterion. In general, this parameter is obtained through laboratory tests (Zoback, 2007). However, due to the lack of laboratory data, empirical correlations are often used to estimate it (Chang et al., 2006). In this work, the empirical relation of Plumb is used to calculate the friction angle, which is addressed below (Plumb, 1994):

$$\varphi = 26.5 - 37.4(1 - \mathrm{NPHI} - \mathrm{V_{shale}}) + 62.1(1 - \mathrm{NPHI} - \mathrm{V_{shale}})^2 \quad (5)$$

V_{shale} is the shale volume, which is obtained from gamma-ray log data:

$$V_{shale} = \frac{GR - GR_{min}}{GR_{max} - GR_{min}} \quad (6)$$

Cohesion (C) is a rock property, which is defined as the ability of adhesive molecules to stick together without getting separated under any tensile loading (Zoback, 2007). The below equation, which is based on the Mohr-Coulomb failure criterion relation, is used to calculate cohesion (Das and Chatterjee, 2017):

$$C = \frac{UCS(1 - \sin\varphi)}{(2\cos\varphi)} \quad (7)$$

The estimated elastic properties, rock strengths, friction angle, and cohesion of Well-A (generally called rock mechanical properties) have been indicated in Fig.4. NISOC drives the relationships, which were used to compute E_{static} and UCS from the actual data of cores gained from laboratory uniaxial or triaxial tests. Also, this company widely deals with these relationships in wellbore stability researches corresponding to the current field. On the other hand, in the AS and SV formations, the results of some uniaxial tests, which had been carried out before, have been acquired. As beheld clearly in Fig.4, the experimental results (black dots) calibrate the estimated UCS and E_{static} properly. Hence, it can be claimed that the constructed profile of mechanical properties is sufficiently reliable for Well-A and this work.

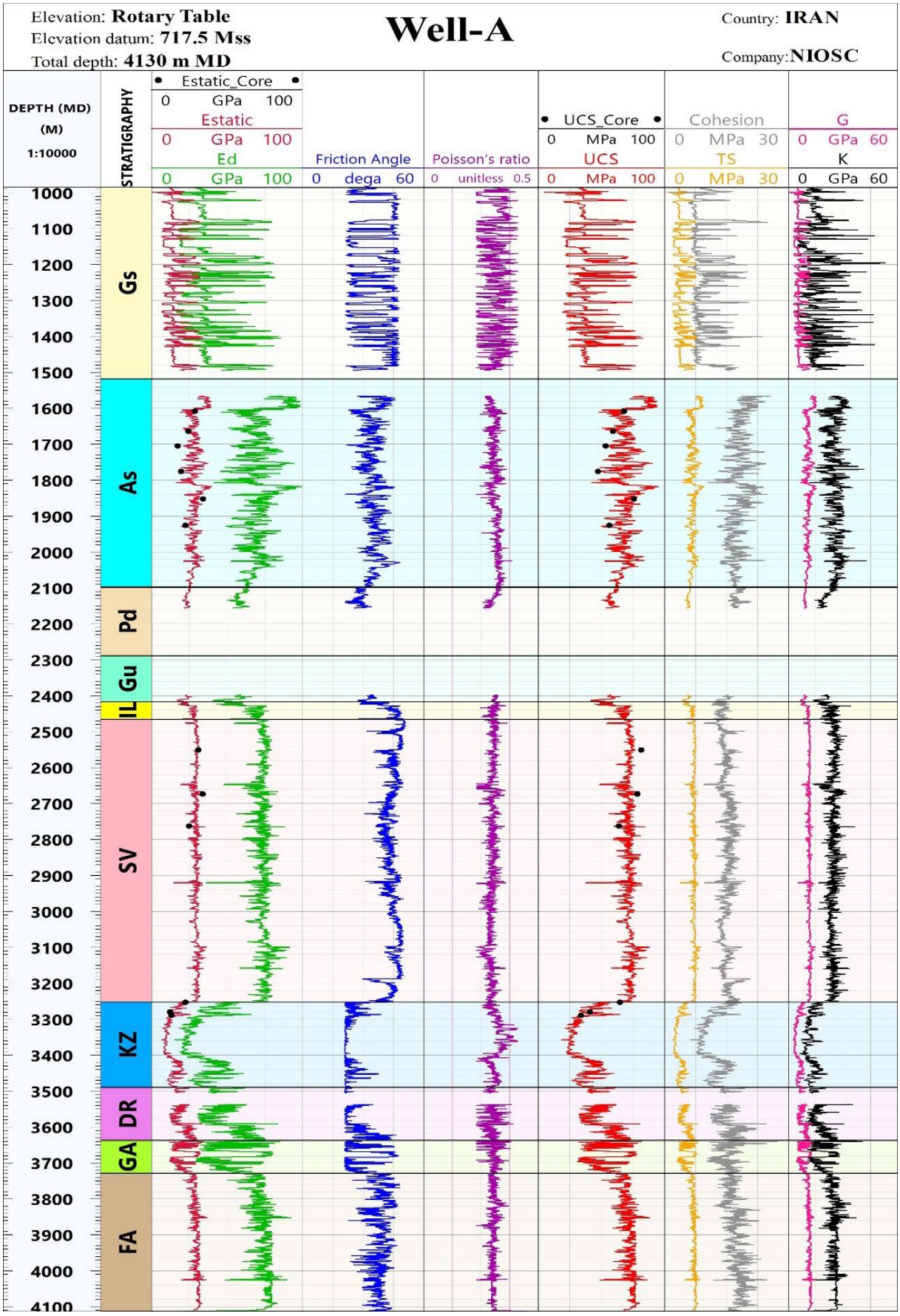

Fig. 4. Estimated rock mechanical properties of Well-A

3.4. Pore Pressure

Pore pressure knowledge during drilling or production operation is essential because the lack of enough information for pore pressure could cause extreme drilling events such as well blowouts, kicks, and fluid influx (Maleki et al., 2014). Pore pressure can be determined by direct and indirect methods. Direct measurements, e.g., Repeat Formation Test (RFT), are costly and time-consuming. Therefore, the indirect methods using log data are recommended (Singha and Chatterjee, 2014). For instance, the Eaton method is commonly used, where sonic or resistivity logs are available (Eaton, 1976). However, some RFT results are needed to calibrate pore pressures estimated from indirect methods. Here, we apply several methods to predict pore pressure because of being diverse geology formations in Well-A.

- Shale and marl formations**:**

Eaton's equation has been used to calculate pore pressure. This equation is formulated as follow (Eaton, 1976):

$$P_p = S_V - (S_V - P_{pn})(\frac{DTCn}{DTC})^3 \quad (8)$$

Where P_p is the pore pressure, P_{pn} is normal pore pressure or hydrostatic pressure, and DTC_n is compressional transit time in normal compaction trend.

- Reservoir formations:

We have calculated pore pressure in all depths of the reservoir formations based on the data, including water-oil contact (WOC), gas-oil contact (GOC), datum depth, the pressure of oil, gas, and water at datum depth, and the pressure gradient of oil, gas, and water. NISOC provided these data from the offset wells. This method is supposed to aim for the most reliable results for pore pressure since the data used in this method were acquired from direct

measurements of offset wells. Moreover, Eaton developed his equation for the shale formations (Zoback, 2007), and the reservoir formations are mainly limestone in Well-A.

- Salt and anhydrite formations

pore pressure has been taken into account as much as differential pressure less than drilling fluid (mud) pressure used in these formations. This manner has been used based on the previous NISOC researches performed in the offsets wells of the current Iranian field.

3.5. In-situ Stresses

In-situ stresses are the stresses, have been developed underneath the surface of the undisturbed rock mass due to the weight of the overlying materials, confinement, and the past stress history (Zoback, 2007). Generally, the in-situ stresses are the vertical stress (S_v) and two horizontal stresses, minimum horizontal stress (S_{hmin}) and maximum horizontal stress (S_{Hmax}). The horizontal stresses, which are due to tectonic confinement loads, are usually unequal in most geological structures (Fjaer et al., 1992). Depending on the order of the in-situ stresses magnitudes, three stress faulting regimes exist (Zoback, 2007); namely normal, reverse, and strike-slip. For a normal regime, the order will be $S_V \geq S_{Hmax} \geq S_{hmin}$, and for the reverse and strike-slip, the order respectively will be $S_{Hmax} \geq S_{hmin} \geq S_V$ and $S_{Hmax} \geq S_V \geq S_{hmin}$.

This study assumes that the vertical stress value is due to the weight of the upper overlaying layers, so the vertical stress has been computed by integrating bulk density logs at any interest point of depth as following (Fjaer et al., 1992):

$$S_V(z) = \int_0^z \rho_b \, g \, dz \tag{9}$$

Where g is the gravity acceleration, and z is the depth of interest.

Calculating horizontal stresses is more complicated than vertical stress. Here, the poroelastic horizontal strain model has been employed to calculate horizontal stresses (Fjaer et al., 1992). The equations of this model are expressed as:

$$S_{Hmax} = S_V\left(\frac{\vartheta}{1-\vartheta}\right) + \left(\frac{1-2\vartheta}{1-\vartheta}\right)\delta P_p + \left(\frac{E_{static}}{1-\vartheta}\right)\varepsilon_y + \left(\frac{\vartheta\, E_{static}}{1-\vartheta}\right)\varepsilon_x \quad (10)$$

$$S_{hmin} = S_v\left(\frac{\vartheta}{1-\vartheta}\right) + \left(\frac{1-2\vartheta}{1-\vartheta}\right)\delta P_p + \left(\frac{E_{static}}{1-\vartheta}\right)\varepsilon_x + \left(\frac{\vartheta\, E_{static}}{1-\vartheta}\right)\varepsilon_Y \quad (11)$$

Where ε_Y and ε_x are horizontal tectonic strains of the field, and δ is Biot's coefficient. Some injectivity field tests such as leak-off test (LOT), extended leak-off test, mini-fracture, etc., should be used to calibrate the minimum horizontal stress value.

Fig.5 shows the profile of in-situ stresses and pore pressure calculated from Eqs. (8) to (11). In this Figure, the second track shows the formations of Well-A. Track 3 displays the lithology of the Well-A formations, and then the fourth track is the stress profile of this well. Moreover, the pink circular and the purple triangular dots show respectively RFT and LOT data used to verify the calculated magnitudes of pore pressure and minimum horizontal stress. As seen in Fig. 5, the LOT results have a good agreement with the estimated S_{hmin} in all four holes. Moreover, the predicted values of pore pressure for AS are matched with the RFT data displaying the accuracy of a method used for predicting pore pressure in AS. For other reservoir formations, the RFT data were not available. Nevertheless, since the same method was used in calculating pore pressure in the reservoir formations, we can conclude that the pore pressure values estimated for other formations are reliable. In addition, because the magnitudes of pore pressure and the minimum horizontal stress were calibrated with LOT and RFT data, so the extent of the maximum horizontal stress is accurate too (Maleki et al., 2014). As a result, it was figured out that a MEM constructed for Well-A is reliable and practical for performing wellbore stability analysis. Lastly, from Fig. 5, it is observed that the reverse fault stress regime is dominant in the first hole. In the second hole and corresponding AS, the strike-slip is a

prevailing stress fault regime, whereas the normal regime is dominant in Pd, third hole, and fourth hole.

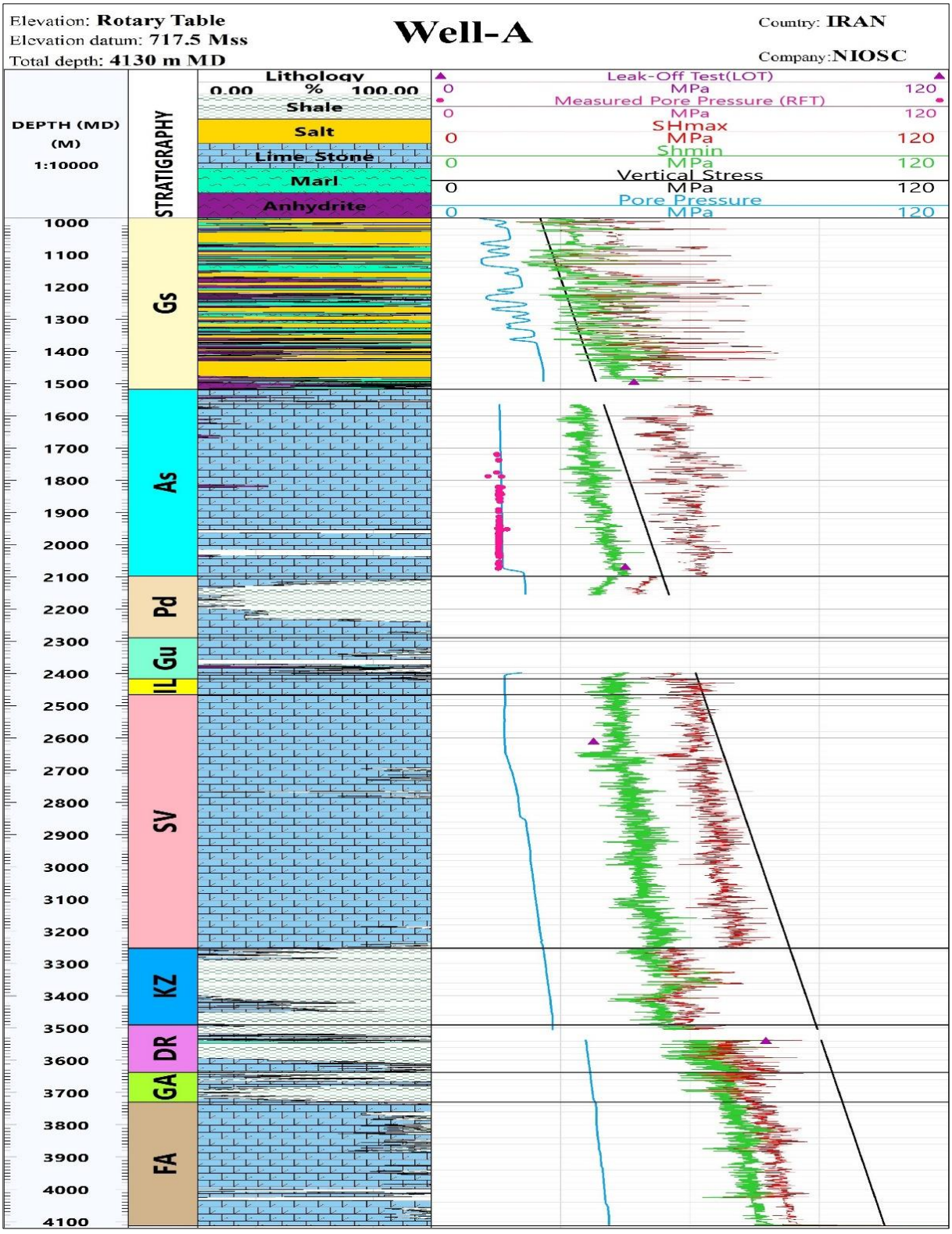

Fig. 5. Pore pressure and in-situ stresses profile of Well-A

3.6. In-situ Stresses Direction

The direction of in-situ stresses is another main section of wellbore stability analysis, and finding their direction might be necessary for designing a worthy trajectory of the wellbore (Ma et al., 2015). In a vertical well, the shear failure or breakout observed from image logs shows the minimum horizontal stress direction. On the other hand, induced fractures (i.e., breakdown) happen in the direction of maximum principal stress (Aadnoy and Looyeh, 2011).

In this study, the borehole image log for the Well-A was investigated. The borehole breakouts observed from the XRMI log demonstrated that the minimum horizontal stress azimuth is about 105° or N75°W/S75°E, and N15°E or the azimuth 15° is the maximum horizontal stress direction. Because this hole has been drilled vertically in the most intervals, the Azimuth 105° can be considered as a reference of minimum horizontal stress direction for Well-A, shown in Fig. 6.

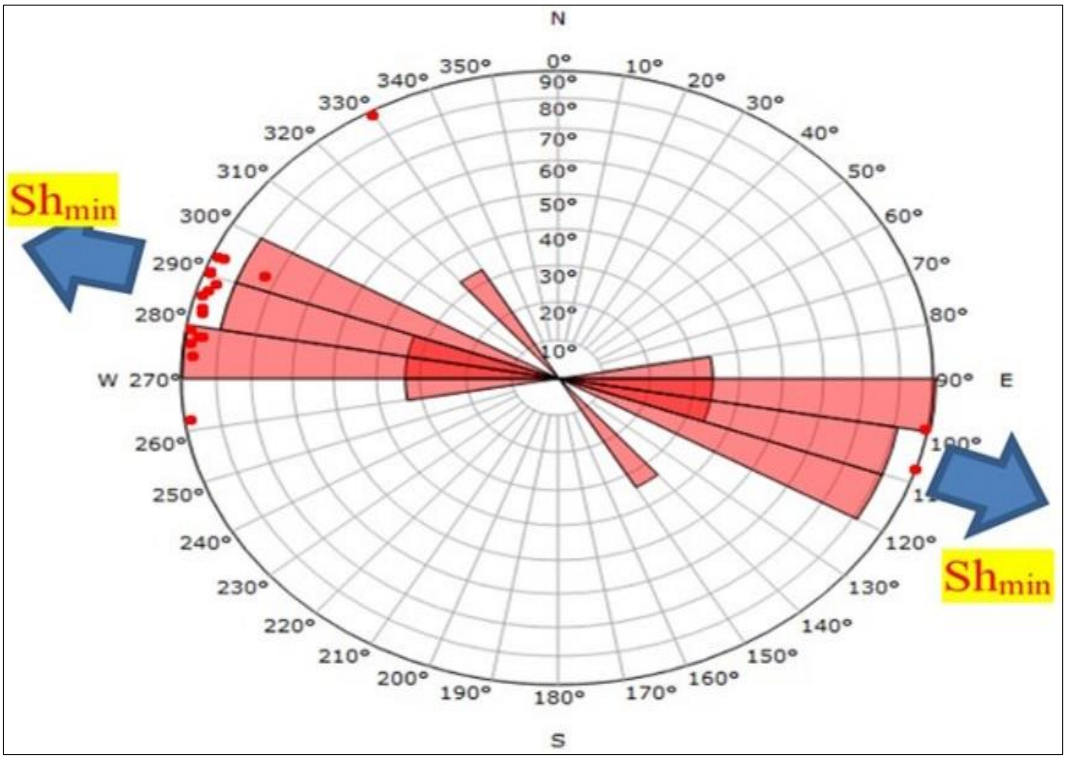

Fig. 6. The borehole breakout or minimum horizontal stress direction in Well-

4. Induced Stresses around the Wellbore

Before drilling, the stress state in underground formations is stable. When a borehole is drilled, and some solid materials are removed, the in-situ stresses state is changed, and a stress concentration occurs around the wellbore and leads to induced stresses (Xu, 2007).

4.1. Induced Stresses around the Vertical Wellbore

The normal induced stresses around the *vertical borehole* are usually expressed in cylindrical coordinates, which include Tangential stress (σ_θ), Radial stress (σ_r), and Axial stress (σ_z) (Maleki et al., 2014). Many different models have already been developed to determine the induced stresses around the wellbore (Aadnoy and Chenevert, 1987). Nonetheless, an analytical solution developed by (Kirsch, 1898) based on a linear elastic model is usually used to determine these stresses. Hence, for isotropic elastic rocks, the induced stresses equations at any point around the borehole are formulated as (Fjaer et al., 1992):

$$\sigma_r = \frac{S_{Hmax}+S_{hmin}}{2}\left(1-\frac{R^2}{r^2}\right)+\frac{S_{Hmax}-S_{hmin}}{2}\left(1+3\frac{R^4}{r^4}-4\frac{R^2}{r^2}\right)cos\,2\Theta+P_w\frac{R^2}{r^2} \quad (12)$$

$$\sigma_\theta = \frac{S_{Hmax}+S_{hmin}}{2}\left(1+\frac{R^2}{r^2}\right)-\frac{S_{Hmax}-S_{hmin}}{2}\left(1+3\frac{R^4}{r^4}\right)cos\,2\Theta-P_w\frac{R^2}{r^2} \quad (13)$$

$$\sigma_z = S_V - 2\vartheta(S_{Hmax}-S_{hmin})\frac{R^2}{r^2}cos\,2\Theta \quad (14)$$

R is the wellbore radius, r is the point of interest distance away from the wellbore center, P_w is mud pressure, and the angle Θ is the azimuth from the maximum horizontal stress direction. The stress concentration at the borehole wall (where R=r), introduced as the critical region, is much higher than other distances due to the sharp rising of tangential stress (Fjaer et al., 1992). The required equations corresponding to the borehole wall are expressed as:

$$\sigma_\theta = (S_{Hmax}+S_{hmin})-2(S_{Hmax}-S_{hmin})\cos 2\Theta-P_w \quad (15)$$

$$\sigma_z = S_v - 2\vartheta(S_{Hmax}-S_{hmin})\cos 2\Theta \quad (16)$$

$$\sigma_r = P_w \tag{17}$$

Based on the above equations, the axial and tangential stresses are dependent on Θ, and Θ changes from 0 to 2π. Also, the tangential and radial stresses are a function of the mud pressure.

The shear failure or breakout occurs when the rock is under maximum tangential stress conditions corresponding to $\Theta = \pm\frac{\pi}{2}$. Tensile failure or breakdown is expected to happen when the minimum tangential stress is applied on the borehole wall, which is 90° away from the breakout location (i.e., Θ=0, π). Three induced stresses in two conditions can be obtained by **1**. $\Theta = \pm\frac{\pi}{2}$:

$$\sigma_\theta{}^{max} = A - P_w \tag{18}$$

$$A = 3S_{Hmax} - S_{hmin} \tag{19}$$

$$\sigma_z = B,\ B = \sigma_v + 2\vartheta(S_{Hmax} - S_{hmin}) \tag{20}$$

And **2.** Θ =0, π:

$$\sigma_\theta{}^{min} = D - P_w \tag{21}$$

$$D = 3S_{hmin} - S_{Hmax} \tag{22}$$

$$\sigma_z = E, E = \sigma_v - 2\vartheta(S_{Hmax} - S_{hmin}) \tag{23}$$

Also, $\sigma_r = P_w$ in both the above conditions. Finally, there are various modes for shear and tensile failures depending on the regime of three induced stresses. Nonetheless, it has been figured out that the state of $\sigma_\theta > \sigma_z > \sigma_r$ is the most prevalent stress regime corresponding to wellbore breakout. Additionally, the case of $\sigma_r > \sigma_z > \sigma_\theta$ is the most common stress regime for the breakdown (Maleki et al., 2014; Das and Chatterjee, 2017; Mansourizadeh et al., 2016).

4.2. Induced Stresses around the Inclined Wellbore

During directional drilling, the azimuth and inclination of the borehole affect the induced and in-situ stresses due to stress coordinate transformations (Kasravi et al., 2017; Ma et al., 2015). Considering directional drilling, Fig.7 indicates that a borehole deviated from the vertical coordinate system (i.e., $(x'.y'.z')$) to the new coordinate system, as denoted ($(x.y.z)$, with the azimuth, α, and inclination, i, from the S_{Hmax} and vertical direction. The components of transformed stresses in the new coordinate system can be expressed by (Fjaer et al., 1992):

$$\sigma_x = (S_{Hmax}\cos(\alpha)^2 + S_{hmin}\sin(\alpha)^2)\cos(i)^2 + S_V\sin(i)^2 \quad (24)$$

$$\sigma^{\circ}_{zz} = (S_{Hmax}\cos(\alpha)^2 + S_{hmin}\sin(\alpha)^2)\sin(i)^2 + S_V\cos(i)^2 \quad (25)$$

$$\sigma_y = (S_{Hmax}\sin(\alpha)^2 + S_{hmin}\cos(\alpha)^2) \quad (26)$$

$$\tau_{xy} = \frac{1}{2}(S_{hmin} - S_{Hmax})\ \sin(2\alpha)\cos(i) \quad (27)$$

$$\tau_{zy} = \frac{1}{2}(S_{hmin} - S_{Hmax})\ \sin(2\alpha)\sin(i) \quad (28)$$

$$\tau_{xz} = \frac{1}{2}(S_{Hmax}\cos(\alpha)^2 + S_{hmin}\sin(\alpha)^2 - S_V)\ \sin(2i) \quad (29)$$

The induced stresses at the wellbore wall can be written in the cylindrical polar system (Fjaer et al., 1992):

$$\sigma_\theta = \sigma_x + \sigma_y - 2(\sigma_x - \sigma_y)\cos 2\Theta - 4\tau_{xy}\sin 2\theta - P_w \quad (30)$$

$$\sigma_r = P_w \quad (31)$$

$$\sigma_z = \sigma^{\circ}_{zz} - \vartheta[2(\sigma_x - \sigma_y)\cos 2\Theta + 4\tau_{xy}\sin 2\theta] \quad (32)$$

$$\tau_{\theta z} = 2(\tau_{yz}\cos 2\Theta - \tau_{xz}\sin\theta) \quad (33)$$

Where θ is the azimuth angle of the wellbore position relative to the x-axis. $\tau_{\theta z}$, $\tau_{\theta r}$, and τ_{rz} are shear stress components of induced stresses.

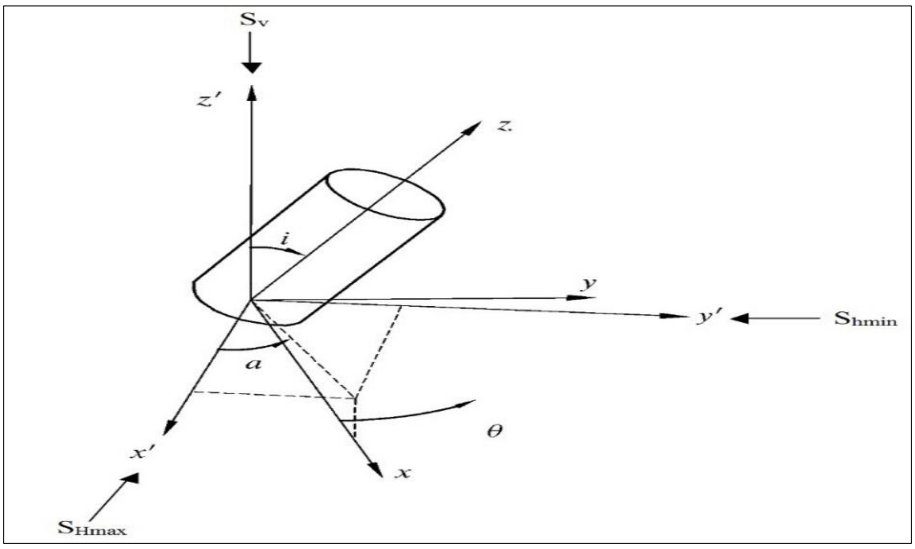

Fig. 7. The stress transformation system for a deviated well (Fjaer et al., 1992)

According to Eq. (33), the shear stress in the Θ-z plane is not zero at the borehole wall compared to the vertical borehole due to azimuth and inclination. Thus, the normal axial and tangential stresses are not applied on a principal stress plane (Θ-z is not a principal plane), and therefore they cannot be considered as the principal stresses. It means that the regimes of $\sigma_\theta>\sigma_z>\sigma_r$ and $\sigma_r>\sigma_z>\sigma_\theta$ are not considered for the borehole breakout and breakdown, and the principal stresses should be determined for the deviated boreholes. The locations of the principal stresses ($\Theta_1.\Theta_2$), where the shear stress is zero, can be obtained by (Al-Ajmi, 2006; Kasravi et al., 2017):

$$\theta_1 = \tan^{-1}\left(\frac{2\tau_{xy}}{\sigma_x+\sigma_y}\right).\ \theta_2 = \theta_1 + \frac{\pi}{2} \tag{34}$$

Moreover, the maximum and minimum principal stresses, as a function of borehole azimuth and inclination, in these locations can be calculated as followed (Zoback, 2007):

$$\sigma_{max} = \frac{1}{2}\left[(\sigma_\theta + \sigma_z) + \sqrt{(\sigma_\theta + \sigma_z)^2 + 4\tau_{\theta z}^2}\right] \tag{35}$$

$$\sigma_{min} = \frac{1}{2}\left[(\sigma_\theta + \sigma_z) - \sqrt{(\sigma_\theta + \sigma_z)^2 + 4\tau_{\theta z}^2}\right] \tag{36}$$

5. Wellbore Stability Analysis based on Elastic Model

The determination of a safe MW window is usually the main aim of performing wellbore stability using the analytical (elastic) solution. In determining a MW window, the breakout and breakdown pressures, known as the lower and upper bounds of the mud window, need to be calculated. For achieving the goal of the MW window determination, rock failure criteria utilization is essential since failure criteria deal with the state of induced stresses that both shear and tensile failure occur around the wellbore. Hence, in this paper, four rock failure criteria, namely Mohr-Coulomb (MC), Hoek-Brown (HB), Mogi-Coulomb (MG), and Modified Lade (ML), have been employed to determine the safe MW window for Well-A. The application of these failure criteria and their equations have been presented at the end of this paper, Appendix A section. The results of various MW windows predicted under rock failure criteria in each hole of Well-A have been rendered in the following subsections.

5.1. MW Window of the 17.5-inch Hole

Fig. 8 represents the predicted MW windows for the first hole of Well-A. In this Figure, the first, second, and third tracks show measured depth (MD), well formations, and lithology. Track 4 to 7 display the predicted different MW windows based on four failure criteria. The real mud weight (Real MW) used to drill this hole is observed in the black line. The grey profile displays the equivalent mud weight of kick (MW_Kick) or pore pressure. The breakout pressure or minimum required MW (MW_Breakout) to prevent breakouts or shear failure has been represented in yellow. The green and blue profiles illustrate mud loss pressure (MW_Loss), which is equal to the minimum horizontal stress value, and the breakdown pressure or maximum allowable MW to avoid borehole fractures, respectively. These profiles express the critical values of a mud window, and all these critical values are in ppg (lbm/gal), which 1 pound per gallon (ppg) = 0.12 gr/cm^3. The white area in the middle of these tracks is the ideal range or safe window of MW. The last track represents the caliper log with the bit

size. The comparison between bit size and caliper log is used to verify the predicted MW windows since changing in caliper data relative to bit size can be a sign of wellbore enlargement or breakout. As observed in Fig. 8, practically, there is no safe window of MW for drilling, and the real MW have been misdesigned in this hole. Severe breakouts are observed from the caliper log data in most intervals of this section, especially 985 to 1200 m. XRMI images have not detected any breakouts due to the large diameter of this hole (i.e., 17.5-inch) and the poor quality of images. Based on this Figure, MC and HB criteria overestimate the minimum required MW. It means both HB and MC are a conservative failure criterion. The conservative approach of the MC and HB criteria is mainly due to the presence of the intermediate principal stress, and they both do not account for the effect of intermediate stress. Accordingly, it can be concluded that the MG and ML failure criteria render more proper predictions compared to the HB and MC. In the end, between MG and ML, both predict the minimum required MW near each other, although the ML criterion has underestimated the breakout pressure for this zone. On the other hand, the GS formation consists of weak rocks with low cohesion, as indicated in Fig. 4 and 5. Besides, for the weaker rocks, a higher breakout pressure is required to prevent shear failure. Consequently, since the MG provides a higher minimum required MW than the ML criterion, we might conclude that the MG criterion and its results are the most reliable approach in drilling the hole with 17.5- inch size.

5.2. MW Window of the 12.25-inch Hole

In the 12.25-inch hole, Fig. 9 displays the predicted MW windows using four failure criteria with the XRMI images. This Figure, indicates clearly that the stable or safe area of the mud window is broader than the 17.5-inch hole. Plus, from the caliper log, a severe breakout is observed in AS formation from 1740 to 1790 m. As the same, the XRMI image represents the borehole breakouts in this interval. Borehole breakouts are detected almost in the depth of 2050 to 2100 m by XRMI images, whereas caliper logs do not show any breakout in this depth.

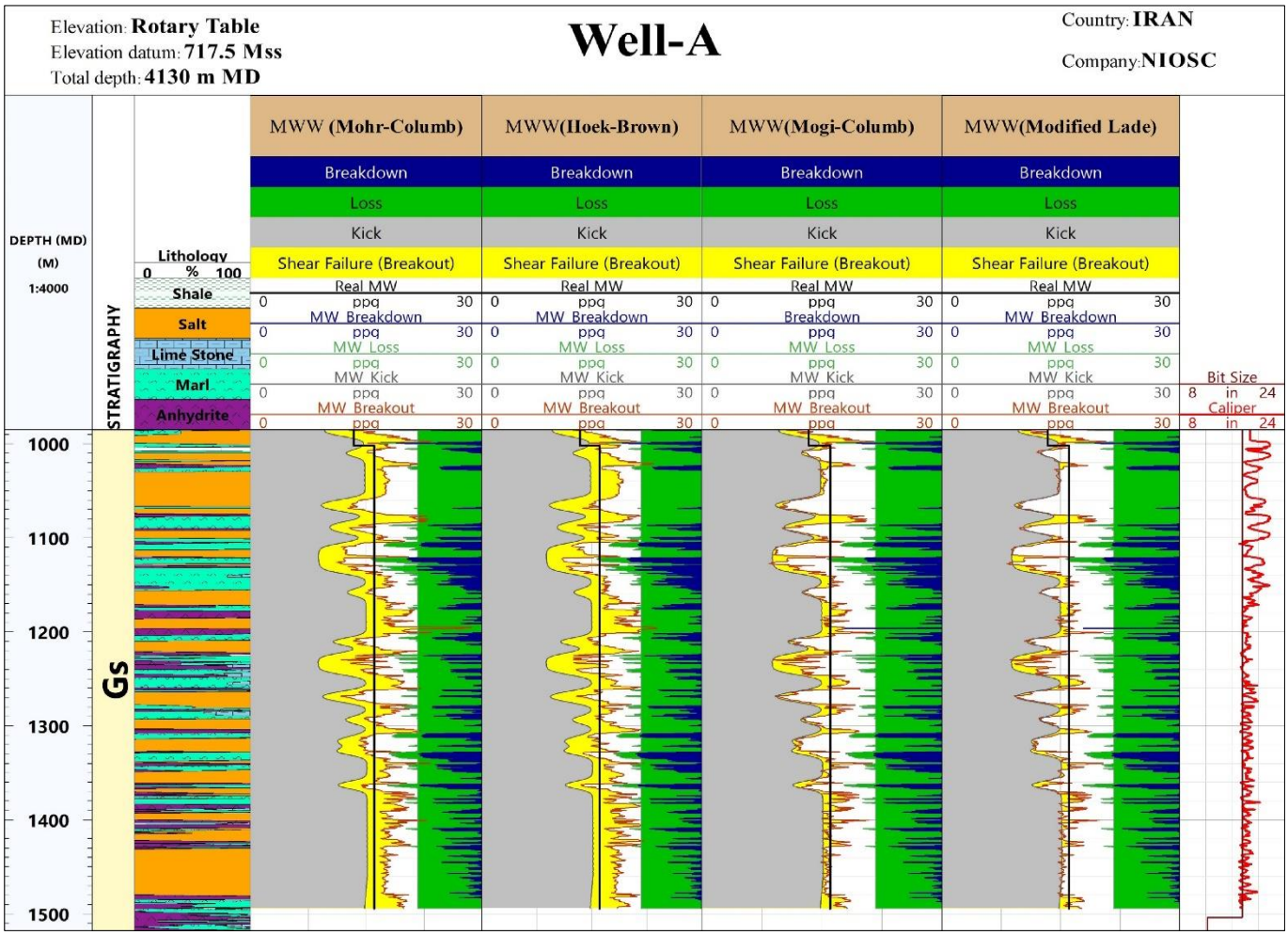

Fig. 8. Mud weight windows for the 17.5-inch hole of Well-A using four different rock failure criteria with real MW, bit/caliper logs, and lithology of GS stratigraphy

Similar to the results of the 17.5-ich hole, the MC and HB failure criteria overestimate the minimum required MW in the 12.25-inch comparing to the MG and ML criteria. Additionally, the ML failure criterion presents a lower minimum required MW than MG. On the other side, the predicted breakouts using the MG failure criterion have a good agreement with the real breakouts observed from the image and caliper logs. Nonetheless, in the depth of 2055-2100 m, the ML criterion does not give an appropriate match with the real breakouts. In consequence, like the 17.5-inch hole, which offers a more robust base to conclude that the MG failure criterion perhaps is the most reliable criterion to consider for the 12.25-inch hole of Well-A.

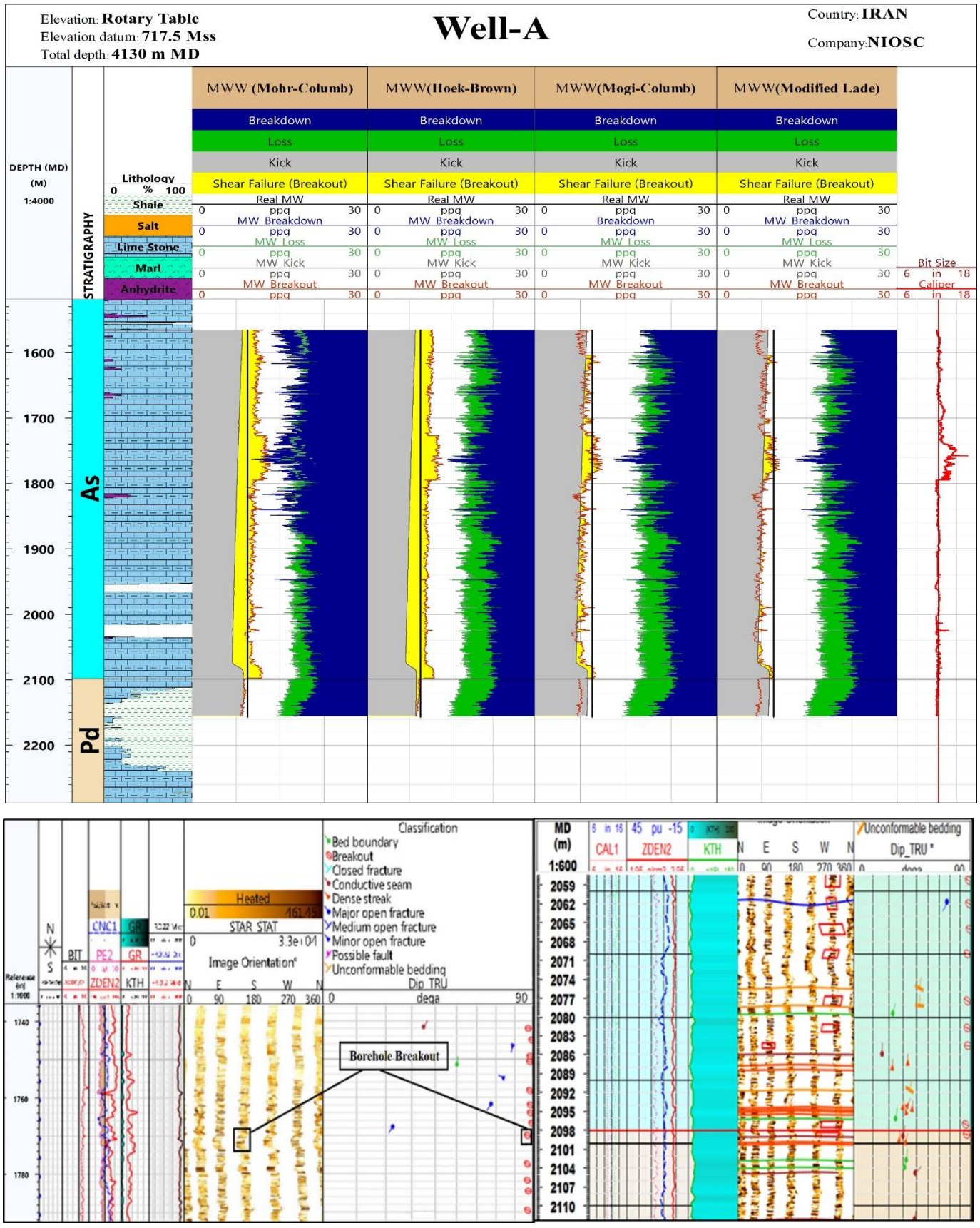

Fig. 9. Mud weight windows for the 12.25-inch hole of Well-A using four different rock failure criteria with real MW, bit /caliper logs, XRMI images, and lithology of AS and Pd

5.3. MW Window of the 8.375-inch Hole

Fig. 10 demonstrates the predicted MW windows. Track 4 shows the borehole azimuth and inclination, which reveal that this hole has been drilled directionally. Moreover, from this Figure, the caliper log indicates some enlargements in the intervals of 2440-2520 m and 3300-3400 m MD. According to Fig. 10, the HB failure criterion overestimates the lower limit of the mud window, whereas the ML criterion underestimates it. Therefore, these two failure criteria are not able to predict the breakouts realistically. The MC failure criterion approximately provides the proper predictions, but it is known that the MC adopts a conservative approach for predicting breakout pressure due to presenting a linear model and neglecting of intermediate stress effect. Besides, despite a proper matching in the interval of 3300-3400 m, the MG criterion predicts no breakouts in the interval 2440 -2540 m. However, the image log was not available to confirm the observations of the caliper in this interval, and these enlargements may be due to another reason, not the shear failure. Generally, because the MG failure criterion is a 3D criterion and has provided the most reliable MW window in the two previous boreholes, the MG criterion might be the best option for the safe MW window determination in the 8.375-inch hole of Well-A.

5.4. MW Window of the 6.125-inch Hole

In the last hole section, the predicted MW windows with the OMRI image log have been represented in Fig. 11. Regarding the caliper, the borehole breakouts have been seen in the intervals of 3540-3600, 3640-3665, and 3685-3730 m MD. Likewise, the OMRI image log shows the borehole breakouts at these intervals. Also, based on this Figure, the MC criterion overestimates the minimum required MW, while the HB gives a better prediction. Furthermore, the predicted MW windows via ML and MG criteria are almost identical and have an excellent agreement with the real breakouts seen from the caliper and OMRI logs. In addition, the ML

and MG criteria present the 3D model. Consequently, the ML and MG Criteria could be finally recommended for specifying the safe MW window in the 6.125-inch hole.

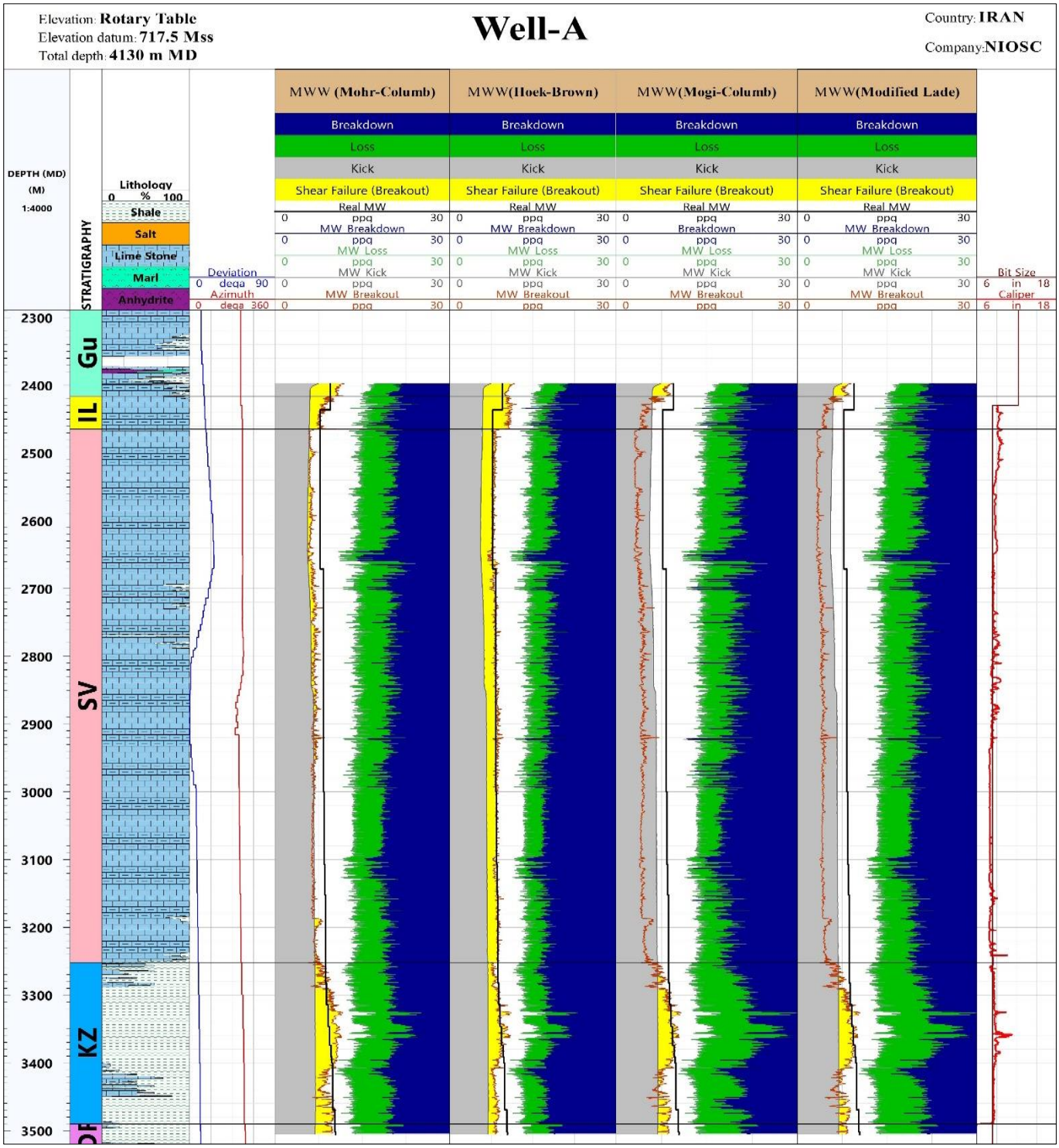

Fig. 10. Mud weight windows for the 8.375-inch hole of Well-A using four different rock failure criteria with real MW, bit/caliper logs, azimuth and inclination of the borehole, and lithology of Gu, IL, SV, and KZ

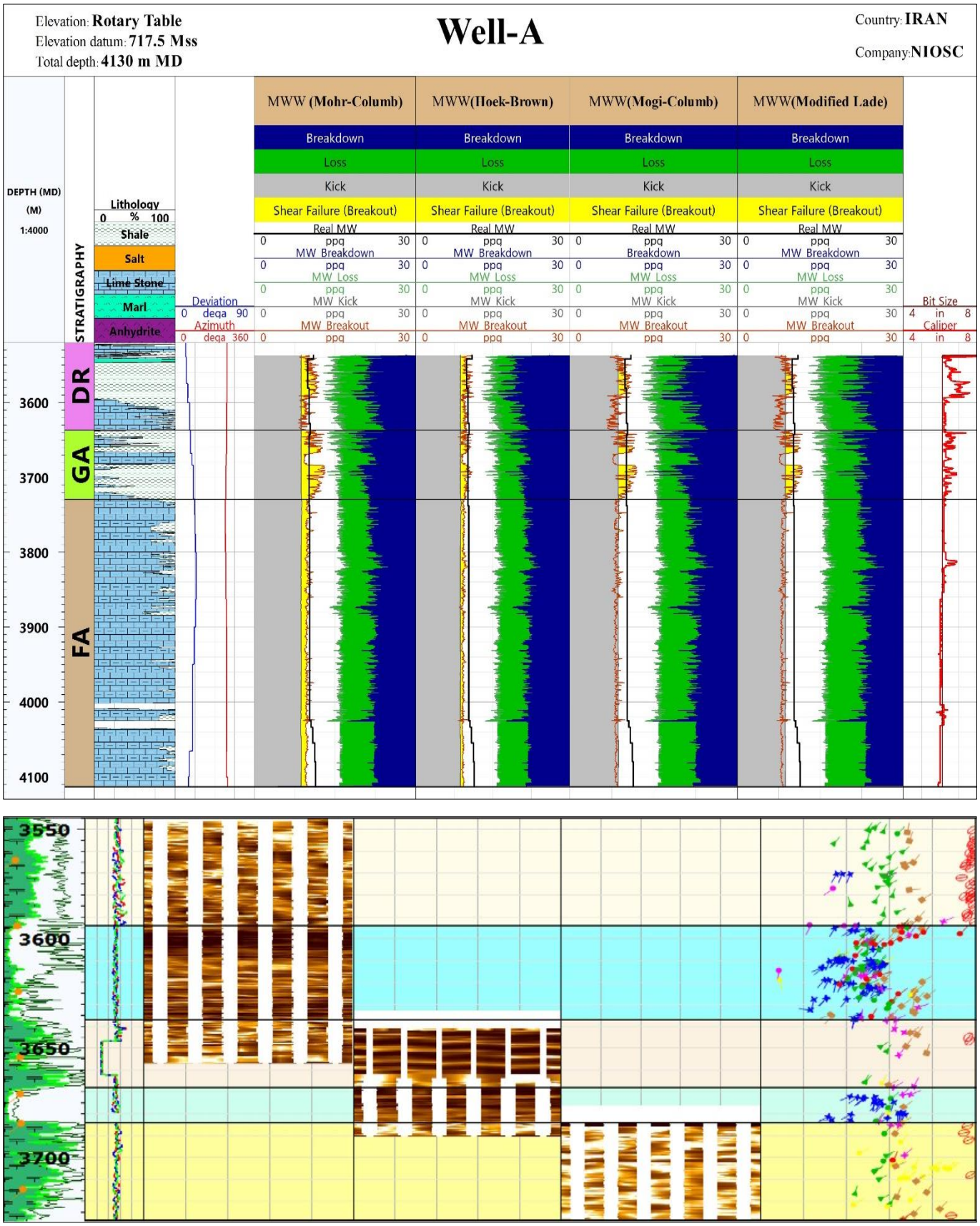

Fig. 11. Mud weight windows for the 6.125-inch hole of well-A using four different rock failure criteria with real MW, bit /caliper logs, OMRI image, azimuth and inclination of the borehole, and lithology of DR, GA, FA

In general, for all holes of Well-A, the MG and ML criteria provide more realistic predictions than the HB and MC criteria. The ML seems to underestimate the minimum required MW, especially in the softer rocks. Hence, the Mogi-coulomb rock failure criterion can be selected as the most appropriate failure criterion for designing the MW and well-planning in Well-A or any similar well in the current Iranian oil field.

Fig. 12 suggests the general MW window determined by the Mogi-Coulomb criterion in all height of Well-A. Track 8 shows the points of depth that shear failures have occurred, expressed before, with the azimuth of these shear failures. Also, the loss of drilling fluids during drilling has been illustrated in track 9. Based on this track, the happened mud loss in Well-A owns the most significant quantity in IL formation. Track 10 indicates a view of the borehole shape, which has been drilled with the caliper log. The last track illustrates a schematic of the Well-A, including the size of casings or liners in every hole, and the depths of the casing shoe. The sixth track shows the predicted shear failure modes. For a vertical borehole, both Wide Breakout and Low Angle Echelon modes occur when the stress regime is $\sigma_\theta > \sigma_z > \sigma_r$. Besides, the Shallow Knockout mode takes place when there is the condition of $\sigma_z > \sigma_\theta > \sigma_r$.

As is evident in Fig. 12, the Wide Breakout (the red one) is a predominant shear failure mode in the vertical 17.5 and 12.5-inch holes. On the other hand, the stress regime of $\sigma_\theta > \sigma_z > \sigma_r$ was considered for predicting the breakout pressure in the vertical depths. Therefore, this consideration and the determined breakout pressures are creditable for Well-A. Also, based on this Figure, the first hole possesses the tightest safe window of MW and the most excessive breakouts in comparison with other formations, so it needs more attention in drilling applications.

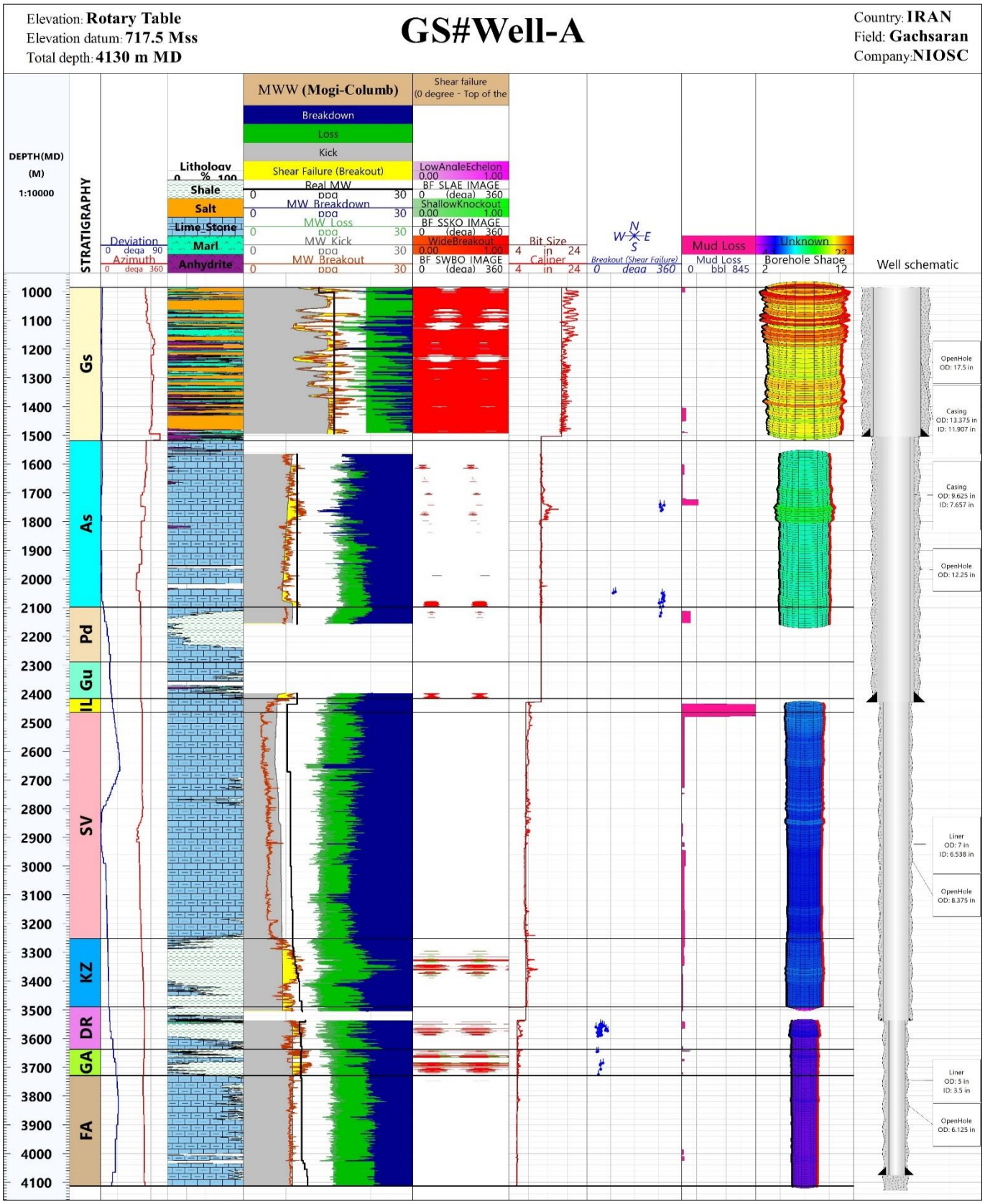

Fig. 12. General mud weight window for Well-A using Mogi-Coulomb failure criterion with predicted shear failure modes, the azimuth of shear failures, mud loss, borehole shape, and well schematic of Well-A

6. Sensitivity Analysis

The sensitivity analysis of well deviation and azimuth based on the elastic solution was conducted in this research using the MG criterion to specify the optimum well trajectory.

6.1. Sensitivity Analysis Results of GS

In this formation, because all single depths indicate approximately similar results, only the results of conducted sensitivity analysis at a single depth of 1080 m MD have been presented. Also, in this depth, the stress faulting regime reveals to be inverse. Fig. 13 (a) and (b) demonstrate the borehole MW corresponding to breakout and breakdown with the wellbore azimuth and deviation. The radial distance represents a deviation of the borehole, and it is zero at the center of the plot and 90˚ the circle circumference. The borehole azimuth at the top of the circle is 0˚ corresponding to the north and increases clockwise to 180˚. From this Figure, the darkest red and blue respectively show the worst and best conditions of stability against both breakout and breakdown instabilities. Hence, the boreholes oriented in the minimum horizontal stress direction are least stable, especially for a high-inclination well. According to Fig. 13 (a), the boreholes drilled in the maximum horizontal stress direction, i.e., azimuth 15˚, with the deviation from 60˚ to 90˚ are most stable against breakouts. On the other side, based on Fig. 13 (b), the maximum horizontal stress direction and an inclination between about 15˚ and 35˚ is the most challenging status for initiating fractures. Generally, because the breakouts were the dominant failures in this formation, it can be concluded that a well with an inclination of 60˚-65˚ and azimuth 15˚ could make experienced the best stability. Nonetheless, because the diameter of the borehole is large in GS (i.e., 17.5-inch), directional drilling with such a high deviation of 60˚ may not be possible practically. Thus, other drilling actions such as hole cleaning or directional drilling with a low inclination should be considered to plan the drilling operation in GS in the best way.

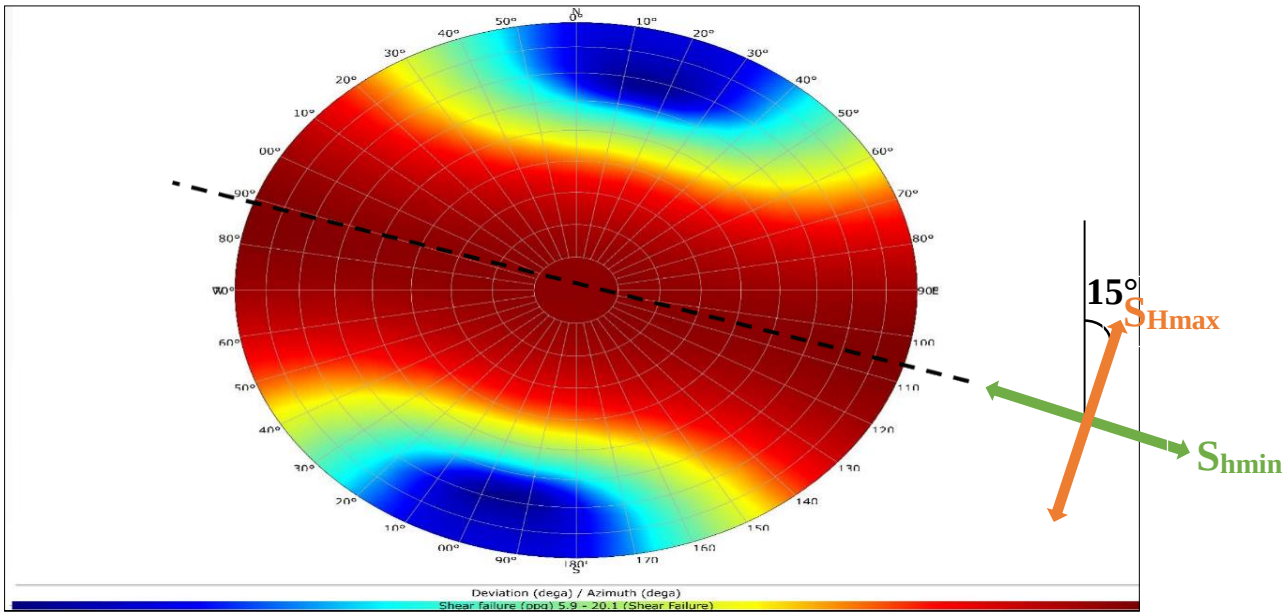

(a)

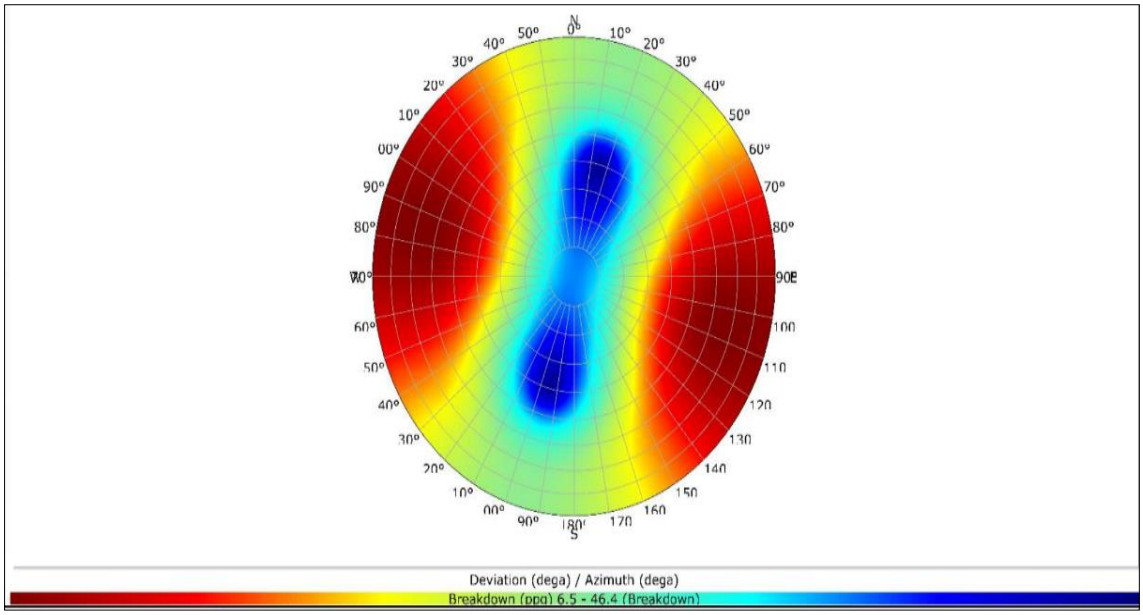

(b)

Fig. 13. Borehole equivalent MW related to (a) breakout, (b) breakdown at a depth of 1080 m MD in GS

6.2. Sensitivity Analysis Results of AS and Pd

The sensitivity analysis was performed for the AS formation at three single depths of 1600, 1780, and 2000 m MD, where the stress regime is strike-slip, and two depths 2100 and 2140 m MD in the Pd formation, where the stress regime is normal. The results of the conducted analysis for the single depths of 1780 m MD and 2100 m MD, where real breakouts were

observed, have been indicated in Fig. 14 and 15, respectively. Based on Fig. 14, the horizontal wells (i.e., deviation of 90˚) with two azimuths 40-50° and 160-170° are most durable in the breakout statuses. Also, fractures are toughest to induce in the horizontal wells with an azimuth from 70° to 140°. Furthermore, vertical wellbores possess the worst condition versus breakout and breakdown, and this could be due to the in-situ stress regime. In the strike-slip regime, the difference between the two horizontal stresses is more significant than the difference between the vertical stress and each of the horizontal stresses. On the other side, a vertical well will be subjected to the maximum and minimum horizontal stresses. In contrast, a horizontal well will be exposed to the vertical stress and maximum horizontal stress or the minimum. The higher stress difference in a vertical well will cause higher shear stresses to generate compared to a horizontal well, which will eventuate less stable wellbore conditions in a vertical well.

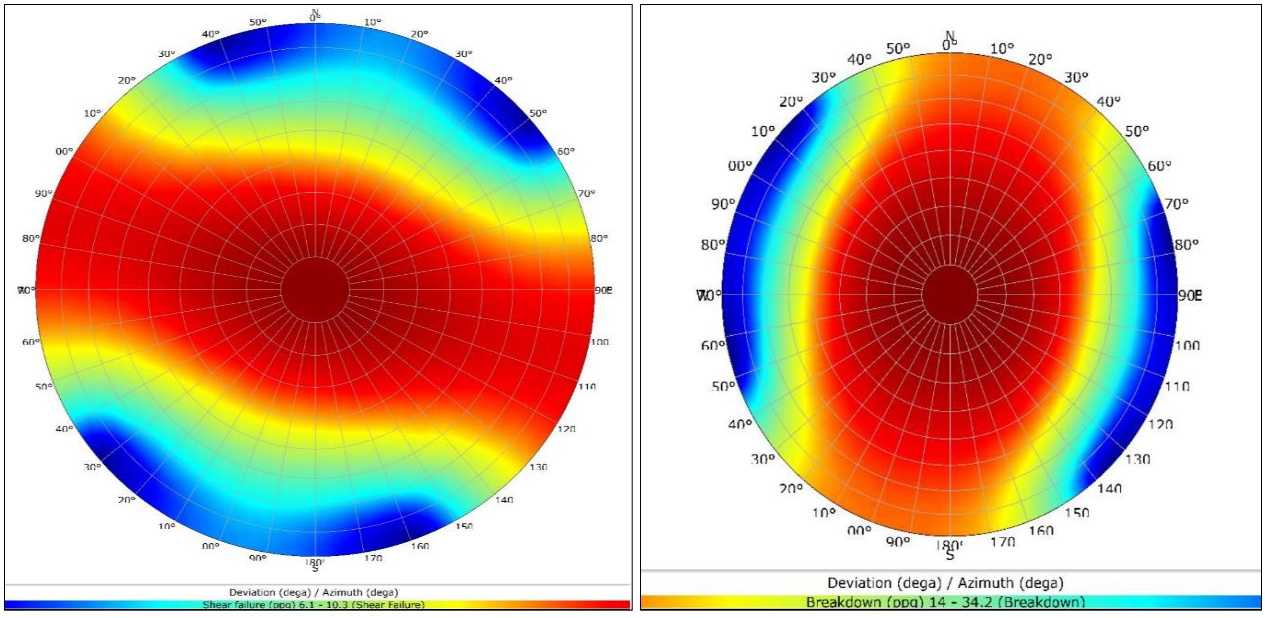

(a) (b)

Fig. 14. Borehole equivalent mud weight related to (a) breakout, (b) breakdown at a depth of 1780 m MD in AS

From Fig. 15, the minimum horizontals stress direction with a deviation from 20 to 50°, and 55 to 65° are respectively the safest orientations for drilling a well relative to the breakout and breakdown. Moreover, it was predictable that the horizontal boreholes drilled in the

maximum horizontal stress azimuth are least stable since the stress regime is a normal fault regime, and shear stresses in this orientation are much higher than in other orientations. As a result, the maximum horizontal stress direction generates the highest shear stresses for a horizontal well, which will lead to a less stable wellbore condition. Overall, it could be concluded that directional drilling would be a more appropriate selection for planning the drilling scenario of Well-A in this Iranian oil field with respect to AS and Pd.

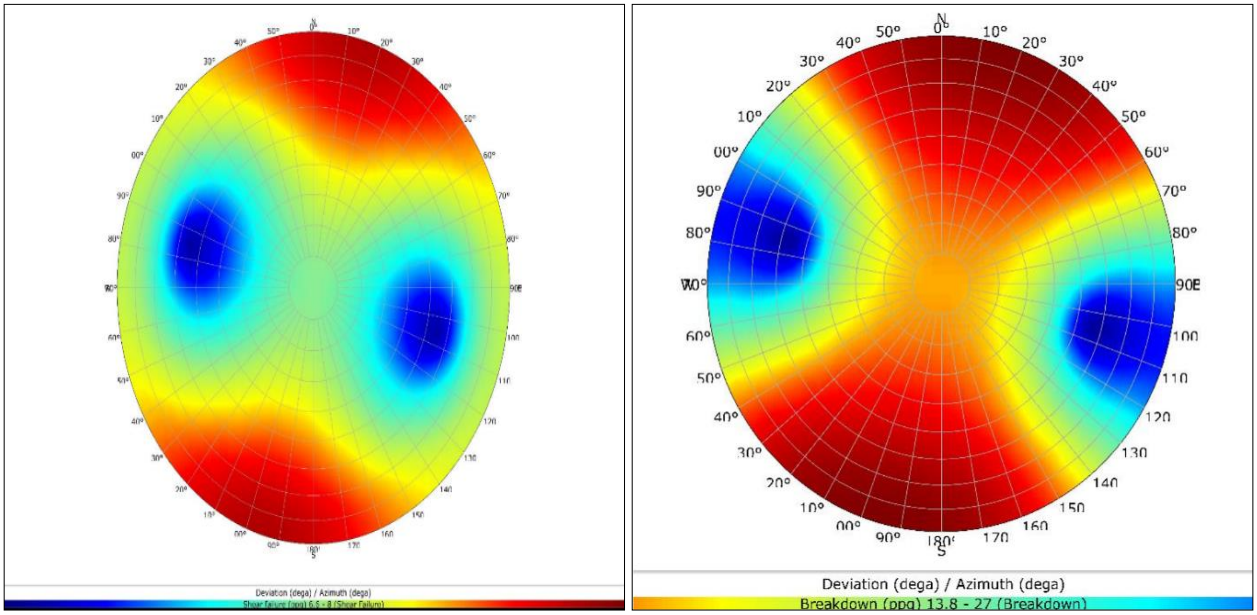

(a) (b)

Fig. 15. Borehole equivalent mud weight related to (a) breakout, (b) breakdown at a depth of 2100 m MD in Pd

6.3. Sensitivity Analysis Results of Gu, IL, and SV

The four individual depths were taken into account for both Gu and IL formations. In the SV formation, five different single depths were evaluated. The stress regime in Gu, IL, and upper depths of SV is mainly normal faulting with really close to the boundary of the strike-slip (i.e., $S_V >= S_{Hmax} \gg S_{hmin}$). The results of the sensitivity analysis conducted in IL formation have been demonstrated in Fig. 16, regarding the depth of 2440 m MD. Based on this Figure, similar to the results of Pd formation, the horizontal wells drilled in the maximum horizontal stress direction are most unstable. Contrarily, the minimum horizontal stress

direction will result in the most proper wellbore condition, and a well drilled in this azimuth with a deviation from about 40 to 55° will be encountered to the least shear failure. However, for the breakdown, this status exists in the deviation of 70- 90°. Finally, the conducted sensitivity analysis for five other depths of 2400, 2410, 2460, 2500, and 2660 m MD has provided the same results since an identical stress faulting regime is prevalent in these depths.

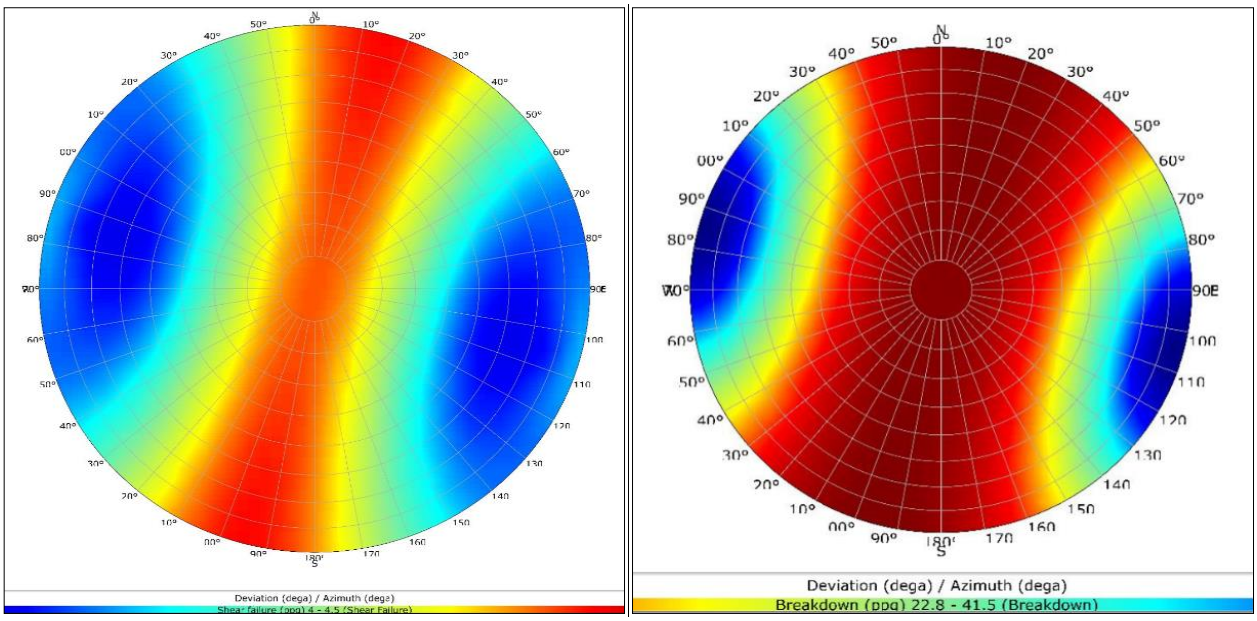

(a) (b)

Fig. 16. Borehole equivalent mud weight related to (a) breakout, (b) breakdown at a depth of 2440 m MD in IL

Three alternative depths of SV represent the normal fault regime at the lower depths, which are 2900, 3100, and 3200 m MD. Only the results of the breakout MW at a depth of 2900 m have been indicated in Fig. 17 since the breakdown results are similar to the 2440 m. As seen in this Figure, the worst and best wellbore conditions are related to the minimum horizontal stress direction. Therefore, a well oriented in the minimum horizontal stress direction with a deviation between 30 and 40° will experience the most desired degree of stability.

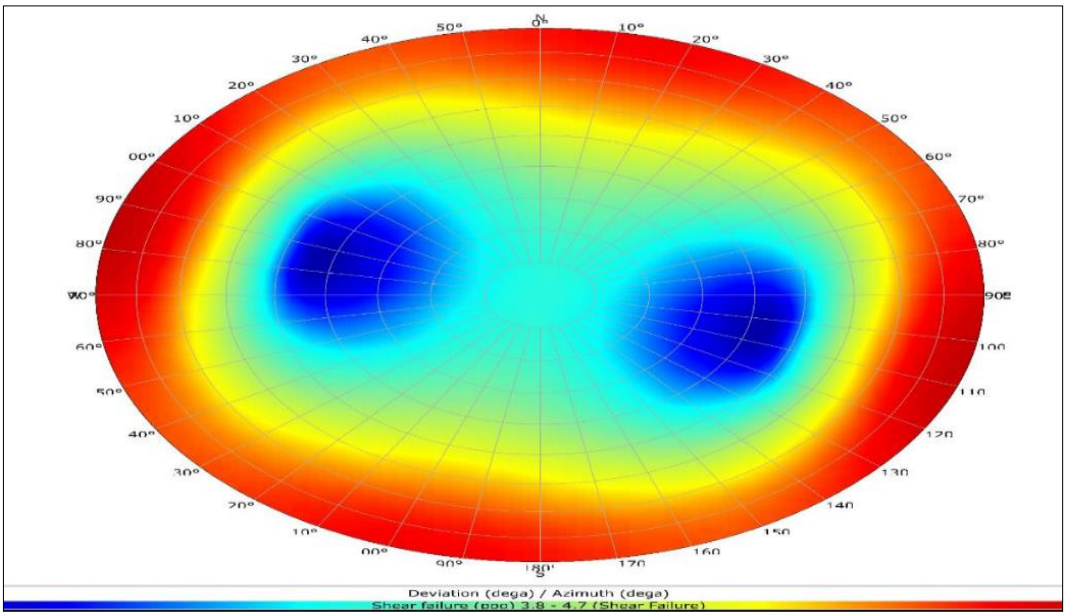

Fig. 17. Borehole equivalent mud weight related to breakout in SV at a depth of 2900 m MD

6.4. Sensitivity Analysis Results of KZ, DR, GA, and FA

The sensitivity analysis performed for all single depths of KZ, GR, GA, and FA indicates approximately the matching results because the stress regime is normal so that $S_V \gg S_{Hmax} > = S_{hmin}$. The selected single depths have been 3270, 3360, and 3470 m MD for KZ, and also 3500, 3580, and 3620 m MD for DR, then 3640, 3700, and 3720 m MD for GA, and lastly, 3740, 3850, 3950, 4025, and 4100 m MD for FA.

Fig. 18 demonstrates the taken resembling results as an example at the depth of 3580 m in which real breakout has been observed. According to this Figure, the high deviations, autonomous of the azimuth variations, can lead to the least constant of the wellbore condition. Contrariwise, a low deviated well like a vertical well is most stable since a vertical wellbore will be exposed to the maximum and minimum horizontal stresses, so the lower shear stresses exist in this direction. Regarding the breakdown, Fig. 18 displays that the fractures are most stick to create in the azimuth of 105°with an inclination of 20-35°. Eventually, we may conclude that the vertical boreholes are the most trustworthy trajectory in KZ, DR, GA, and FA.

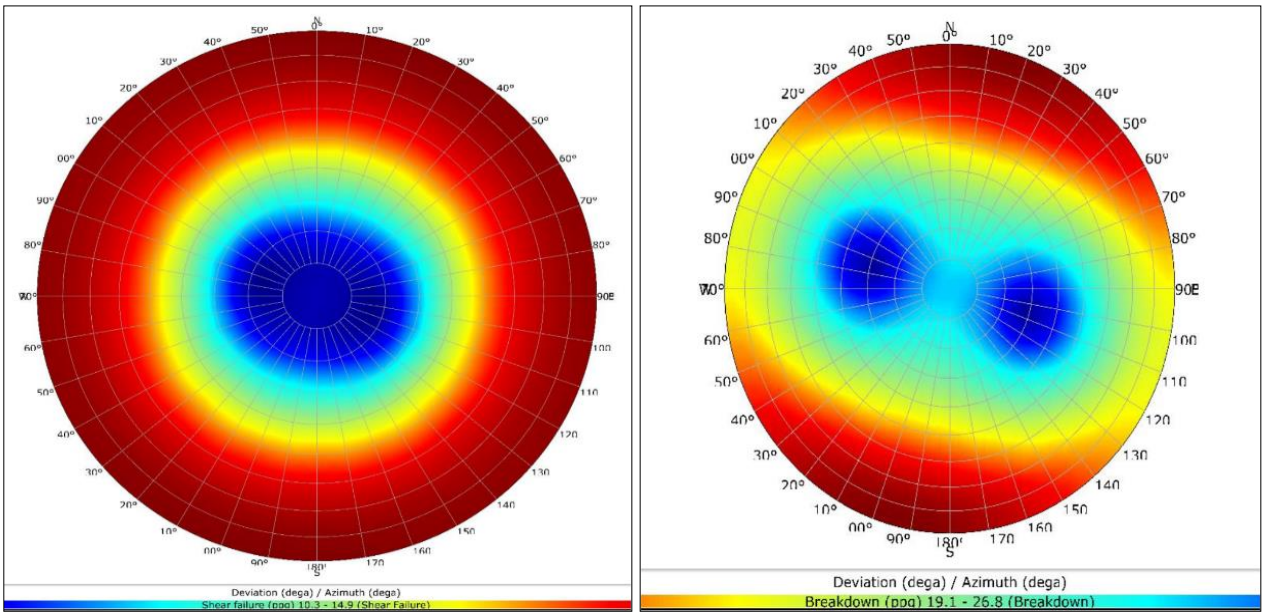

(a) (b)

Fig. 18. Borehole equivalent mud weight related to (a) breakout, (b) breakdown at a depth of 3580 m MD in DR

Generally, based on the results obtained from the sensitivity analysis of Well-A, directional drilling would be a wise decision for the drilling operation in the shallower formations (i.e., GS, AS, Pd, Gu, IL, and SV). On the contrary, the deeper formations present a better response to the vertical drilling for achieving the most favorable degree of stability. This diversity of optimum well trajectory determined for Well-A c due to varying the regimes of in-situ stresses.

7. Numerical Solution of Wellbore Stability Based on Elastoplastic Model

In the previous sections, the analytical solutions were discussed to analyze the wellbore stability of Well-A. The linear elastic model is the most popular approach due to its simplicity and less required inputs. However, this model cannot achieve reliable results, and rock properties often exhibit elastoplastic yielding behavior in deep drilling (Salehi et al., 2010; Chen and Abousleiman, 2017). Consequently, a qualified elastoplastic model is required to confirm the results of the elastic model and to perform wellbore stability analysis more realistic.

The Normalized Yielded Zone Area (NYZA) parameter is often used to specify the wellbore instability risk (Hawkes and Mclellan, 1999). The NYZA parameter is defined as the cross-sectional area or volume of the plastic (yielded) zone around the borehole divided into the borehole's original area or volume, shown in Fig. 19. According to the former researches, the difficulties of borehole instability are related to the NYZA more than 1.0, which is considered as a critical value (Kasravi et al., 2017; Salehi et al., 2010; Elyasi and Goshtasbi, 2015). The NYZA less than 1.0 indicates that the mud pressure is in optimum status.

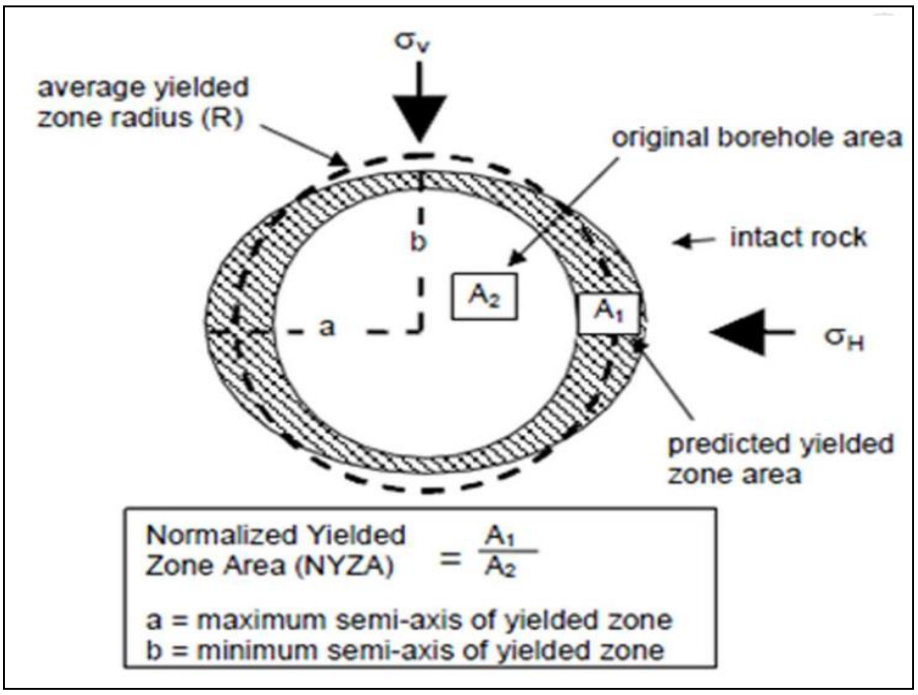

Fig. 19. NYZA parameter concept (Kasravi et al., 2017)

In this paper, a finite difference code, FLAC3D, based on the elastoplastic model assumptions, was employed to (1) evaluate the analytical solution results of wellbore stability analysis (i.e., the MW window determined by the MG failure criterion) (2) to determine the optimum MW for the case study Well-A. Also, the regions of Well-A in which the real breakouts have been detected from caliper/image logs were simulated. For instance, Fig. 20 shows a geometrical model generated in FLAC3D for a deviated borehole of Well-A.

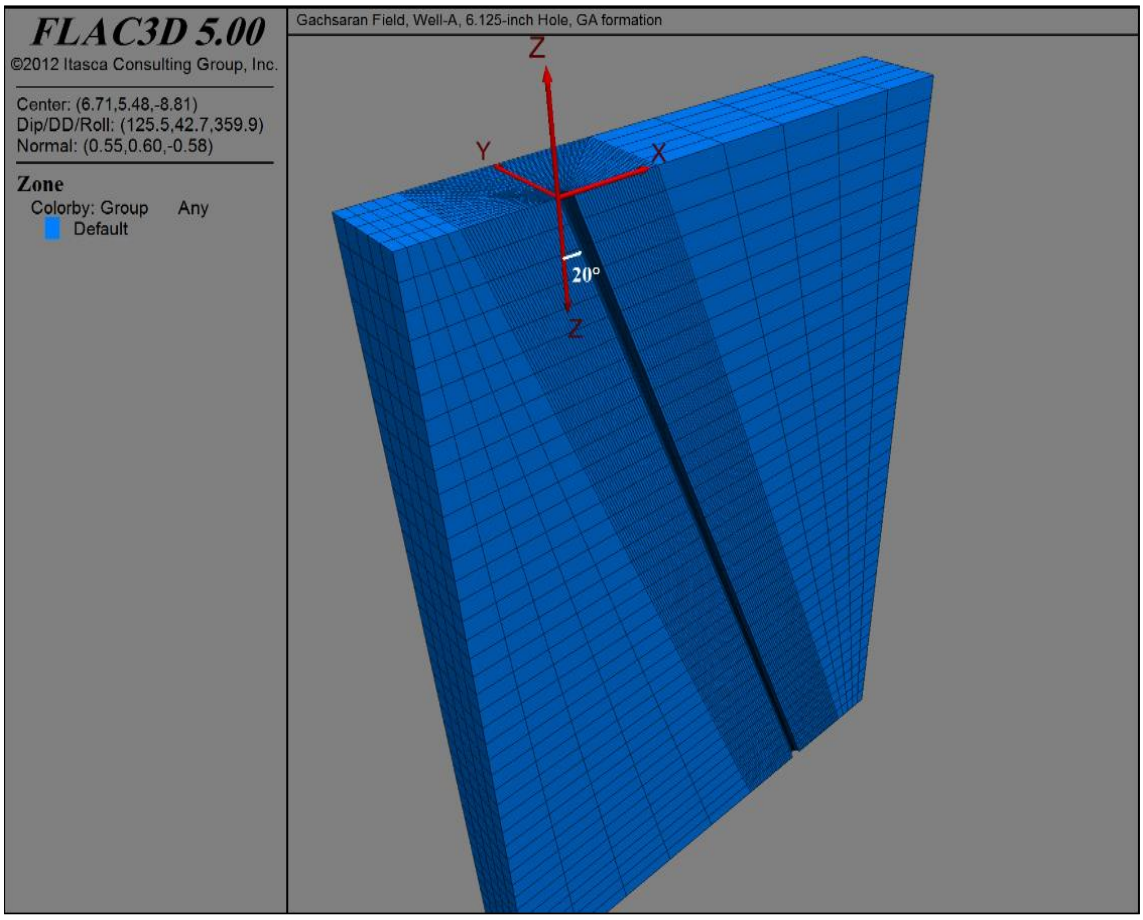

Fig. 19. Schematic view of a generated model for the 6.125-inch hole of Well-A

7.1. Numerical Simulation of 17.5-inch Hole

In this hole, separate simulations were conducted for six intervals. The obtained NYZAs versus different MWs have been indicated in Fig. 21. According to this Figure, the NYZA reduces with increasing MW. Also, For the interval from 990 to 1020 m, the best curve has been fitted to the calculated NYZAs for determining the optimum MW from the curve formula, and the optimum MW ranges from 16.6 to 17.33 ppg, corresponding to the NYZA of 0.8 to 1.0, which 0.8 is considered as a safety margin (Salehi et al., 2010). From the other graphs, the optimum range of MW is recommended to be 21.5-21.75 ppg, 20.5-22.46 ppg, 19.8-20.64 ppg, 17.6-18.8 ppg, and 20.1-20.85 ppg at the intervals of 1020-1050, 1050-1080,1080-1110, 1110-1140, and 1140-1180 m respectively. Based on Fig. 21, the calculated NYZAs for each real MW used to drill these intervals (the red dots) are more than 1.0, which means the rocks around

the wellbore have been yielded or failed. Therefore, the simulation results obtained from FLAC3D are acceptable since they have a good agreement with the real observations of the caliper log. On the other hand, the determined MW window by the MG failure criterion predicted the breakouts correctly and indicated that the real MWs have been unsuitable for drilling these intervals. Consequently, this point manifests that the analytical results present proper accordance with numerical results and so will prove the accuracy of the analytical results of this hole.

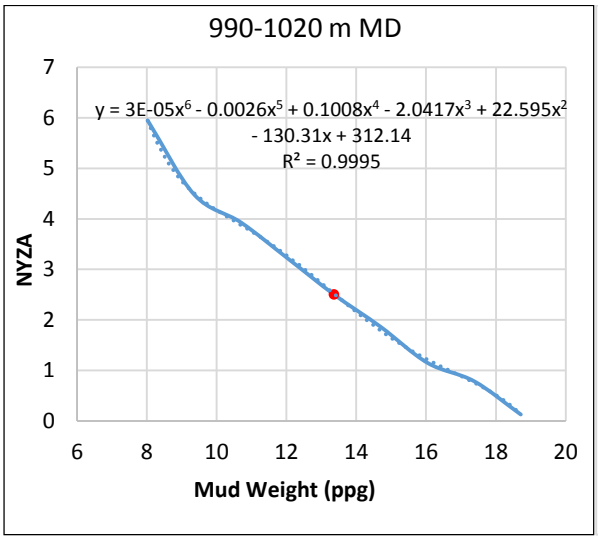

(a)

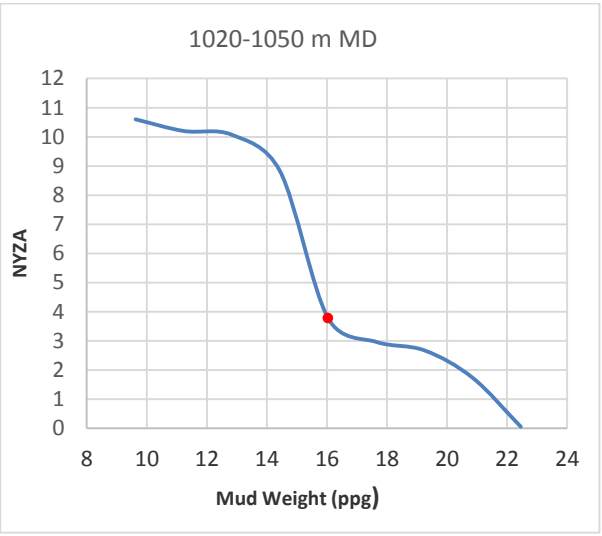

(b)

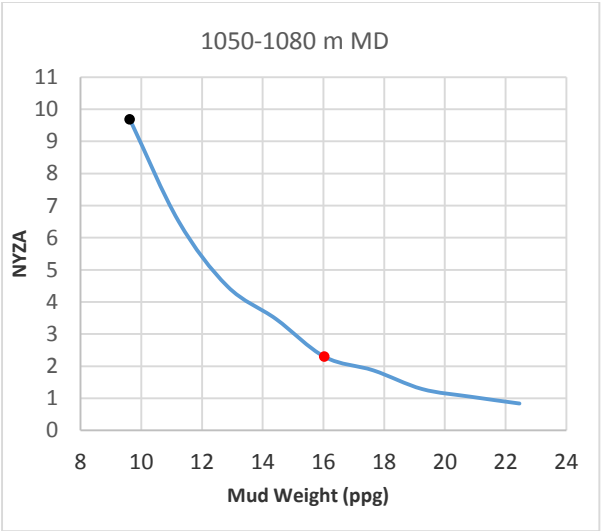

(c)

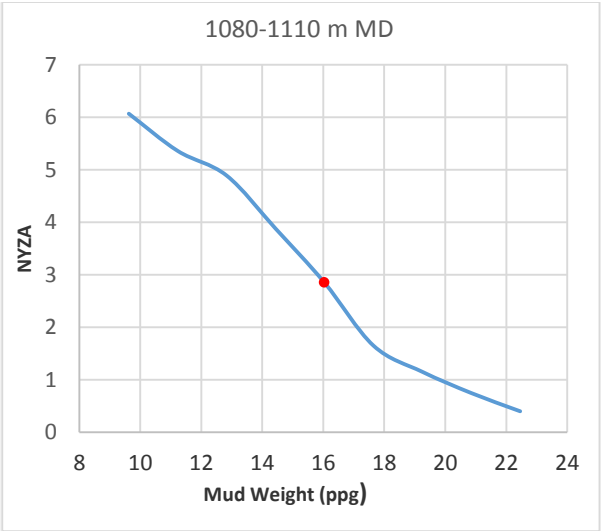

(d)

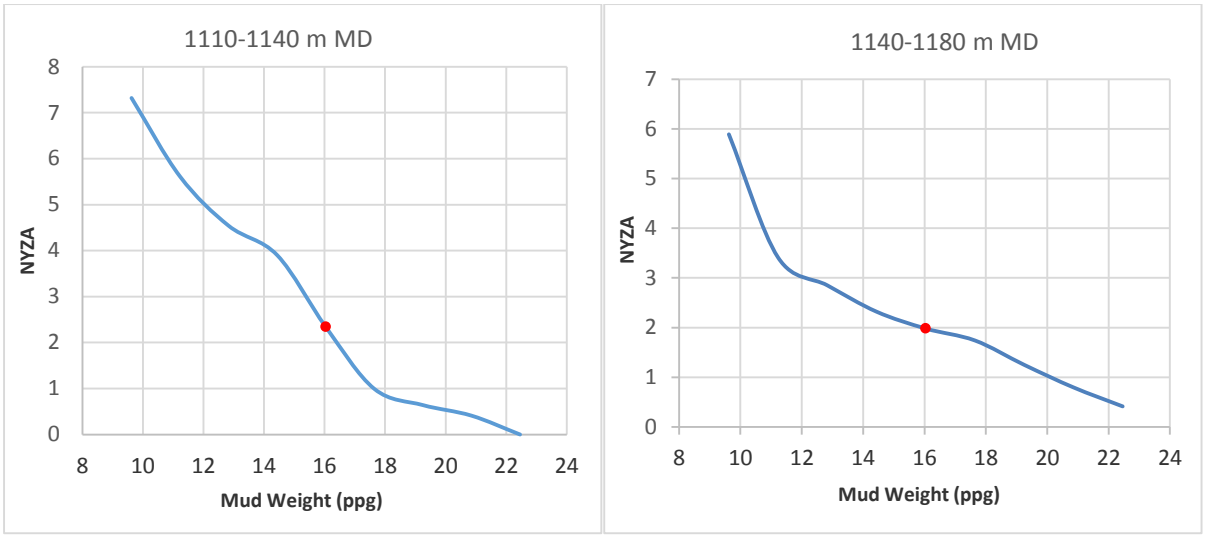

(e) (f)

Fig. 20. NYZA Versus mud weight in the 17.5-inch hole of Well-A for for the depth of (a) 990 to 1020 m, (b) 1020-1050, (c) 1050-1080, (d) 1080-110, (e) 1110-1140, and (f) 1140-1180 m MD

The computation procedure of NYZA for the interval from 1050 to 1080 m has been displayed in Fig. 22. Based on this Figure, only the shear failures have occurred around the borehole (i.e., blue and red regions), not tensile failures, which have a good agreement with the real observations of the breakout. Also, this Figure represents the black point in Fig. 21 (c).

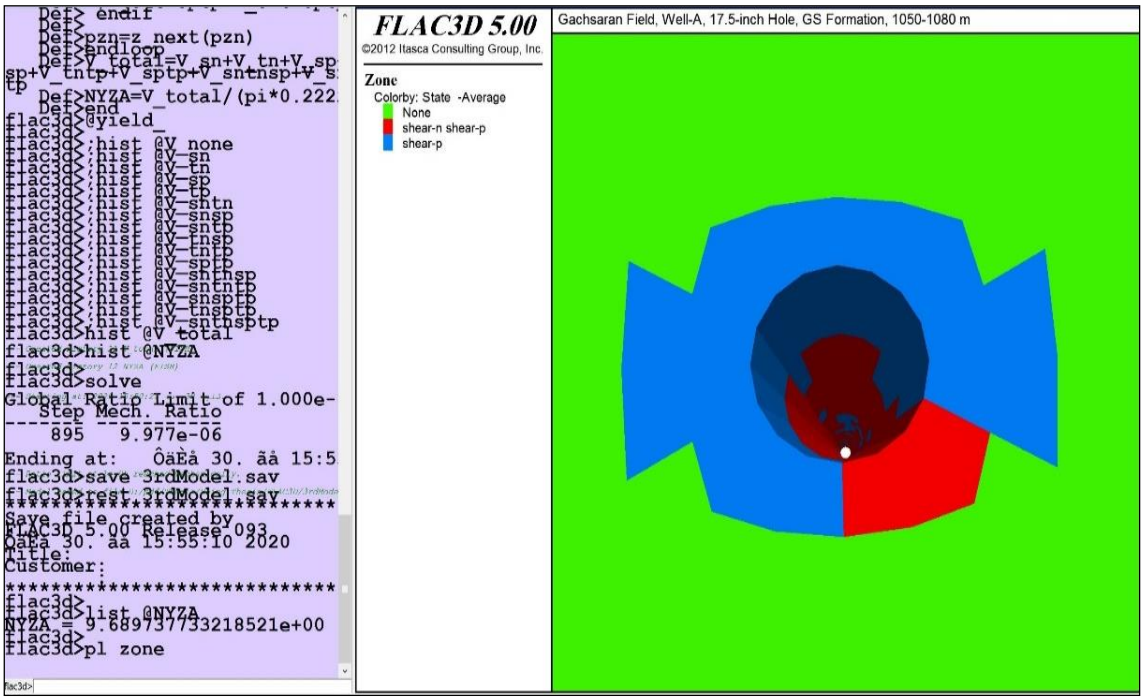

Fig. 21. Computation of NYZA using FLAC3D code at the depth interval of 1050-1080 m MD

7.2. Numerical Simulation of 12.25-inch Hole

In this hole, numerical simulations were performed for four intervals between (1) 1735 and 1750m, (2) 1750 and 1765 m, (3) 1765 and 1780 m, (4) 1780 and 1795 m, which are related to the AS formation. Fig.23 illustrates the results of NYZA, taking into account the various MWs. As seen clearly from this Figure, the real MW (9.492 ppg) is not acceptable due to providing the NYZA more than 1.0, which means the wellbore has been yielded. Besides, the optimum range of MW consists of 10.2-10.84 ppg, 10.8-11.62 ppg, 10.5-11.01 ppg, and 10.2-10.72 ppg for the interval of 1735-1750 m, 1750-1765 m, 1765-1780 m, and 1780-1795 m respectively. The optimum range of MW offered for the interval 1735-1795 m could be acceptable for another region in which real breakouts were observed, i.e., 2055 to 2100 m, since it was specified that Pd requires lower MW than AS based on the predicted breakout pressures.

7.3. Numerical Simulation of 8.375-inch Hole

In this section and from 3300 to 3400 m, four simulations were conducted to determine the optimum range of MW.

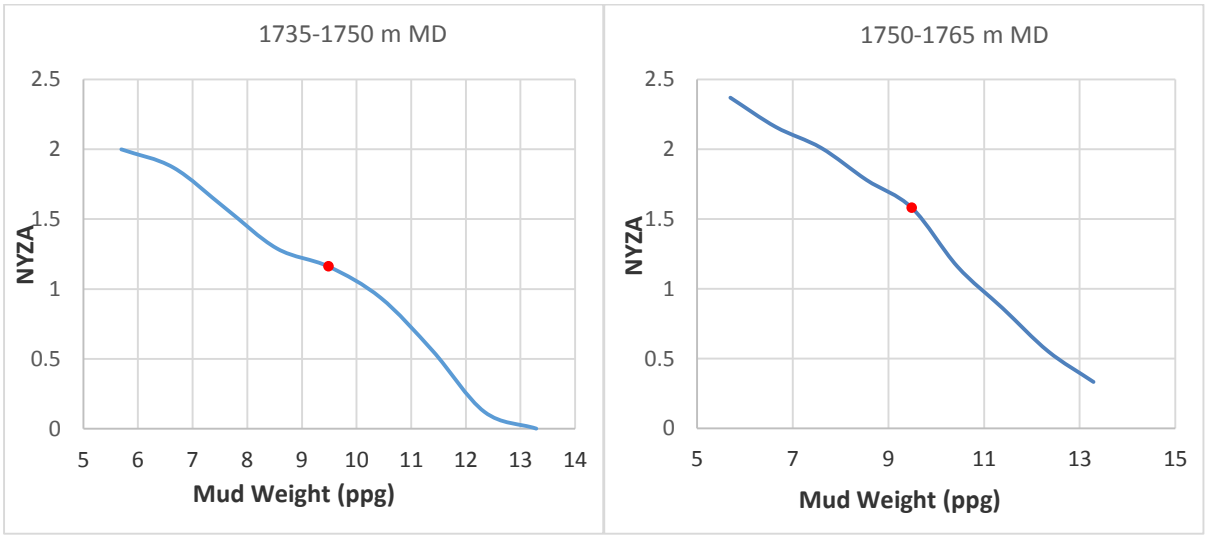

(a) (b)

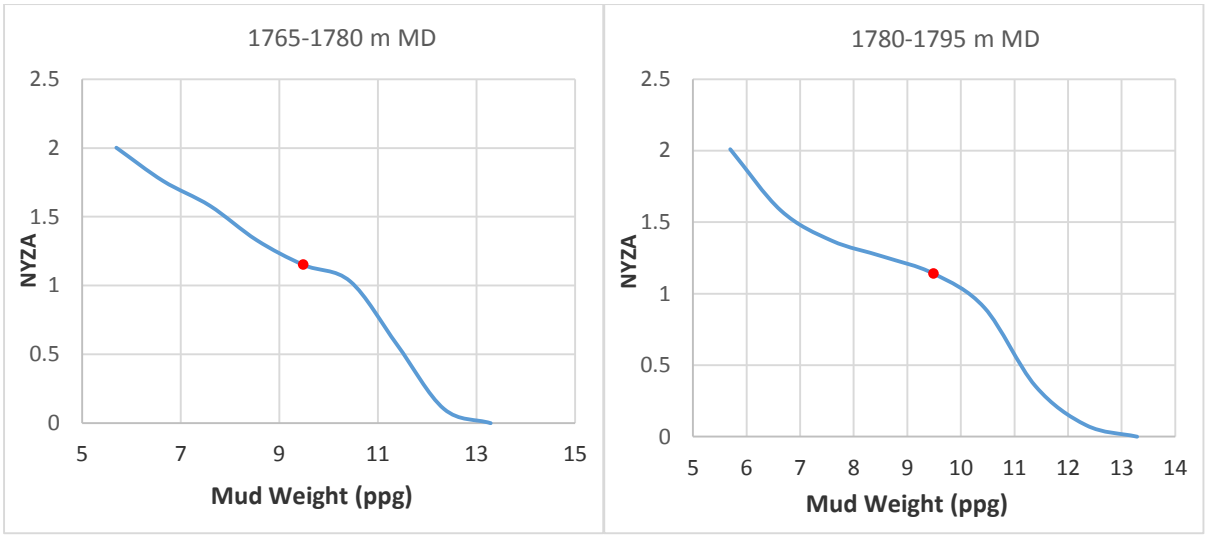

(c) (d)

Fig. 22. NYZA versus mud weight in the 12.25-inch hole of well-A for the depth of (a) 1735-1750, (b) 1750-1765, (c) 1765-1780, (d) 17850-1795 m MD

Fig. 24 shows the results of numerical simulation. As it is evident in this Figure, the real MWs make the NYZA more than 1.0. In consequence, the actual MWs have not been appropriate for drilling this interval, and the MW should be taken into account in ranges from 10.1 to 10.46 ppg, 10.7 to 11.02 ppg, 9.9 to 10.78 ppg, and 10.2 to 10.88 ppg as an optimum range respectively for drilling the interval of 3300-3325 m, 3325-3350 m, 3350-3375 m, and 3375-3400 m.

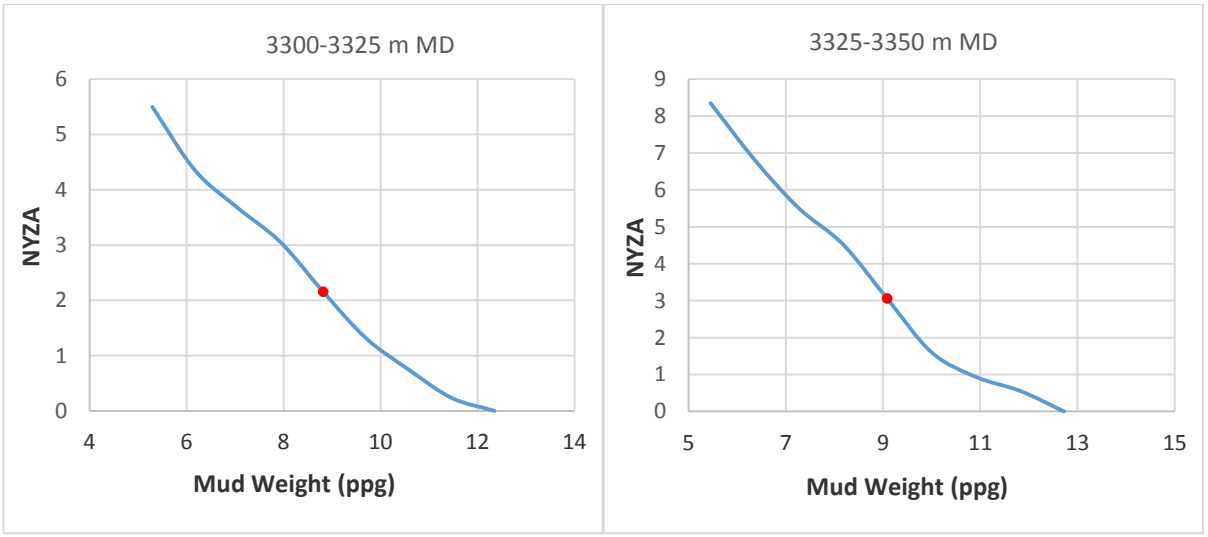

(a) (b)

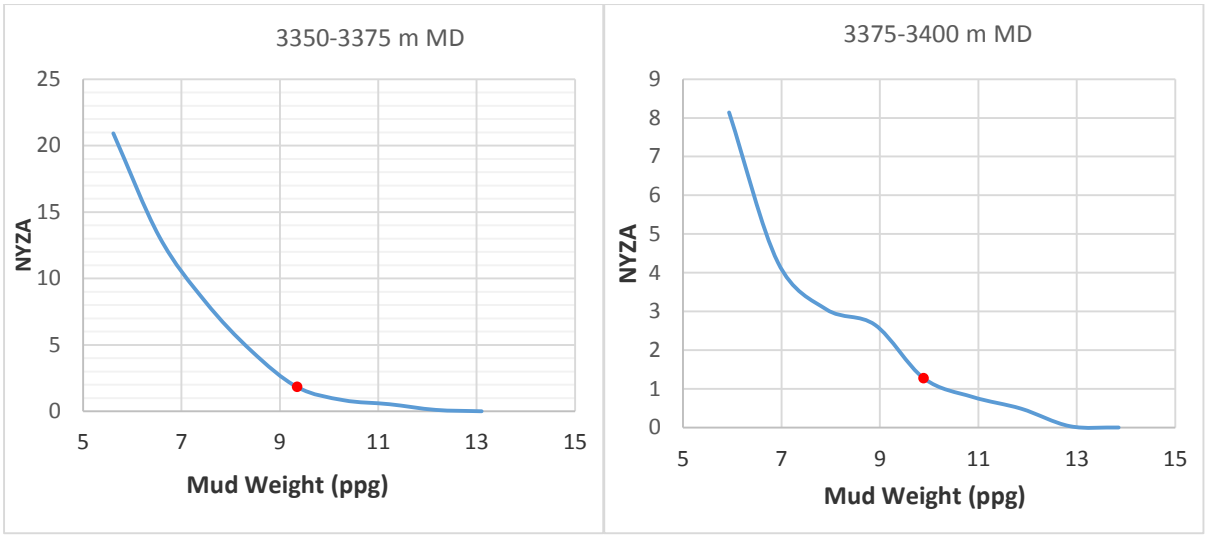

(c) (d)

Fig. 23. NYZA versus mud weight in the 8.375-inch hole of Well-A for the depth of (a) 3300-3325, (b) 3325-3350, (c) 3350-3375, (d) 3375-3400 m MD

7.4. Numerical Simulation of 6.125-inch Hole

For the final section, five numerical simulations were implemented, and the computed normalized yielded zone areas versus different MWs have been displayed in Fig. 254. Like the 17.5, 12.25, and 8.375-inch holes, in the real breakouts regions, the real MWs lead to the NYZA more than 1.0. Additionally, the optimum range of MW would be considered 10.6-10.87 ppg, 11-11.39 ppg, 11.3-11.84 ppg, 11.8-12.11 ppg, and 10.9-11.23 ppg for the intervals of 3540-3570 m, 3570-3600 m, 3640-3670 m, 3670-3700 m, and 3700-3730 m respectively to prevent breakouts or shear failures.

Generally, the numerical results obtained from FLAC3D, which have a proper match with the real observations, indicate that the actual MWs used to drill Well-A at the mentioned intervals are not appropriate due to leading to the yielded wellbores. As a result, we can conclude that the numerical solution results are desirable and reliable, and they confirm the results of the analytical solution sufficiently.

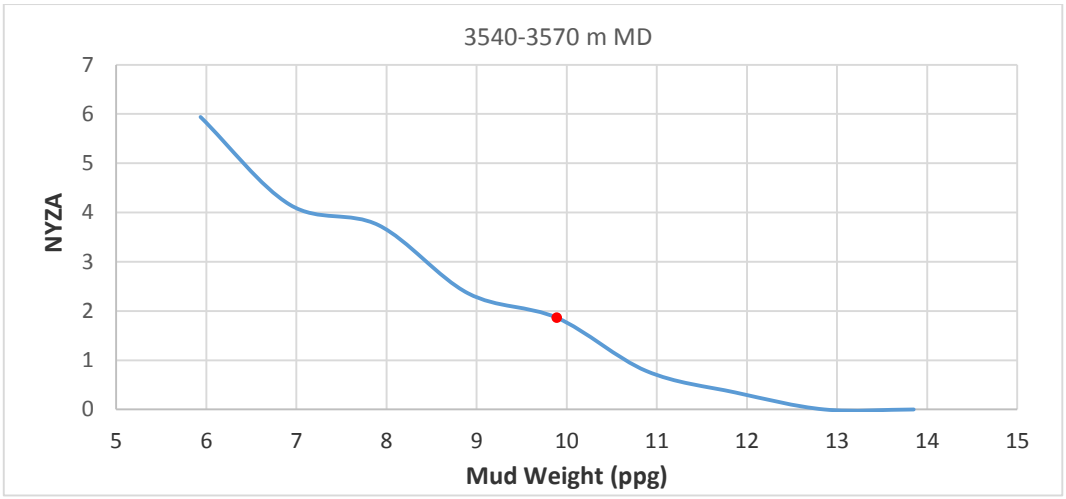

(a)

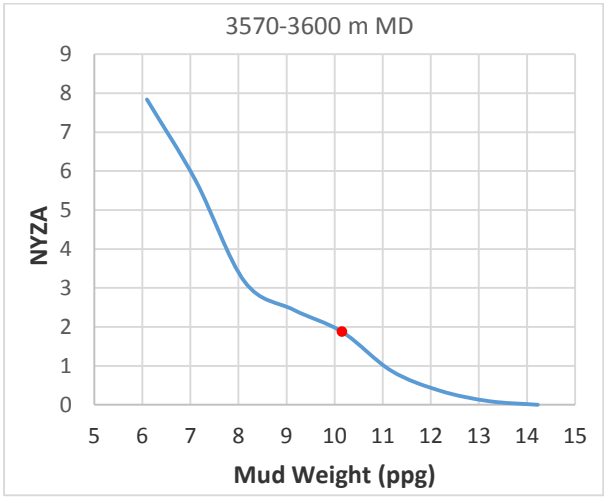

(b)

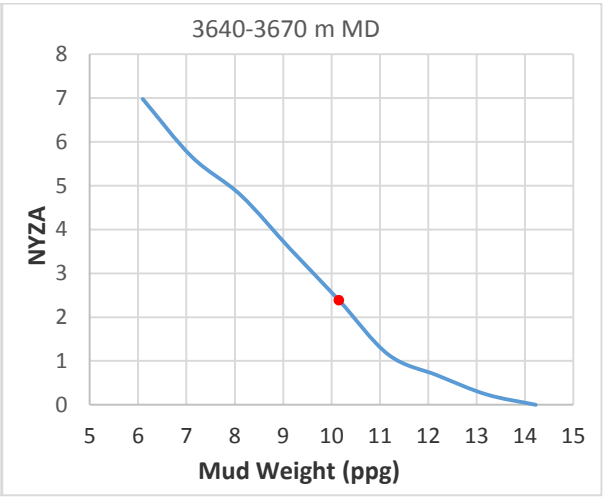

(c)

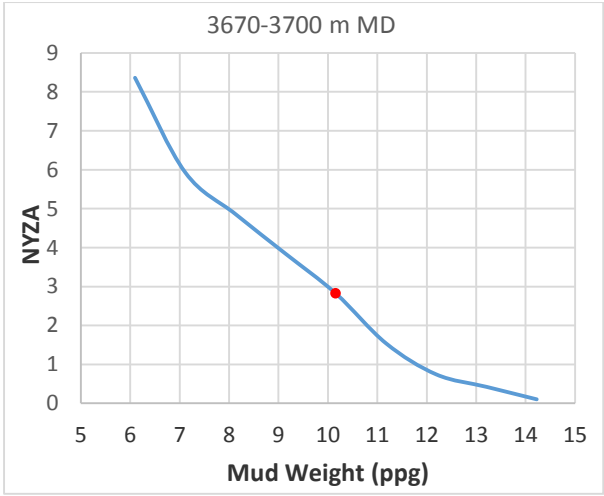

(d)

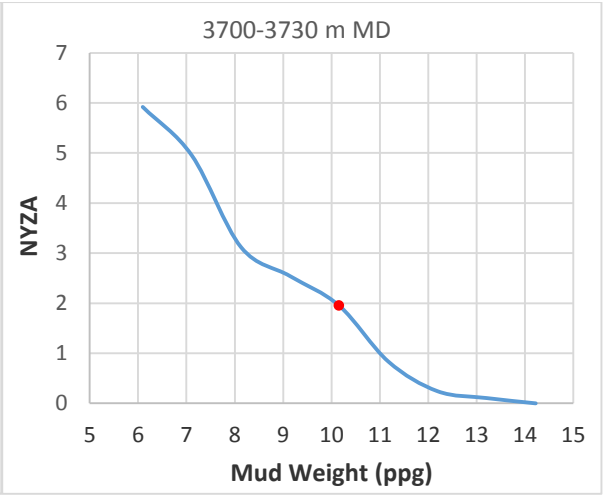

(e)

Fig. 24. NYZA versus mud weight in the 6.125-inch hole of Well-A for the depth of (a) 3540-3570, (b) 3570-3600, (c) 3640-3670, (d) 3670-3700, (e) 3700-3730 m MD

8. Comparison and Discussion

To arrange and verify the results of the numerical simulation and the analytical solution, Table 1 presents the related results for each hole comprehensively. In this table, the results deal with problematic depths confronted with real shear failures or breakouts. From this table, it can be clearly figured out that the stable windows of mud weight procured from analytical solution (i.e., MG failure criterion) have a good agreement with the optimum range of mud weight obtained from FLAC3D. Besides, the real mud weights used for drilling Well-A does not belong to the safe or optimum ranges of mud weight expressed in the table at all depths corresponding to actual shear failures. Moreover, from the comparison between the analytical and numerical results, Table 2 presents an optimum MW with an optimum trajectory. It is recommended for drilling the formations of Well-A or a similar well in the future. The optimum MW offered in this Table has been considered between the minimum required MW and mud loss in the MW window determined by the Mogi-Coulomb failure criterion.

Based on Table 2, for the 17.5-inch hole (GS formation), the optimum MWs are recommended to respectively be 20.5 and 18.5 ppg for the depth interval of 990-1085 and 1085-1495 m MD. These optimum MWs have been regarded carefully to be related to the safe area of the mud window, which is extremely narrow in GS. Nonetheless, the suggested MWs are significantly high for drilling this hole. Such high MWs are rarely utilized in operational applications of drilling since they can cause many drilling difficulties. On the other hand, being MW far from the optimum condition can increase the possibility of breakout occurrence. Consequently, increasing the MW as close to the optimum values as possible with some practical actions (e.g., hole cleaning) would be used operationally in drilling the 17.5-inch hole to reduce the possibility of both breakout and drilling hazards.

Table 1

Results of numerical simulation and analytical solution at the relevant depths to real breakouts

Hole Size	Interval Depth of Real Breakouts (m)	Stable Mud Weight Window (ppg)	Optimum Range of Mud Weight (ppg)	Real Mud Weight (ppg)
17.5-inch	990-1020	**16 to 21**	**16.6 to 17.33**	13.37
	1020-1050	**18 to 22**	**21.5 to 21.75**	16.04
	1050-1080	**19 to 22**	**20.5 to 22.46**	
	1080-1110	**18 to 21**	**19.8 to 20.64**	
	1110-1140	**15 to 19**	**17.6 to 18.8**	
	1140-1180	**18 to 21**	**20.1 to 20.85**	
12.25-inch	1735-1750	**10 to 16**	**10.2 to 10.84**	9.492
	1750-1765	**10.5 to 13**	**10.8 to 11.62**	
	1765-1780	**10.5 to 13.5**	**10.5 to 11.01**	
	1780-1795	**10 to 15**	**10.2 to 10.72**	
8.375-inch	3300-3325	**10 to 13**	**10.1 to 10.46**	8.82
	3325-3350	**10.5 to 13**	**10.7 to 11.02**	9.09
	3350-3375	**10 to 13**	**9.9 to 10.78**	9.36
	3375-3400	**9.5 to 11**	**10.2 to 10.88**	9.89
6.125-inch	3540-3570	**10.5 to 13**	**10.6 to 10.87**	9.89
	3570-3600	**10 to 12.5**	**11 to 11.39**	10.16
	3640-3670	**10.5 to 13.5**	**11.3 to 11.84**	
	3670-3700	**10 to 14**	**11.8 to 12.11**	
	3700-3730	**10.5 to 15**	**10.9 to 11.23**	

Table 2

Optimum mud weight with an optimum well trajectory suggested for Well-A

Hole Size	Formation	Measured Depth Interval (m)	Optimum Mud Weight (ppg)	Optimum Azimuth (degree)	Optimum Deviation (degree)
17.5-inch	GS	990-1085	high as possible	15	Low Deviation
		1085-1495	high as possible		
12.25-inch	AS	entirely	11.2	50	Directional drilling
	Pd	entirely	11.2	105	25-30
8.375-inch	Gu and IL	entirely	10	70	Directional drilling
	SV	entirely	10	105	30
	KZ	3252-3400	11	105	0-20
		3400-3505	10		
6.125-inch	DR	entirely	11.35	105	0-20
	GA	entirely	12.11	105	0-20
	FA	entirely	10.6	105	0-20

In the end, this study's outputs generally reveal that the results of the numerical and analytical solutions have an appropriate agreement with real observations gained from caliper and image logs in all four holes of Well-A. Hence, this revelation renders us a robust foundation to conclude that the elastoplastic model used for stability analysis in Well-A would be taken as a successful approach due to authenticating the analytical solution results and determining the optimum mud weight. In addition, the 3D numerical simulation using a finite difference code, FLAC3D, was prosperous in Well-A.

9. Conclusions

This study aimed to perform wellbore stability analysis for a well (Well-A) in one Iranian southwest field, considering two elastic and elastoplastic models. Usually, one of the analytical (elastic) or numerical (elastoplastic) solution has been used in most of the previous literature. Besides, the prior works have been conducted for the particular section of a well, not the whole due to lack of the required information or other problems. In this paper, firstly, a comprehensive MEM was built for Well-A in all depth. Also, for making this earth model reliable, the constructed MEM was calibrated versus direct data of field tests, including RFT and LOT. Secondly, an analytical solution based on the elastic model was employed to predict the MW window using four rock failure criteria, including MC, HB, MG, and ML. Also, the caliper and image logs, as the real observations, were used to investigate the predicted MW windows. After that, the sensitivity analysis was conducted to find the optimum trajectory of Well-A. Ultimately, the numerical simulations using FLAC3D code were performed to appraise the analytical solution results and to determine the optimum MWs. It was deduced that the Mogi-Coulomb provides the most realistic MW window due to having the most proper agreement with the real breakouts observed from caliper and image logs. Furthermore, the results achieved from the numerical simulations demonstrated appropriate accordance with the real observations. Therefore, these results were admitted to be reliable. Besides, the numerical results could successfully affirm the mud weight window determined from the analytical solution. Consequently, an elastoplastic model would be qualified to determine the optimum MW and to analyze wellbore stability for Well-A or a similar well in this Iranian field.

Appendix A. Rock Failure Criteria for the MW Window Determination

A. 1. Mohr-Coulomb (MC) failure criterion

The MC criterion is the most common failure criterion used widely in geomechanics and wellbore stability studies. The MC criterion presents a linear relationship form, which is a function of shear stress (τ) and normal stress (σ_n) as followed (Mohr, 1900):

$$\tau = C + \sigma_n \tan\varphi \tag{A-1}$$

The MC failure criterion can be expressed in terms of principal stresses, which is written as (Fjaer et al., 1992):

$$\sigma_1 = UCS + q\sigma_3 \text{ where, } q = \frac{(1+\sin\varphi)}{(1-sin\varphi)} \tag{A-2}$$

σ_1 and σ_3 respectively are maximum and minimum principal stresses, and q is the flow factor. Also, the MC criterion is a 2D linear failure criterion, which does not regard the effect of intermediate principal stresses. For the breakout and considering $\sigma_\theta = \sigma_1$ and $\sigma_r = \sigma_3 = P_w$, the MC criterion in terms of principal stresses is written as:

$$(\sigma_\theta - P_p) = UCS + q(P_w - P_p) \tag{A-3}$$

By substituting the values of Eqs. (18) and (19) in the above equation, the minimum required mud pressure to prevent breakouts, $P_{w(BO)}$, will be:

$$P_{w(BO)} = \frac{3S_{Hmax} - S_{hmin} - UCS + P_p(q-1)}{(1+q)} \tag{A-4}$$

On the other hand, the maximum allowable mud pressure to avoid fractures (breakdowns), $P_{w(Break)}$, will be obtained by introducing Eqs. (21) and (22) and substituting them in the Eq. (A-2) under $\sigma_\theta = \sigma_3$, $\sigma_z = \sigma_2$, and $\sigma_r = \sigma_1 = P_w$, which is followed below:

$$P_{w(Break)} = \frac{UCS + P_p(1-q) + q(3S_{hmin} - S_{Hmax})}{(1+q)} \tag{A-5}$$

A. 2. Hoek-Brown (HB) failure criterion

(Hoek & Brown, 1980, 1997) established a rock failure criterion according to the empirical model. In the HB criterion, both fracture and rock mass properties were considered, and then the relationship between the maximum and minimum horizontal stresses at the failure plane was defined as:

$$\sigma_1 = \sigma_3 + UCS(s + m\frac{\sigma_3}{UCS})^{0.5} \quad \text{(A-6)}$$

The HB criterion is a 2D nonlinear failure criterion. Besides, it takes into account UCS and introduces two dimensionless constant parameters, s, and *m*. These parameters depend on both rock and fracture characteristics. For the intact rock, the parameter *s* is equal to 1, while the parameter *m* has diverse values corresponding to different rock types (Zoback, 2007).

The same calculation manners described in the MC section can be pursued to predict the MW window of Well-A by assuming the HB failure criterion and Eq. (A-6). The results are expressed as:

$$P_{w(BO)} = \frac{(4A+mUCS)-\sqrt{(4A+mUCS)^2-16(A^2+mUCSP_p-sUCS^2)}}{8} \quad \text{(A-7)}$$

$$P_{w(Break)} = \frac{(4D-mUCS)+\sqrt{(4D-mUCS)^2-16(D^2-mUCSD+mUSCP_p-sUCS^2)}}{8} \quad \text{(A-8)}$$

A. 3. Mogi-Coulomb (MG) failure criterion

Mogi (1971) implemented triaxial experimental tests on various rock types and concluded that the intermediate principal stress affects rock strength. He discovered that the failure plane happens along the intermediate stress direction. As a result, he developed a new failure criterion which considers the effect of intermediate principal stress, defined as below:

$$\tau_{oct} = f(\sigma_{m.2}) \quad \text{(A-9)}$$

Where τ_{oct} is octahedral shear stress and $\sigma_{m,2}$ is the effective mean normal stress resisting the fracture plane creation. τ_{oc} and $\sigma_{m,2}$ are formulated by (Mogi, 1971):

$$\tau_{oct} = \frac{1}{3}\sqrt{(\sigma_1 - \sigma_2)^2 + (\sigma_3 - \sigma_1)^2 + (\sigma_2 - \sigma_3)^2} \quad \text{(A-10)}$$

$$\sigma_{mean} = \frac{\sigma_3 + \sigma_1}{2} \quad \text{(A-11)}$$

Parameter *f* is a nonlinear function. Al-Ajmi and Zimmerman (2005) found a linear relation form for τ_{oct} and $\sigma_{m,2}$ with two material constants (a and b). The related equations are followed below:

$$\tau_{oct} = a + b\sigma_{m.2} \quad \text{(A-12)}$$

$$a = \frac{2\sqrt{2}}{3} C \cos\varphi \quad \text{(A-13)}$$

$$b = \frac{2\sqrt{2}}{3} sin\varphi \quad \text{(A-14)}$$

In terms of the first and second invariants, I_1 and I_2, using the MG criterion are expressed by:

$$\sqrt{(I_1^2 - 3I_2^2)} = a' + b'(I_1 - \sigma_2) \quad \text{(A-15)}$$

$$I_1 = \sigma_1 + \sigma_2 + \sigma_3 \quad \text{(A-16)}$$

$$I_2 = \sigma_1\sigma_2 + \sigma_1\sigma_3 + \sigma_2\sigma_3 \quad \text{(A-17)}$$

Where $a' = 2C\ cos\ \varphi$ and $b' = sin\varphi$.

The stress invariants in the MG failure criterion at the maximum and minimum tangential stress will be:

$$\Theta = \pm\frac{\pi}{2} : I_1 = \sigma_\theta + \sigma_z + \sigma_r = A + B \text{ and } I_2 = AB + AP_w - {P_w}^2 \quad \text{(A-18)}$$

$$\Theta = 0, \pi: I_1 = D + E \text{ and } I_2 = DE + DP_w - {P_w}^2 \quad \text{(A-19)}$$

The MG criterion in terms of stress invariants is regarded to determine lower and upper bounds of mud window (i.e., $P_{w(BO)}$ and $P_{w(Break)}$) similar to the procedures used in the two previous subsections. The breakout and breakdown pressures by following the MG criterion will be:

$$P_{w(BO)} = \frac{A}{2} - \frac{1}{6}\sqrt{12[a' + b'(A - 2P_p)]^2 - 3(A - 2B)^2} \quad \text{(A-20)}$$

$$P_{w(Break)} = \frac{D}{2} + \frac{1}{6}\sqrt{12[a' + b'(D - 2P_p)]^2 - 3(D - 2E)^2} \quad \text{(A-21)}$$

A. 4. Modified Lade (ML) failure criterion

Lade (1977) inferred that the internal friction angle reduces by raising the mean normal stress value for cohesionless soil. The Modified Lade criterion was established by Ewy (1999). In the ML, the constant material m is zero, and the ML has offered a new procedure with effective stresses and introduction of the parameter S being function of cohesion. The ML criterion is defined as the following form (Ewy, 1998).

$$\frac{I_1''^3}{I_3''} = 27 + \eta \quad \text{(A-22)}$$

Where the I_3'' and I_1'' are expressed as:

$$I_1'' = (\sigma_1 + S) + (\sigma_2 + S) + (\sigma_3 + S) \quad \text{(A-23)}$$

$$I_3'' = (\sigma_1 + S)(\sigma_2 + S)(\sigma_3 + S) \quad \text{(A-24)}$$

Also, the parameters S and η in the above equations can be formulated by:

$$S = \frac{C}{\tan(\varphi)} \quad \text{(A-25)}$$

$$\eta = 4(tan\,\varphi)^2 \frac{(9 - 7\sin\varphi)}{(1 - \sin\varphi)} \quad \text{(A-26)}$$

The lower and upper limits of the mud window under the ML criterion are given by:

$$P_{w(BO)} = \frac{P-\sqrt{Q}}{2R} \ldots\ldots\ldots\ldots\ldots \quad \text{(A-27)}$$

Where $R = B + S - P_p$, $P = RA$,

$$Q = P^2 - 4R\left[U - R(S - P_p)(A + S - P_p)\right], \text{ and } U = \frac{(A+B+3S-3P_p)^3}{27+\eta}.$$

$$P_{w(Break)} = \frac{P+\sqrt{Q}}{2R} \ldots\ldots\ldots\ldots\ldots \quad \text{(A-28)}$$

Where $R = E + S - P_p$, $P = RD$,

$$Q = P^2 - 4R\left[U - R(S - P_p)(D + S - P_p)\right], \text{ and } U = \frac{(D+E+3S-3P_p)^3}{27+\eta}.$$

The above equations have been used to predict the MW window for the Vertical intervals of Well-A. In the Inclined intervals, as explained before, it is not allowed to consider the conditions of $\sigma_\theta > \sigma_z > \sigma_r$ and $\sigma_r > \sigma_z > \sigma_\theta$. Accordingly, for any azimuth and inclination angles, Eqs. (35) and (36) must be substituted as the maximum and minimum principal stresses in the relationships of all four failure criteria to estimate the MW windows in Well-A.

In the end, because some rock failure criteria overestimate the breakdown pressure, tensile cut-off should be considered for estimating the maximum allowable MW (Maleki et al., 2014). This cut-off is known as the tensile failure criterion, which is expressed as (Zhang et al., 2010):

$$\sigma_3 = \sigma_\theta{}^{min} = D - P_w = TS \quad \text{(A-29)}$$

The estimated mud pressures from the above equation should be compared to the values of breakdown pressure calculated under four rock failure criteria. The less value has to be considered as the upper bound of the MW window.

Acknowledgments

The authors would like to express their thanks to Mr. M. Heidari for his help and NISOC for their permission to publish the results of this work.

Nomenclatures

DDR	Daily Drilling Report
DTC	Compressional Slowness Sonic (μs/ft)
DTC_n	Normal Trend of Compressional Slowness Sonic (μs/ft)
RHOB, ρ_b	Bulk Density (gr/cm^3)
GR	Gamma Ray (API)
NPHI	Neutron Porosity (decimal)
V_{shale}	Shale Volume Fraction (%)
E_{Static}	Static Young's Modulus (GPa)
E_d	Dynamic Young's Modulus
φ	Friction Angle (dega)
K	Bulk Modulus (GPa)
UCS	Uniaxial Compressive Strength (MPa)
TS	Tensile Strength (MPa)
C	Cohesion (MPa)
ϑ	Poisson's Ratio (unitless)
G	Shear Modulus (GPa)
P_p	Pore Pressure (MPa)
P_{pn}	Normal Pore Pressure (MPa)
P_w	Mud (Wellbore) Pressure (MPa)
S_V	Vertical Stress (MPa)
S_{Hmax}	Maximum Horizontal Stress (MPa)
S_{hmin}	Minimum Horizontal Stress (MPa)
S_1,S_2, S_3	Maximum, Intermediate, Minimum Principal Stresses

σ_r	Radial stress
σ_z	Axial Stress
σ_θ	Tangential Stress
τ	Shear Stress
τ_{oct}	Octahedral Shear Stress
$\tau_{\theta z}$, $\tau_{\theta r}$, τ_{rz}	Shear Stress Components of Induced Stresses
σ_x, σ_y, σ_{zz}, τ_{xy}, τ_{xz}, τ_{yz}	Transformed Stress Components
g	Gravity Acceleration (m/s^2)
δ	Biot's Coefficient
i	Borehole Deviation
α	Borehole Azimuth
θ	Azimuth of any point around the wellbore with respect to the Maximum horizontal stress direction
ε_Y, ε_x	Horizontal Tectonic Strains
R	Borehole Radius (in)
dega,$^\circ$	Degree
ppg (lbm/gal)	Pounds per Gallon
a, a'	Material Constants in Mogi-Coulomb Failure Criterion
b, b'	Material Constants in Mogi-Coulomb Failure Criterion
m, s	Hoek-Brown Material Constants
Mss	Evaluation from Sub Sea Level
in	Inch

References

Aadnoy BS, Chenevert ME. Stability of Highly Inclined Boreholes (includes associated papers 18596 and 18736). SPE Drilling Engineering 1987;2:364–74. https://doi.org/10.2118/16052-pa.

Aadnoy BS, Looyeh R. Petroleum rock mechanics. [recurso electrónico] : drilling operations and well design. Gulf Professional Publishing; 2011.

Al-Ajmi A. Wellbore stability analysis based on a new true-triaxial failure criterion. University of KTH Royal Institute of Technology, 2006.

Al-Ajmi AM, Zimmerman RW. Relation between the Mogi and the Coulomb failure criteria. International Journal of Rock Mechanics and Mining Sciences 2005;42:431–9. https://doi.org/10.1016/j.ijrmms.2004.11.004.

Chang C, Zoback MD, Khaksar A. Empirical relations between rock strength and physical properties in sedimentary rocks. Journal of Petroleum Science and Engineering 2006;51:223–37. https://doi.org/10.1016/j.petrol.2006.01.003.

Chen SL, Abousleiman YN. Wellbore stability analysis using strain hardening and/or softening plasticity models. International Journal of Rock Mechanics and Mining Sciences 2017;93:260–8. https://doi.org/10.1016/j.ijrmms.2017.02.007.

Das B, Chatterjee R. Wellbore stability analysis and prediction of minimum mud weight for few wells in Krishna-Godavari Basin, India. International Journal of Rock Mechanics and Mining Sciences 2017;93:30–7. https://doi.org/10.1016/j.ijrmms.2016.12.018.

Dusseault MB. Analysis of borehole stability. Computer Methods and Advances in Geomechanics, 1994, p. 125–37.

Eaton BA. Graphical Method Predicts Geopressures Worldwide. World Oil

1976;183:100–4.

Elyasi A, Goshtasbi K. The impact of sidetracking on the wellbore stability. Advances in Energy Research 2015;3:1–10. https://doi.org/10.12989/eri.2015.3.1.001.

Ewy RT. Wellbore-stability predictions using a modified Lade criterion. JPT, Journal of Petroleum Technology 1998;50:64–6. https://doi.org/10.2118/1198-0064-jpt.

Fjaer E, Holt RM, Horsrud P, Raaen AM, Risnes R. Petroleum related rock mechanics. Elsevier; 1992. https://doi.org/10.1016/0920-4105(93)90066-n.

Gholami R, Moradzadeh A, Rasouli V, Hanachi J. Practical application of failure criteria in determining safe mud weight windows in drilling operations. Journal of Rock Mechanics and Geotechnical Engineering 2014;6:13–25. https://doi.org/10.1016/j.jrmge.2013.11.002.

Hawkes C, Mclellan P. New model for predicting time-dependent failure of shales: Theory and application. Journal of Canadian Petroleum Technology 1999;38:49–55. https://doi.org/10.2118/99-12-02.

Hoek E, Brown ET. Practical estimates of rock mass strength. International Journal of Rock Mechanics and Mining Sciences 1997;34:1165–86. https://doi.org/10.1016/S1365-1609(97)80069-X.

Hoek E, Brown ET. Empirical strength criterion for rock masses. Journal of the Geotechnical Engineering Division, ASCE 1980;106:1013–35. https://doi.org/10.1016/0148-9062(81)90766-x.

Hossain ME, Islam R. Drilling engineering problems and solutions : a field guide for engineers and students. John Wiley & Sons; 2018. https://doi.org/10.1002/9781118998632.

Hsieh PA. Fundamentals of Rock Mechanics. vol. 9. John Wiley & Sons; 2009. https://doi.org/10.1111/j.1468-8123.2009.00251.x.

Huang C. a Numerical Investigation of Wellbore Stability Problems Using an Elastoplastic Model. University of Louisiana State, 2014.

Kasravi J, Safarzadeh MA, Hashemi A. A population-feedback control based algorithm for well trajectory optimization using proxy model. Journal of Rock Mechanics and Geotechnical Engineering 2017;9:281–90. https://doi.org/10.1016/j.jrmge.2016.07.010.

Kirsch EG. Die Theorie der Elastizität und die Bedürfnisse der Festigkeitslehre. Zeitschrift Des Vereins Deutscher Ingenieure 1898;42:797–807.

Lade P V. Elasto-plastic stress-strain theory for cohesionless soil with curved yield surfaces. International Journal of Solids and Structures 1977;13:1019–35. https://doi.org/10.1016/0020-7683(77)90073-7.

Ma T, Chen P, Yang C, Zhao J. Wellbore stability analysis and well path optimization based on the breakout width model and Mogi-Coulomb criterion. Journal of Petroleum Science and Engineering 2015;135:678–701. https://doi.org/10.1016/j.petrol.2015.10.029.

Maleki S, Gholami R, Rasouli V, Moradzadeh A, Riabi RG, Sadaghzadeh F. Comparison of different failure criteria in prediction of safe mud weigh window in drilling practice. Earth-Science Reviews 2014;136:36–58. https://doi.org/10.1016/j.earscirev.2014.05.010.

Mansourizadeh M, Jamshidian M, Bazargan P, Mohammadzadeh O. Wellbore stability analysis and breakout pressure prediction in vertical and deviated boreholes using failure criteria – A case study. Journal of Petroleum Science and Engineering 2016;145:482–92. https://doi.org/10.1016/j.petrol.2016.06.024.

Mogi K. Effect of the triaxial stress system on the failure of dolomite and limestone. Tectonophysics 1971;11:111–27. https://doi.org/10.1016/0040-1951(71)90059-X.

Mohr CO. Welche Umstände Bedingen die Elastizitätsgrenze und den Bruch eines Materiales? (What Conditions Affect the Yield Surface and Failure of Materials). Zeitschrift

Des Vereines Deutscher Ingenieure 1900;44:1524–30.

Najibi AR, Ghafoori M, Lashkaripour GR, Asef MR. Empirical relations between strength and static and dynamic elastic properties of Asmari and Sarvak limestones, two main oil reservoirs in Iran. Journal of Petroleum Science and Engineering 2015;126:78–82. https://doi.org/10.1016/j.petrol.2014.12.010.

Plumb RA. Detection of overpressure zones and a statistical model for pore pressure estimation from well logs in the Krishna-Godavari Basin, India. Society of Petroleum Engineers - Rock Mechanics in Petroleum Engineering 1994, Society of Petroleum Engineers; 1994, p. 13–20. https://doi.org/10.2118/28022-ms.

Rasouli V, Pallikathekathil ZJ, Mawuli E. The influence of perturbed stresses near faults on drilling strategy: A case study in Blacktip field, North Australia. Journal of Petroleum Science and Engineering 2011;76:37–50. https://doi.org/10.1016/j.petrol.2010.12.003.

Salehi S, Hareland G, Nygaard R. Numerical simulations of wellbore stability in under-balanced-drilling wells. Journal of Petroleum Science and Engineering 2010;72:229–35. https://doi.org/10.1016/j.petrol.2010.03.022.

Singha DK, Chatterjee R. Detection of overpressure zones and a statistical model for pore pressure estimation from well logs in the Krishna-Godavari Basin, India. Geochemistry, Geophysics, Geosystems, vol. 15, American Rock Mechanics Association; 2014, p. 1009–20. https://doi.org/10.1002/2013GC005162.

Weijermars R. Principles of rock mechanics. Alboran Science Publishing; 1997.

Xu G. Wellbore stability in geomechanics. University of Nottingham, 2007.

Zhang JJ. Borehole stability. Applied Petroleum Geomechanics 2019;38:375–440. https://doi.org/10.1016/b978-0-12-814814-3.00010-1.

Zhang L, Cao P, Radha KC. Evaluation of rock strength criteria for wellbore stability analysis. International Journal of Rock Mechanics and Mining Sciences 2010;47:1304–16. https://doi.org/10.1016/j.ijrmms.2010.09.001.

Zoback MD. Reservoir Geomechanics. London: Cambridge University Press; 2007. https://doi.org/10.1017/CBO9780511586477.

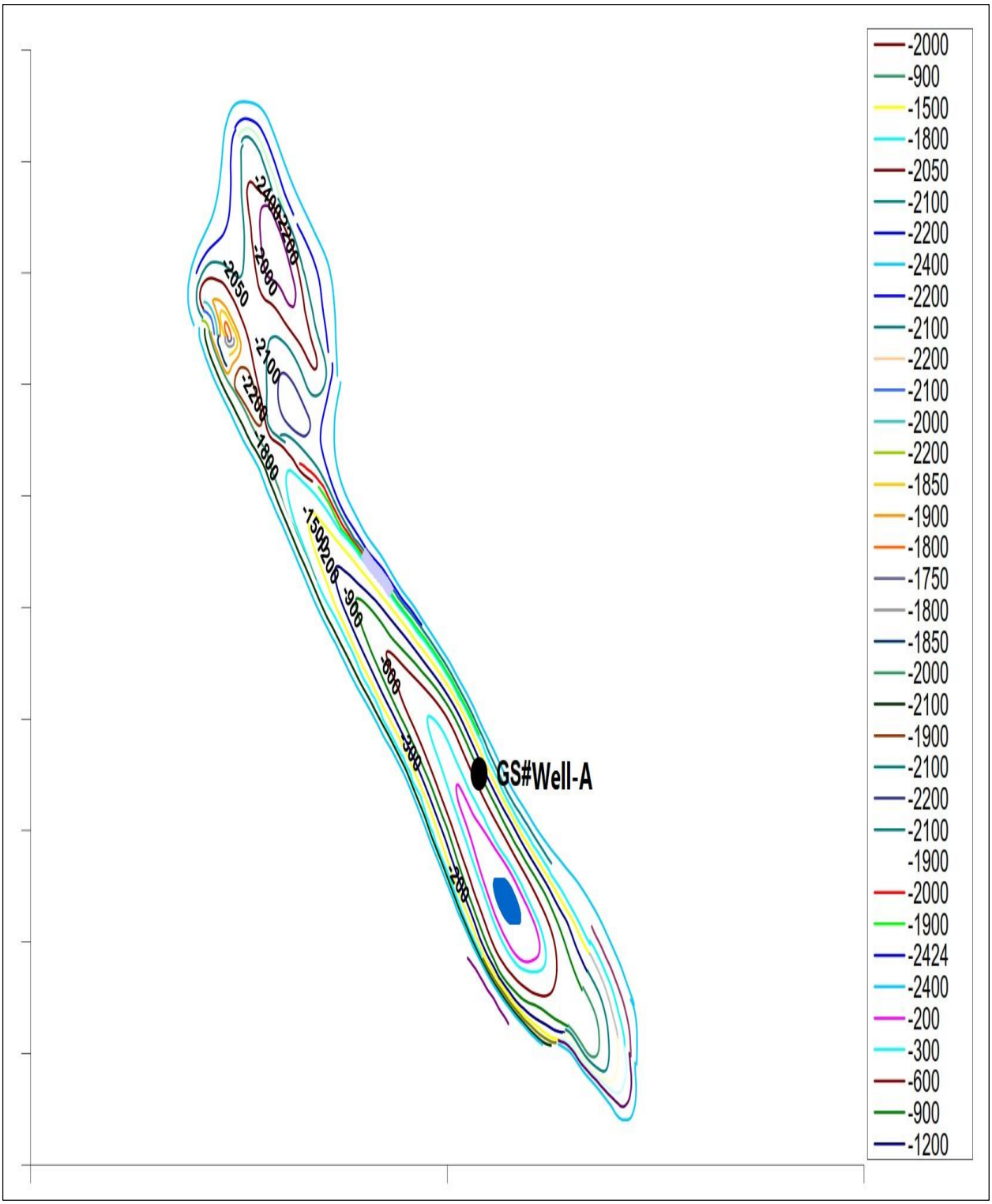

Fig. 1

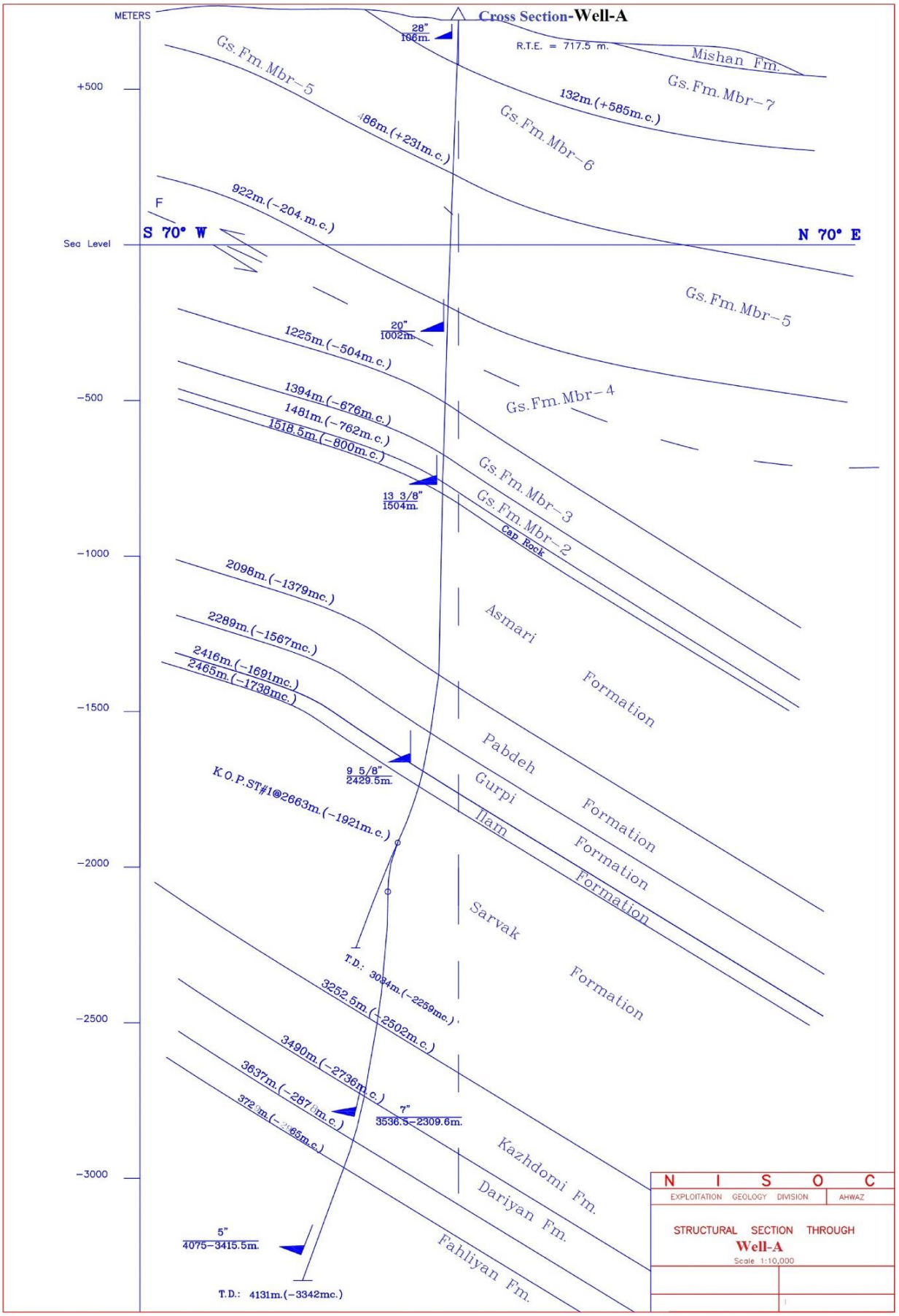
Cross Section-Well-A
METERS
28" 196m.
R.T.E. = 717.5 m.
Mishan Fm.
Gs. Fm. Mbr-5
Gs. Fm. Mbr-7
132m.(+585m.c.)
486m.(+231m.c.)
Gs. Fm. Mbr-6
922m.(-204.m.c.)
F
S 70° W
N 70° E
Sea Level
Gs. Fm. Mbr-5
20" 1002m.
1225m.(-504m.c.)
Gs. Fm. Mbr-4
1394m.(-676m.c.)
1481m.(-762m.c.)
1518.5m.(-800m.c.)
13 3/8" 1504m.
Gs. Fm. Mbr-3
Gs. Fm. Mbr-2
Cap Rock
2098m.(-1379mc.)
Asmari Formation
2289m.(-1567mc.)
2416m.(-1691mc.)
2465m.(-1738mc.)
Pabdeh Formation
9 5/8" 2429.5m.
Gurpi Formation
K.O.P.ST#1@2663m.(-1921m.c.)
Ilam Formation
Sarvak Formation
T.D.: 3084m.(-2259mc.)
3252.5m.(-2502m.c.)
3490m.(-2736m.c.)
7" 3536.5-2309.6m.
3637m.(-2870m.c.)
3723m.(-2965m.c.)
Kazhdomi Fm.
Dariyan Fm.
Fahliyan Fm.
5" 4075-3415.5m.
T.D.: 4131m.(-3342mc.)
+500
-500
-1000
-1500
-2000
-2500
-3000
N I S O C
EXPLOITATION GEOLOGY DIVISION AHWAZ
STRUCTURAL SECTION THROUGH
Well-A
Scale 1:10,000

Fig. 2

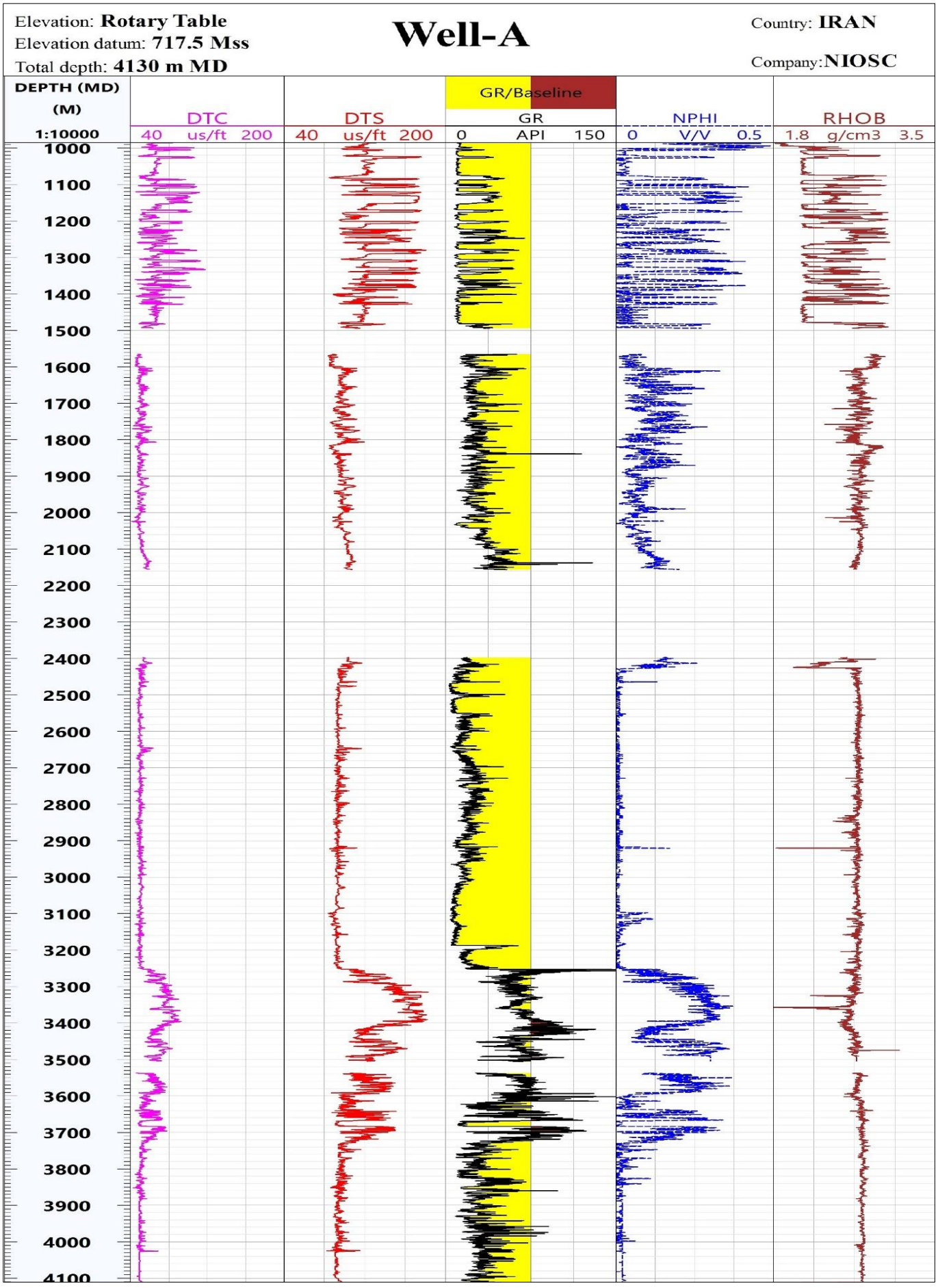
Elevation: Rotary Table
Elevation datum: 717.5 Mss
Total depth: 4130 m MD
Well-A
Country: IRAN
Company: NIOSC
DEPTH (MD)
(M)
1:10000
DTC
40 us/ft 200
DTS
40 us/ft 200
GR/Baseline
GR
0 API 150
NPHI
0 V/V 0.5
RHOB
1.8 g/cm3 3.5
1000
1100
1200
1300
1400
1500
1600
1700
1800
1900
2000
2100
2200
2300
2400
2500
2600
2700
2800
2900
3000
3100
3200
3300
3400
3500
3600
3700
3800
3900
4000
4100

Fig. 3

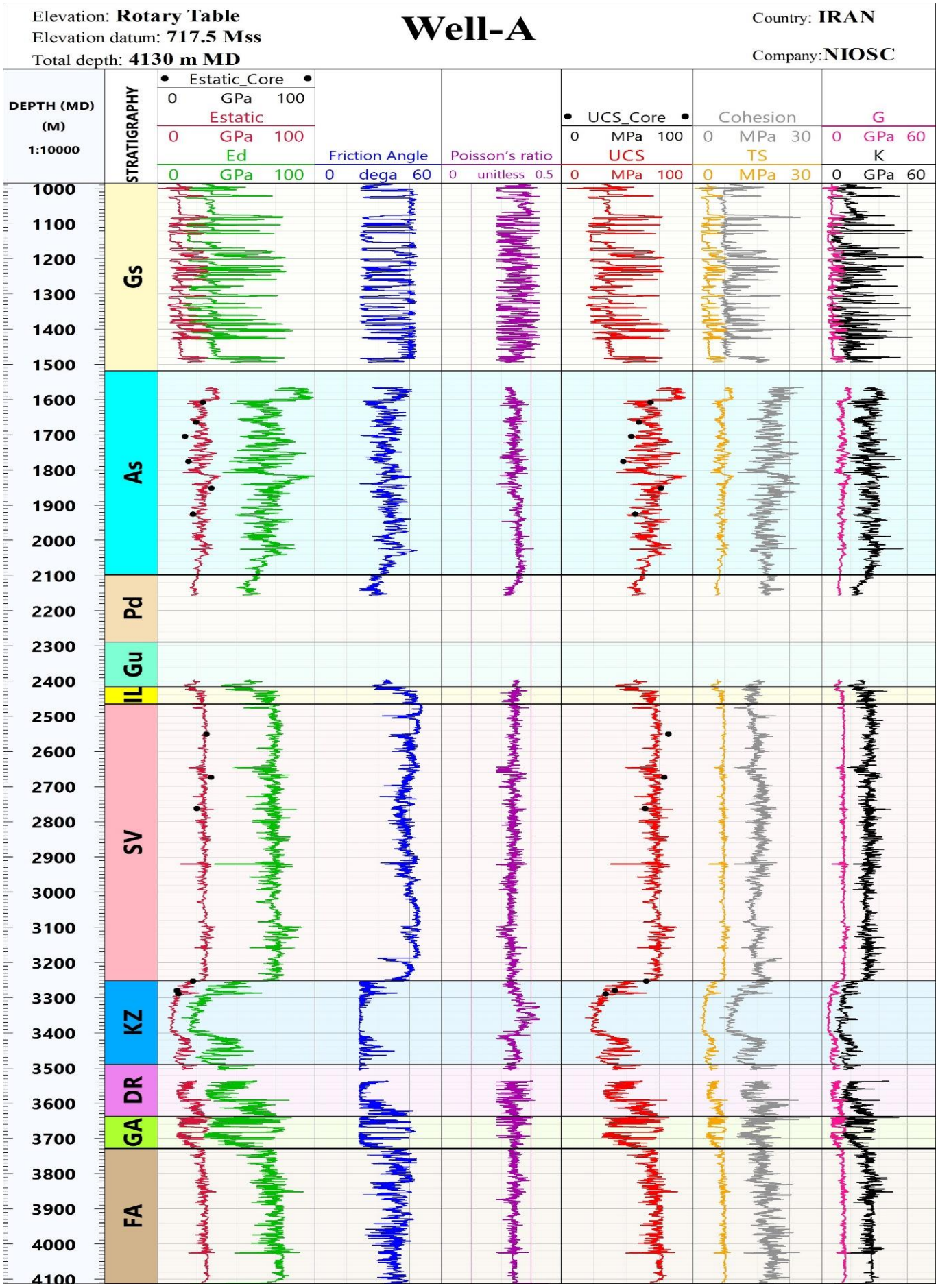
Elevation: Rotary Table
Elevation datum: 717.5 Mss
Total depth: 4130 m MD
Well-A
Country: IRAN
Company: NIOSC
DEPTH (MD) (M) 1:10000
STRATIGRAPHY
Estatic_Core
0 GPa 100
Estatic
0 GPa 100
Ed
0 GPa 100
Friction Angle
0 dega 60
Poisson's ratio
0 unitless 0.5
UCS_Core
0 MPa 100
UCS
0 MPa 100
Cohesion
0 MPa 30
TS
0 MPa 30
G
0 GPa 60
K
0 GPa 60
1000
1100
1200
1300
1400
1500
1600
1700
1800
1900
2000
2100
2200
2300
2400
2500
2600
2700
2800
2900
3000
3100
3200
3300
3400
3500
3600
3700
3800
3900
4000
4100
Gs
As
Pd
Gu
IL
SV
KZ
DR
GA
FA

Fig. 4

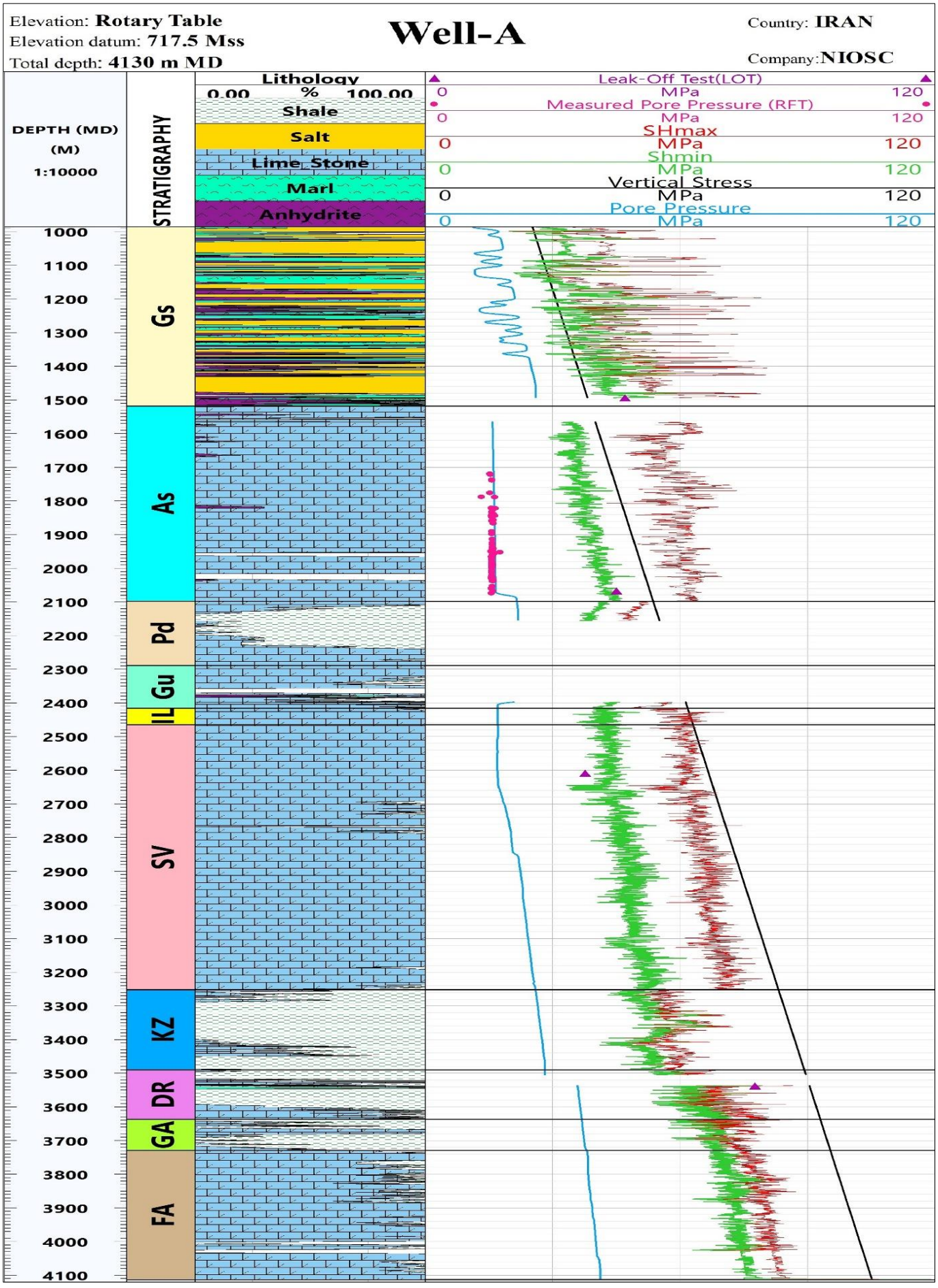
Elevation: Rotary Table
Elevation datum: 717.5 Mss
Total depth: 4130 m MD
Well-A
Country: IRAN
Company: NIOSC
DEPTH (MD)
(M)
1:10000
STRATIGRAPHY
Lithology
0.00 % 100.00
Shale
Salt
Lime Stone
Marl
Anhydrite
Leak-Off Test(LOT)
0 MPa 120
Measured Pore Pressure (RFT)
0 MPa 120
SHmax
0 MPa 120
Shmin
0 MPa 120
Vertical Stress
0 MPa 120
Pore Pressure
0 MPa 120
1000
1100
1200
1300
1400
1500
1600
1700
1800
1900
2000
2100
2200
2300
2400
2500
2600
2700
2800
2900
3000
3100
3200
3300
3400
3500
3600
3700
3800
3900
4000
4100
Gs
As
Pd
Gu
IL
SV
KZ
DR
GA
FA

Fig. 5

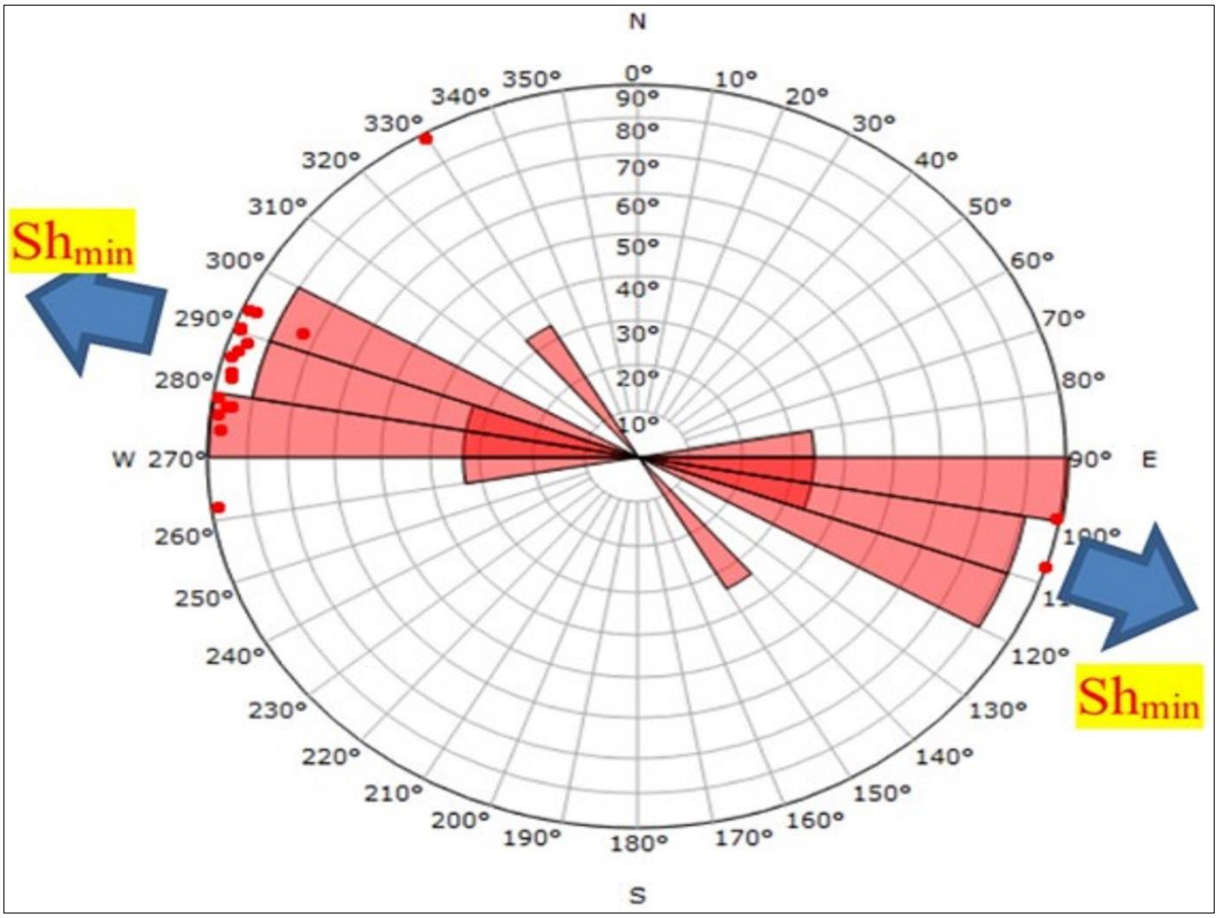
N
S
W
E
0°
10°
20°
30°
40°
50°
60°
70°
80°
90°
100°
120°
130°
140°
150°
160°
170°
180°
190°
200°
210°
220°
230°
240°
250°
260°
270°
280°
290°
300°
310°
320°
330°
340°
350°
Shmin
Shmin

Fig. 6

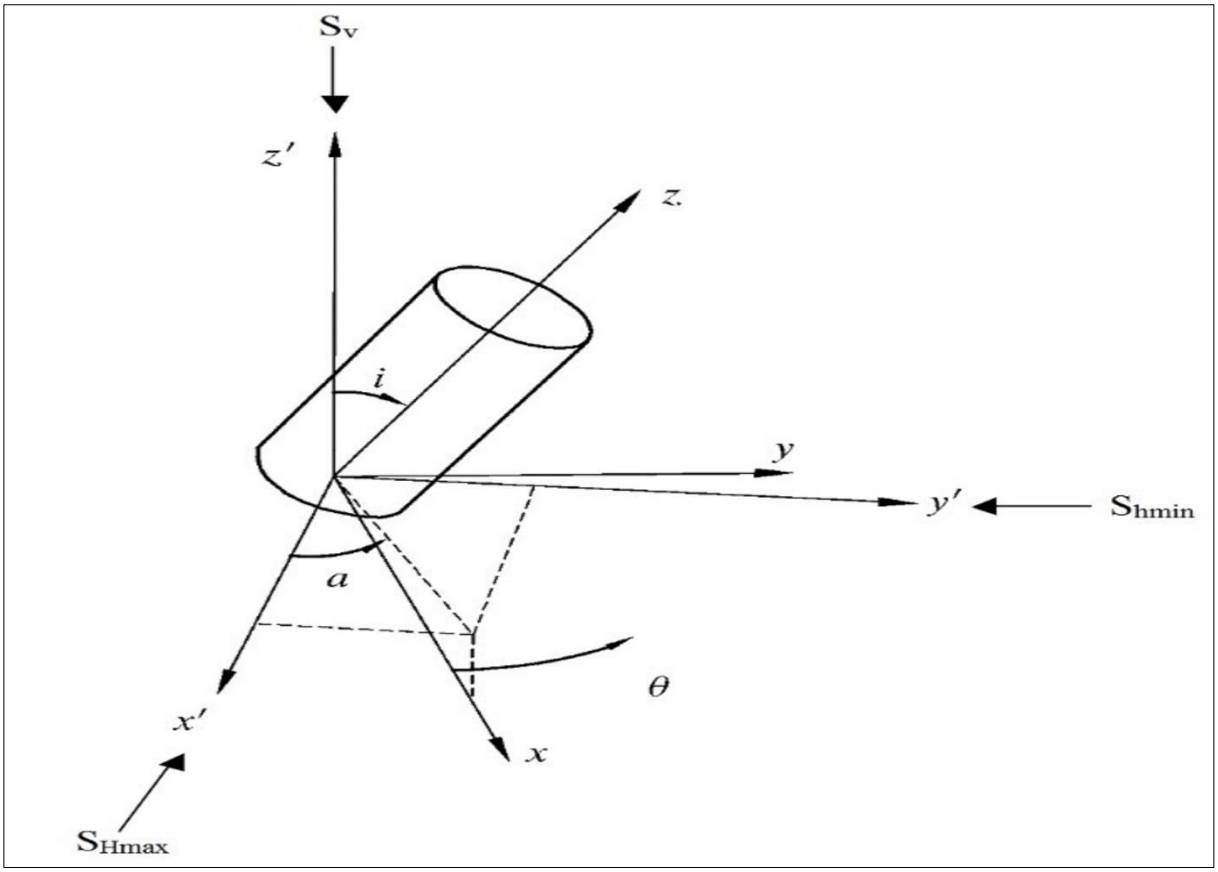
Sv
z′
z
i
y
y′
Shmin
a
θ
x′
x
SHmax

Fig. 7

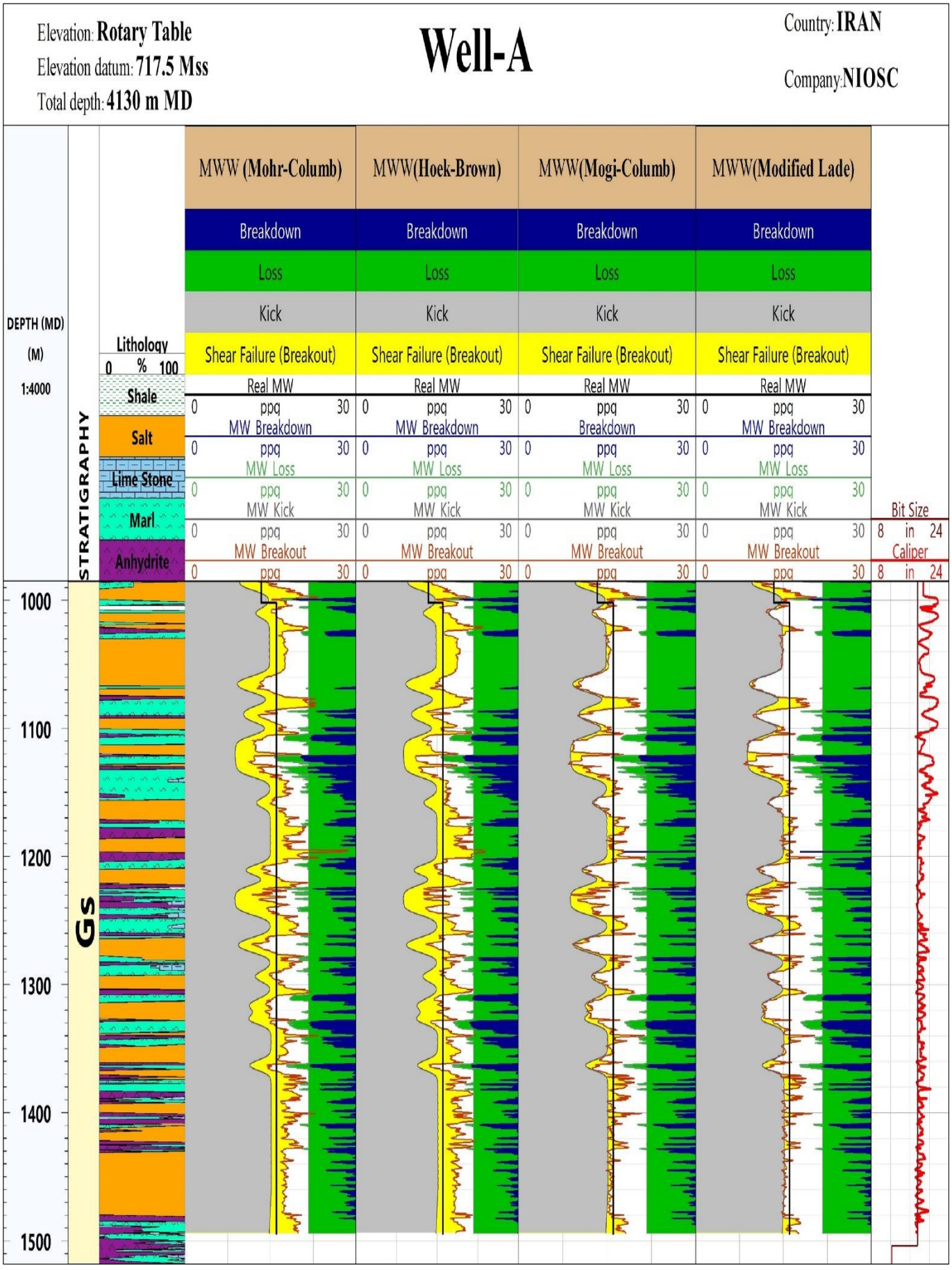
Elevation: Rotary Table
Elevation datum: 717.5 Mss
Total depth: 4130 m MD
Well-A
Country: IRAN
Company: NIOSC
MWW (Mohr-Columb)
MWW(Hoek-Brown)
MWW(Mogi-Columb)
MWW(Modified Lade)
Breakdown
Loss
Kick
Shear Failure (Breakout)
Real MW
0 ppg 30
MW Breakdown
MW Loss
MW Kick
MW Breakout
DEPTH (MD)
(M)
1:4000
STRATIGRAPHY
Lithology
0 % 100
Shale
Salt
Lime Stone
Marl
Anhydrite
Bit Size
8 in 24
Caliper
Gs
1000
1100
1200
1300
1400
1500

Fig. 8

Elevation: **Rotary Table**
Elevation datum: **717.5 Mss**
Total depth: **4130 m MD**

Well-A

Country: **IRAN**
Company: **NIOSC**

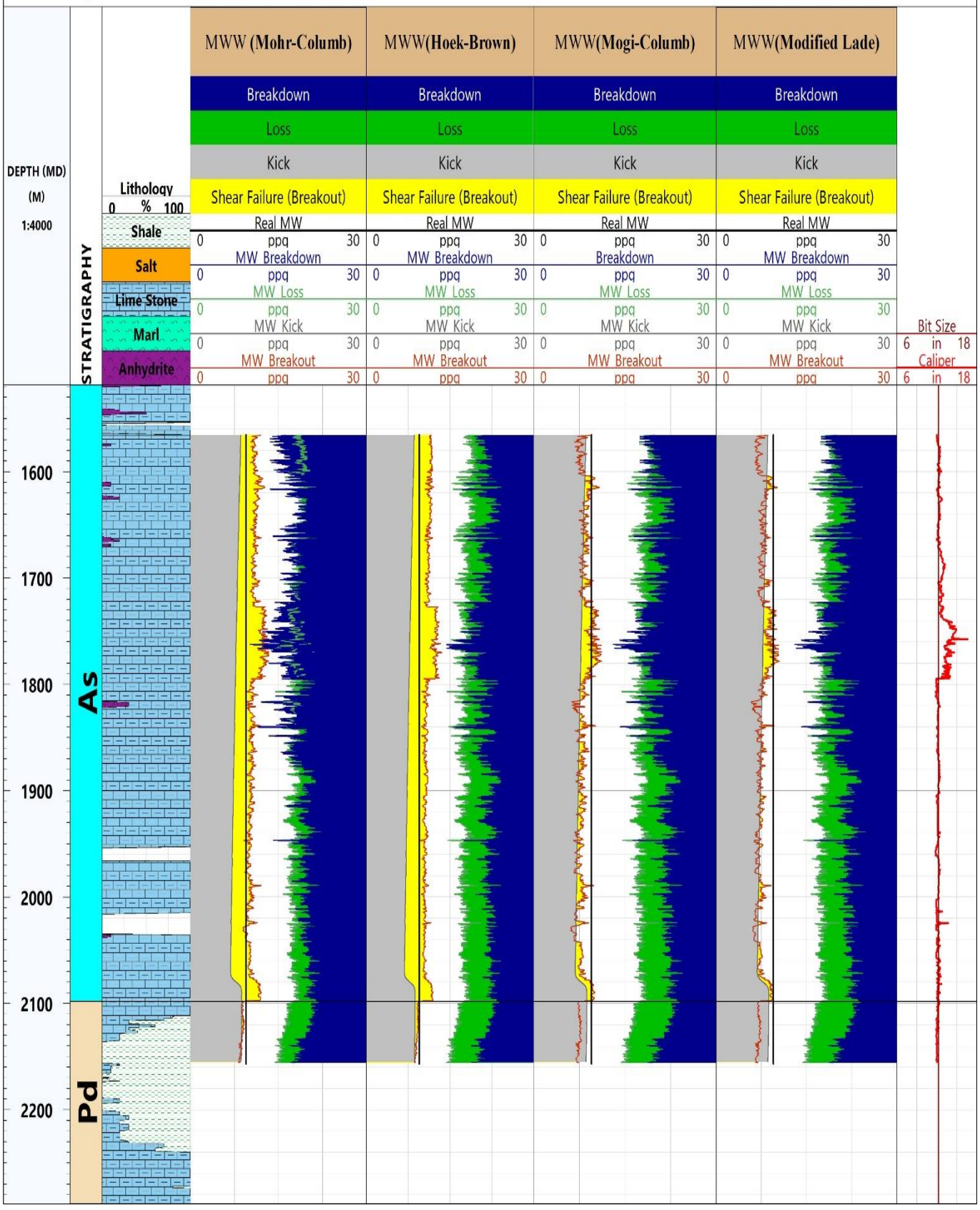

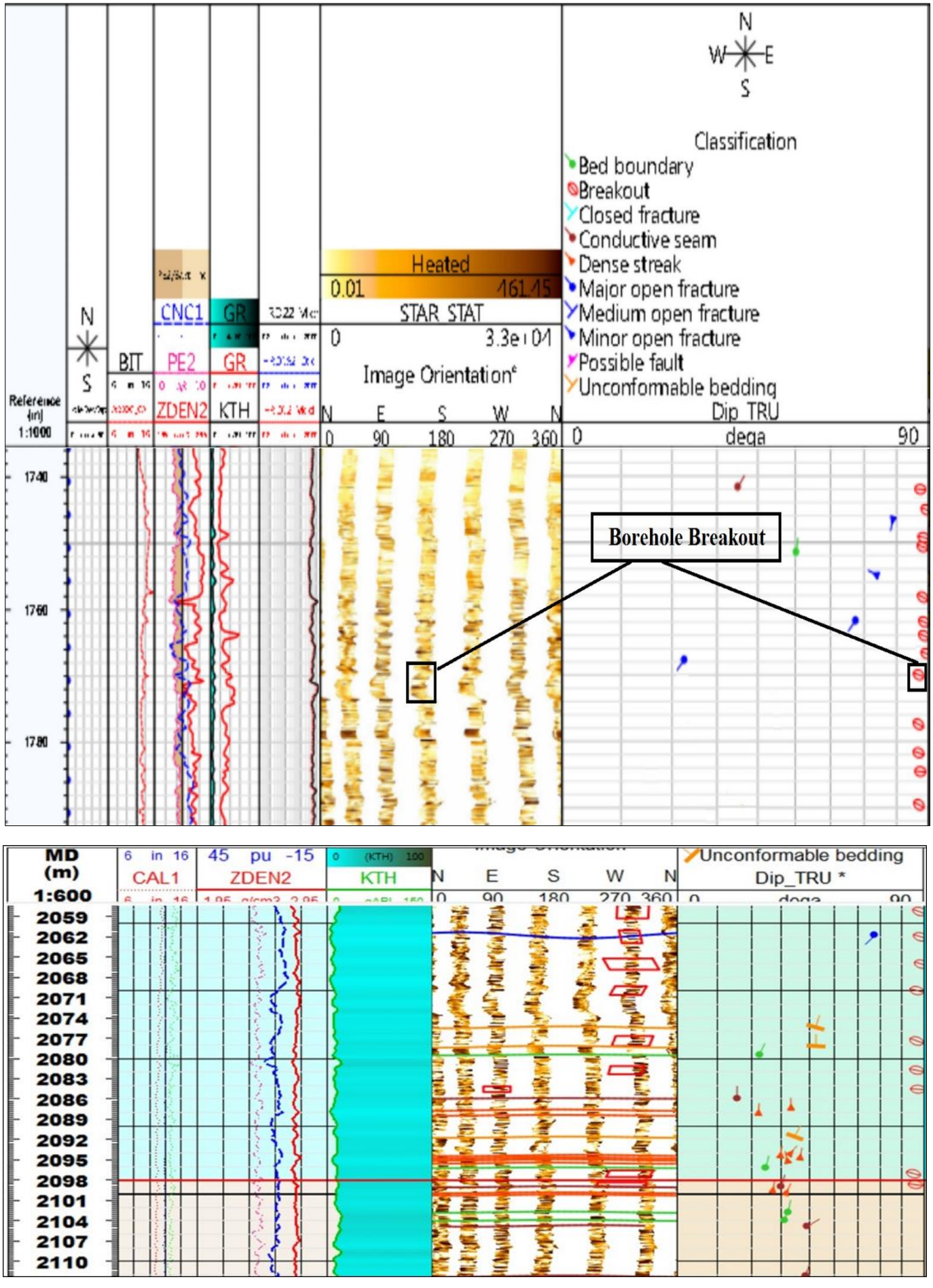
N
W
E
S
Classification
Bed boundary
Breakout
Closed fracture
Conductive seam
Dense streak
Major open fracture
Medium open fracture
Minor open fracture
Possible fault
Unconformable bedding
Heated
0.01
161.15
STAR_STAT
CNC1
GR
BIT
PE2
GR
ZDEN2
KTH
Reference (in) 1:1000
0
3.3e+04
Image Orientation°
N E S W N
0 90 180 270 360
Dip_TRU
0
deg
90
1740
1760
1780
Borehole Breakout
MD (m)
1:600
6 in 16
CAL1
45 pu -15
ZDEN2
0 (KTH) 100
KTH
Unconformable bedding
Dip_TRU *
2059
2062
2065
2068
2071
2074
2077
2080
2083
2086
2089
2092
2095
2098
2101
2104
2107
2110

Fig. 9

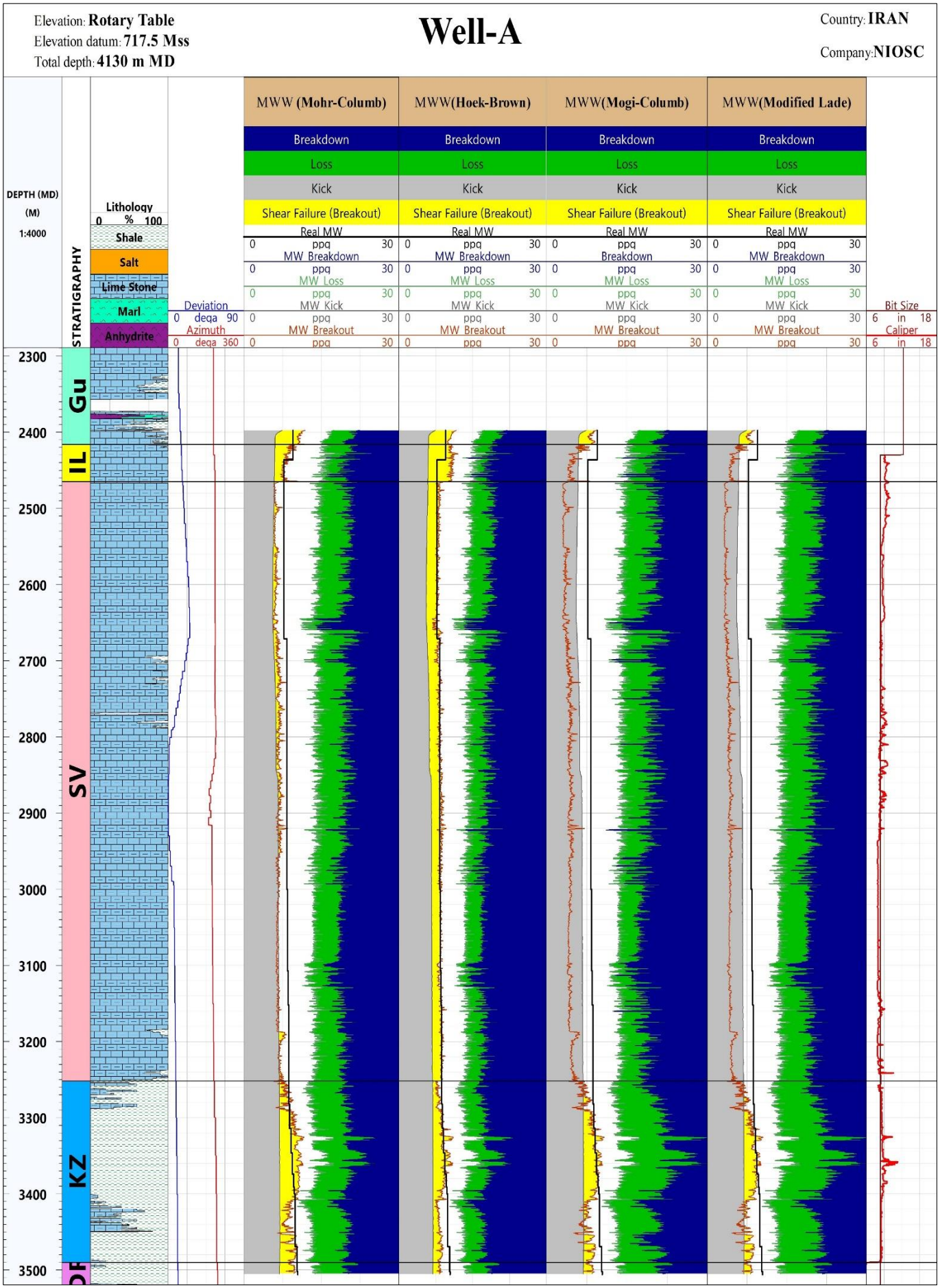
Elevation: Rotary Table
Elevation datum: 717.5 Mss
Total depth: 4130 m MD
Well-A
Country: IRAN
Company: NIOSC
MWW (Mohr-Columb)
MWW(Hoek-Brown)
MWW(Mogi-Columb)
MWW(Modified Lade)
Breakdown
Loss
Kick
Shear Failure (Breakout)
Real MW
MW Breakdown
MW Loss
MW Kick
MW Breakout
Breakdown
DEPTH (MD)
(M)
1:4000
STRATIGRAPHY
Lithology
0 % 100
Shale
Salt
Lime Stone
Marl
Anhydrite
Deviation
0 deqa 90
Azimuth
0 deqa 360
0 ppg 30
Bit Size
6 in 18
Caliper
Gu
IL
SV
KZ
2300
2400
2500
2600
2700
2800
2900
3000
3100
3200
3300
3400
3500

Fig. 1

Elevation: **Rotary Table**
Elevation datum: **717.5 Mss**
Total depth: **4130 m MD**

Well-A

Country: **IRAN**
Company: **NIOSC**

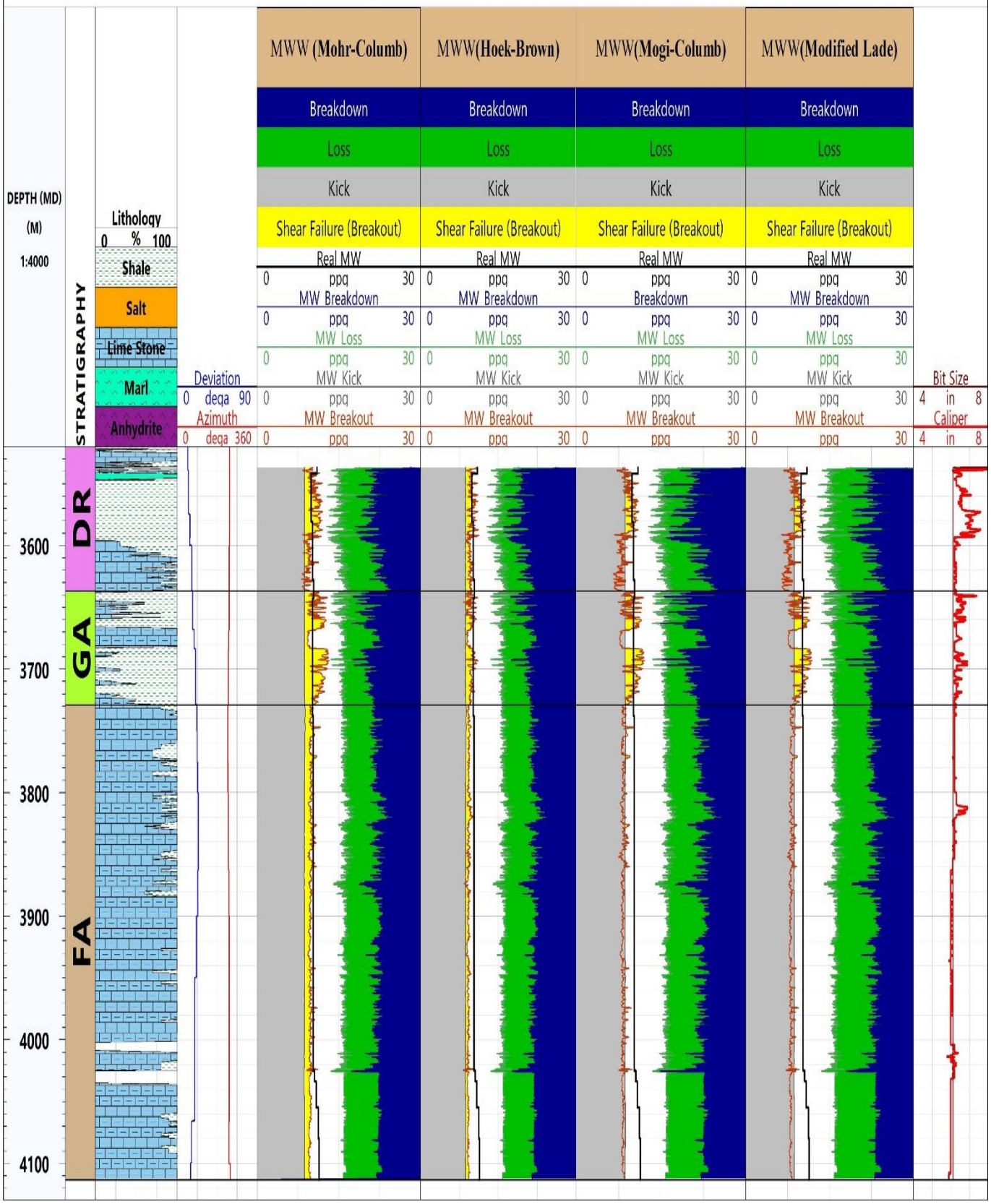

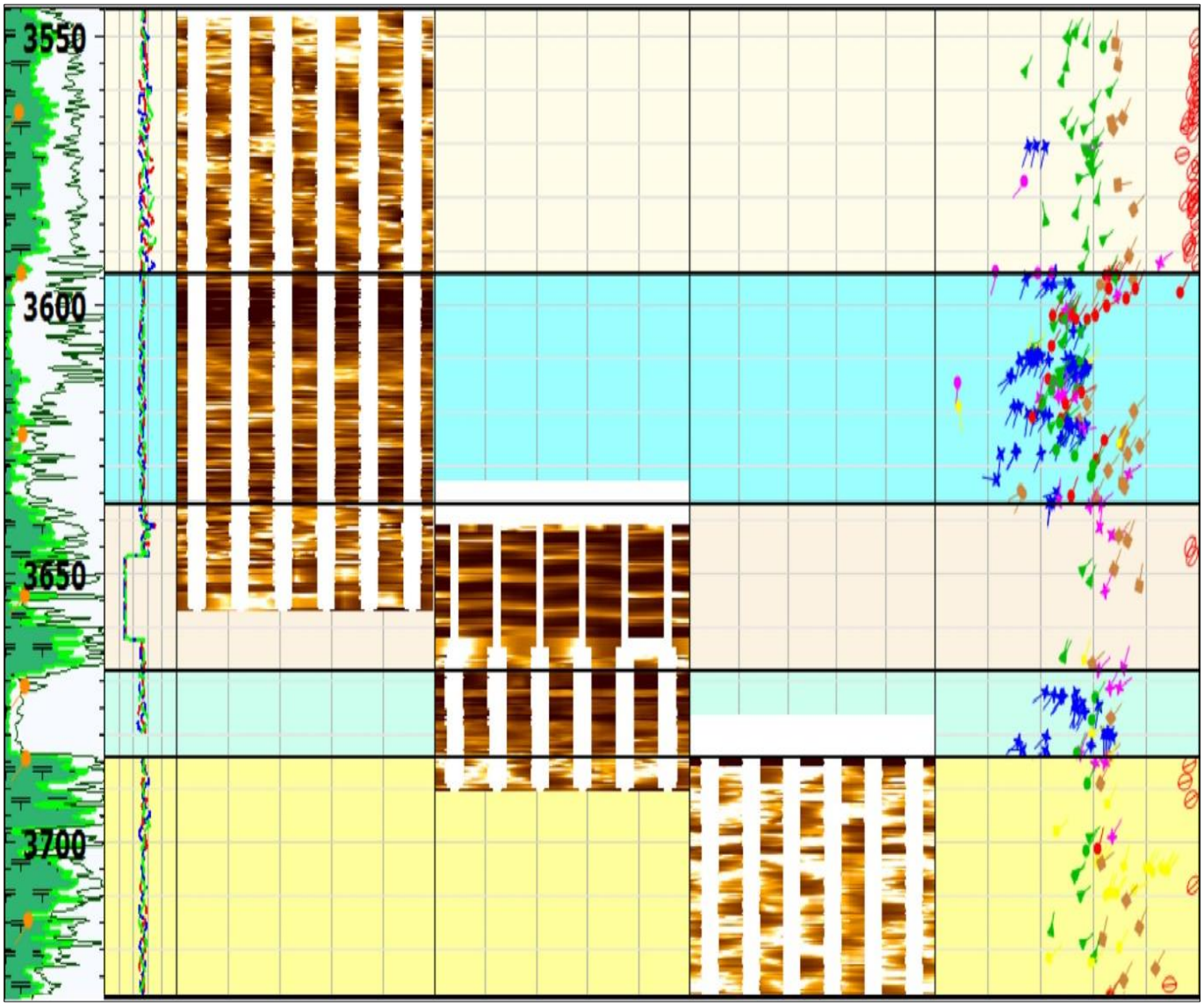

Fig. 2

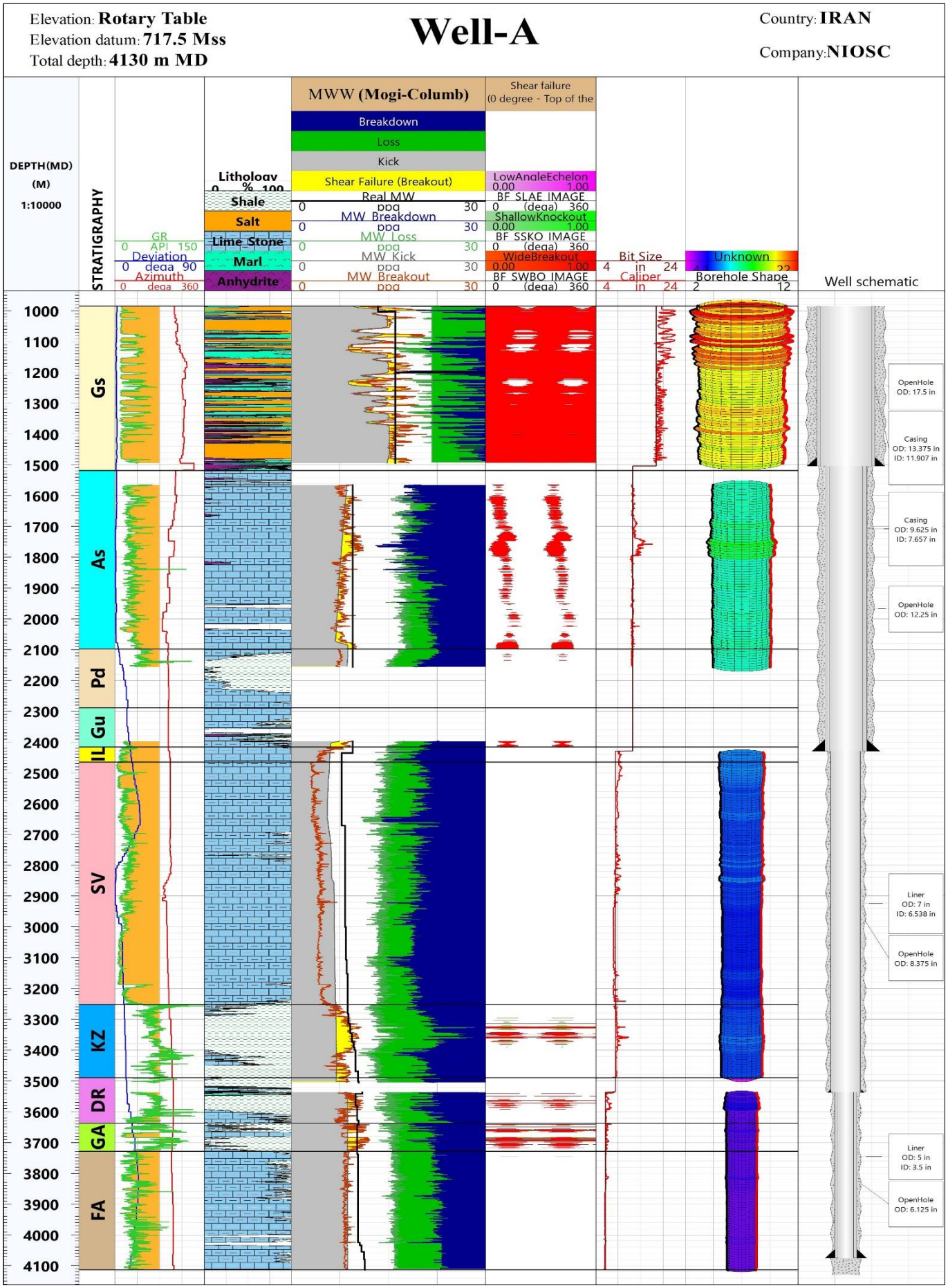
Elevation: Rotary Table
Elevation datum: 717.5 Mss
Total depth: 4130 m MD
Well-A
Country: IRAN
Company: NIOSC
DEPTH(MD)
(M)
1:10000
STRATIGRAPHY
GR
0 API 150
Deviation
0 dega 90
Azimuth
0 dega 360
Lithology
0 % 100
Shale
Salt
Lime Stone
Marl
Anhydrite
MWW (Mogi-Columb)
Breakdown
Loss
Kick
Shear Failure (Breakout)
Real MW
0 ppg 30
MW_Breakdown
0 ppg 30
MW_Loss
0 ppg 30
MW_Kick
0 ppg 30
MW_Breakout
0 ppg 30
Shear failure
(0 degree - Top of the
LowAngleEchelon
0.00 1.00
BF_SLAE_IMAGE
0 (dega) 360
ShallowKnockout
0.00 1.00
BF_SSKO_IMAGE
0 (dega) 360
WideBreakout
0.00 1.00
BF_SWBO_IMAGE
0 (dega) 360
Bit Size
4 in 24
Caliper
4 in 24
Unknown
Borehole Shape
2 12
Well schematic
1000
1100
1200
1300
1400
1500
1600
1700
1800
1900
2000
2100
2200
2300
2400
2500
2600
2700
2800
2900
3000
3100
3200
3300
3400
3500
3600
3700
3800
3900
4000
4100
Gs
As
Pd
Gu
IL
SV
KZ
DR
GA
FA
OpenHole
OD: 17.5 in
Casing
OD: 13.375 in
ID: 11.907 in
Casing
OD: 9.625 in
ID: 7.657 in
OpenHole
OD: 12.25 in
Liner
OD: 7 in
ID: 6.538 in
OpenHole
OD: 8.375 in
Liner
OD: 5 in
ID: 3.5 in
OpenHole
OD: 6.125 in

Fig. 3

Breakout vs Orientation @ 1080 m MD
Azimuth (Circular Angle) Deviation(0-Center, 90-Circumference)
Schmidt - Pole - Upper hemisphere

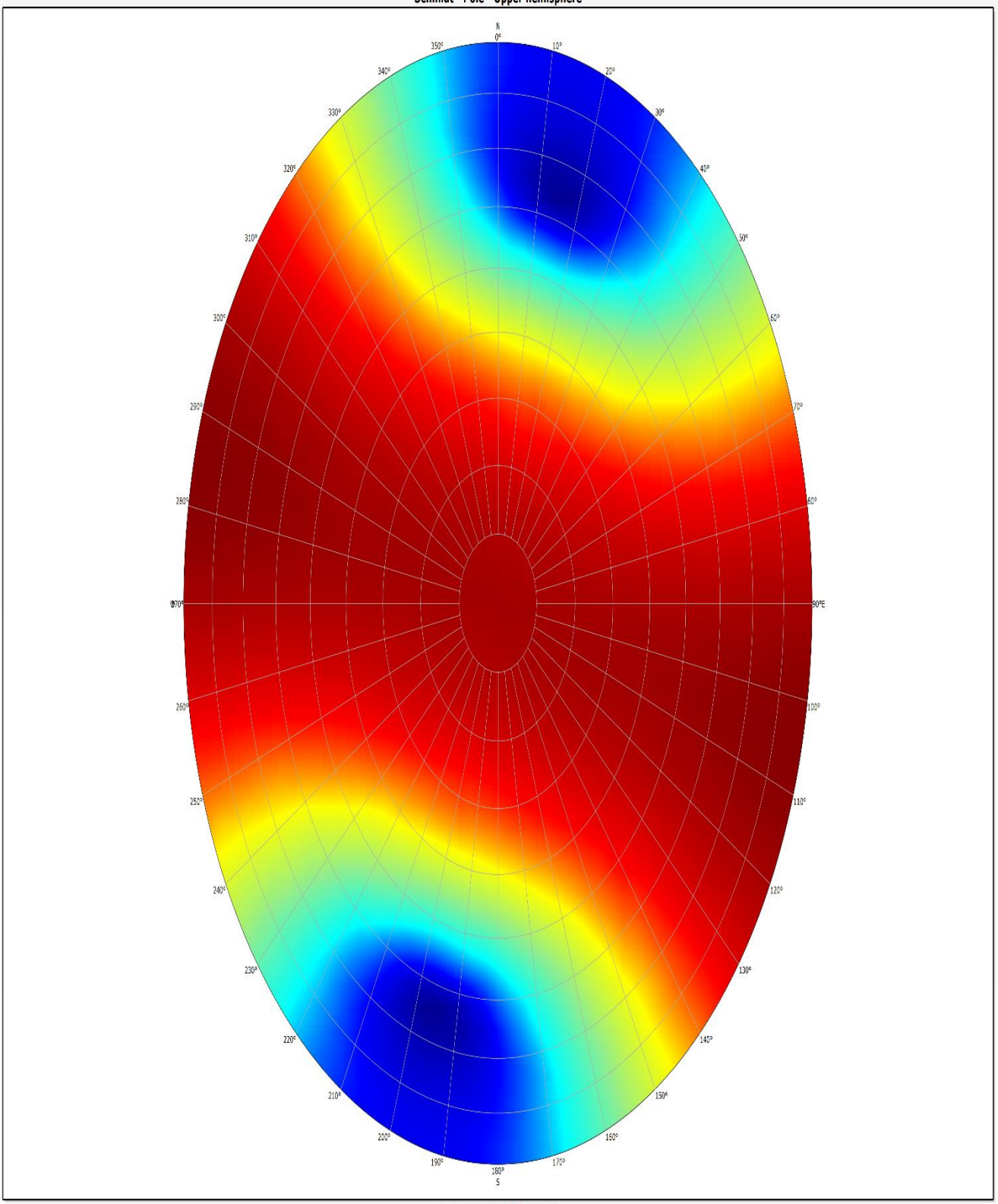

Deviation (dega) / Azimuth (dega)

4.1 Shear failure (ppg) 4.1 - 15.2 (Shear Failure) 15.2

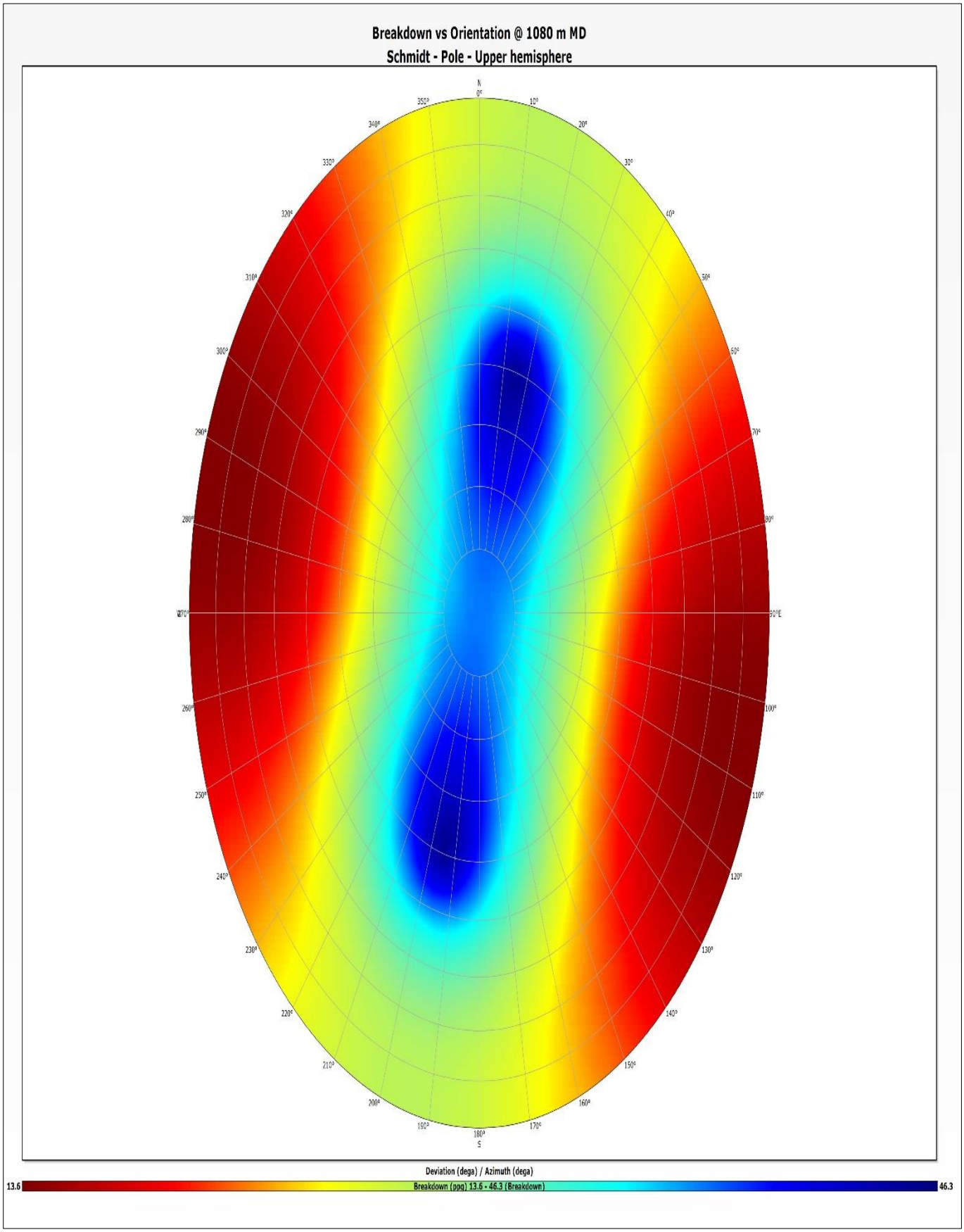
Breakdown vs Orientation @ 1080 m MD
Schmidt - Pole - Upper hemisphere
N
0°
10°
20°
30°
40°
50°
60°
70°
80°
90°E
100°
110°
120°
130°
140°
150°
160°
170°
180°
S
190°
200°
210°
220°
230°
240°
250°
260°
270°W
280°
290°
300°
310°
320°
330°
340°
350°
Deviation (dega) / Azimuth (dega)
13.6
Breakdown (ppg) 13.6 - 46.3 (Breakdown)
46.3

Fig. 4

Breakout @ 1780 m MD

Schmidt - Pole - Upper hemisphere

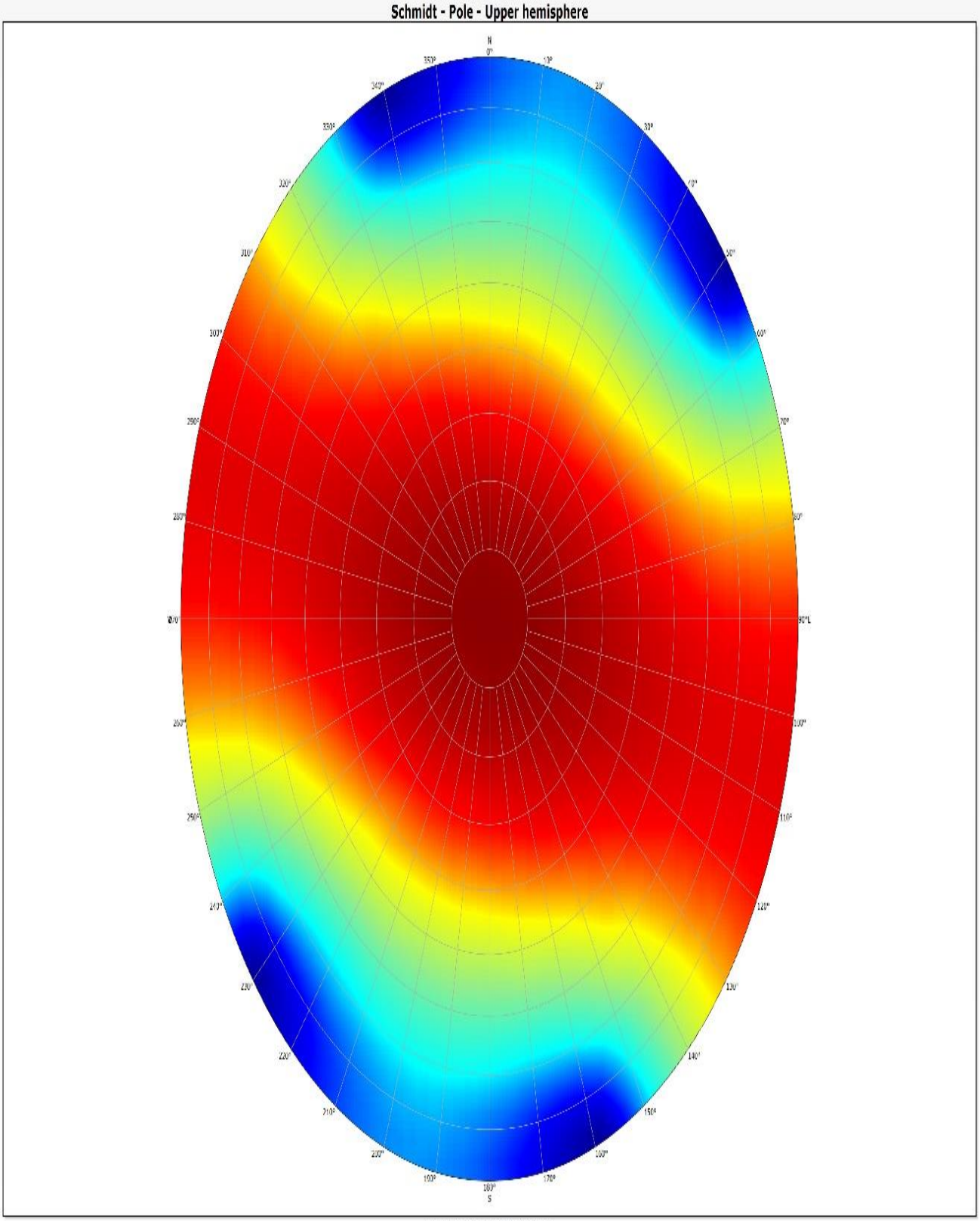

Deviation (dega) / Azimuth (dega)

6.1 Shear failure (ppg) 6.1 - 10.3 (Shear Failure) 10.3

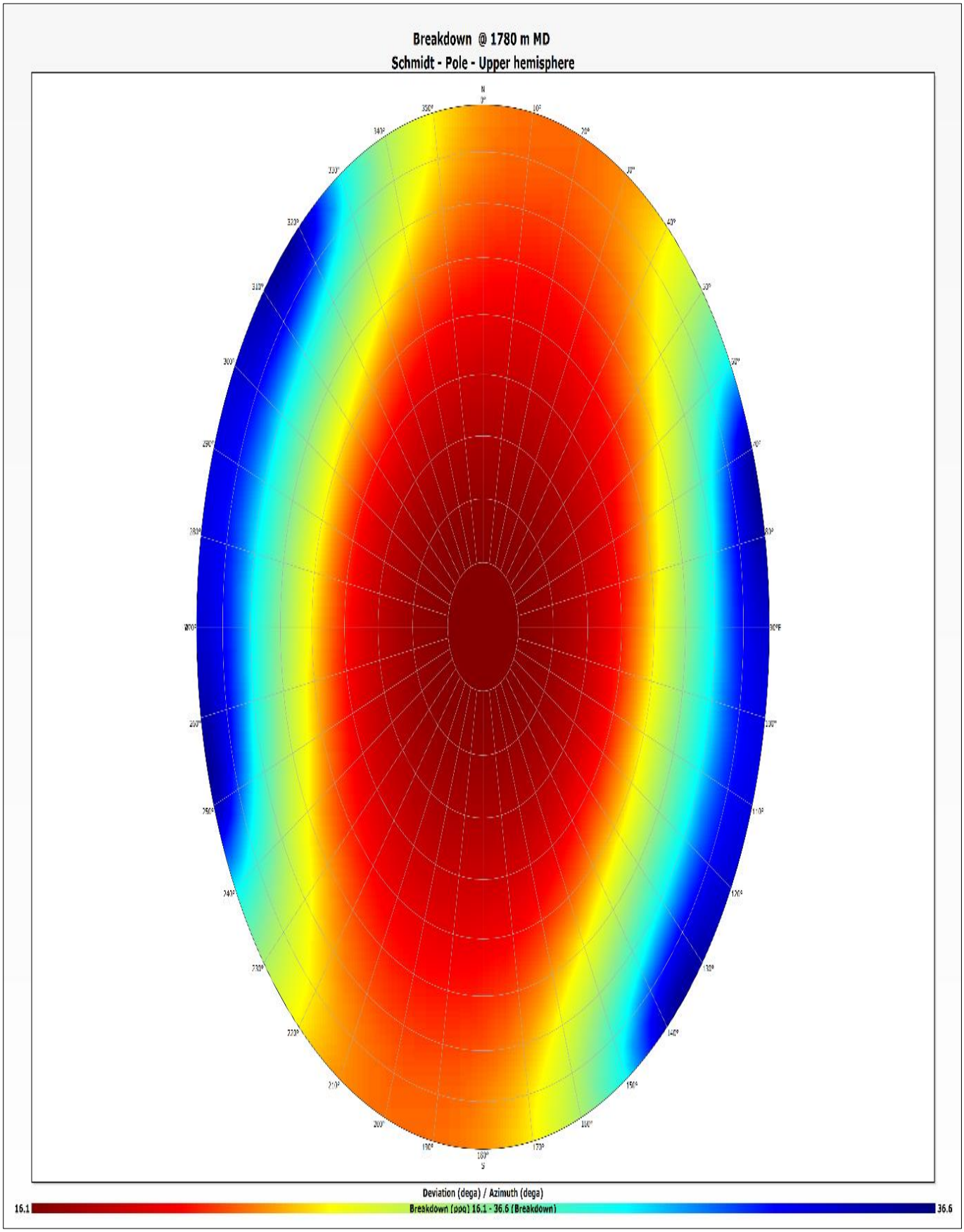
Breakdown @ 1780 m MD
Schmidt - Pole - Upper hemisphere
N
S
Deviation (dega) / Azimuth (dega)
16.1
Breakdown (ppg) 16.1 - 36.6 (Breakdown)
36.6

Fig. 5

Breakout @ 2100 m MD

Schmidt - Pole - Upper hemisphere

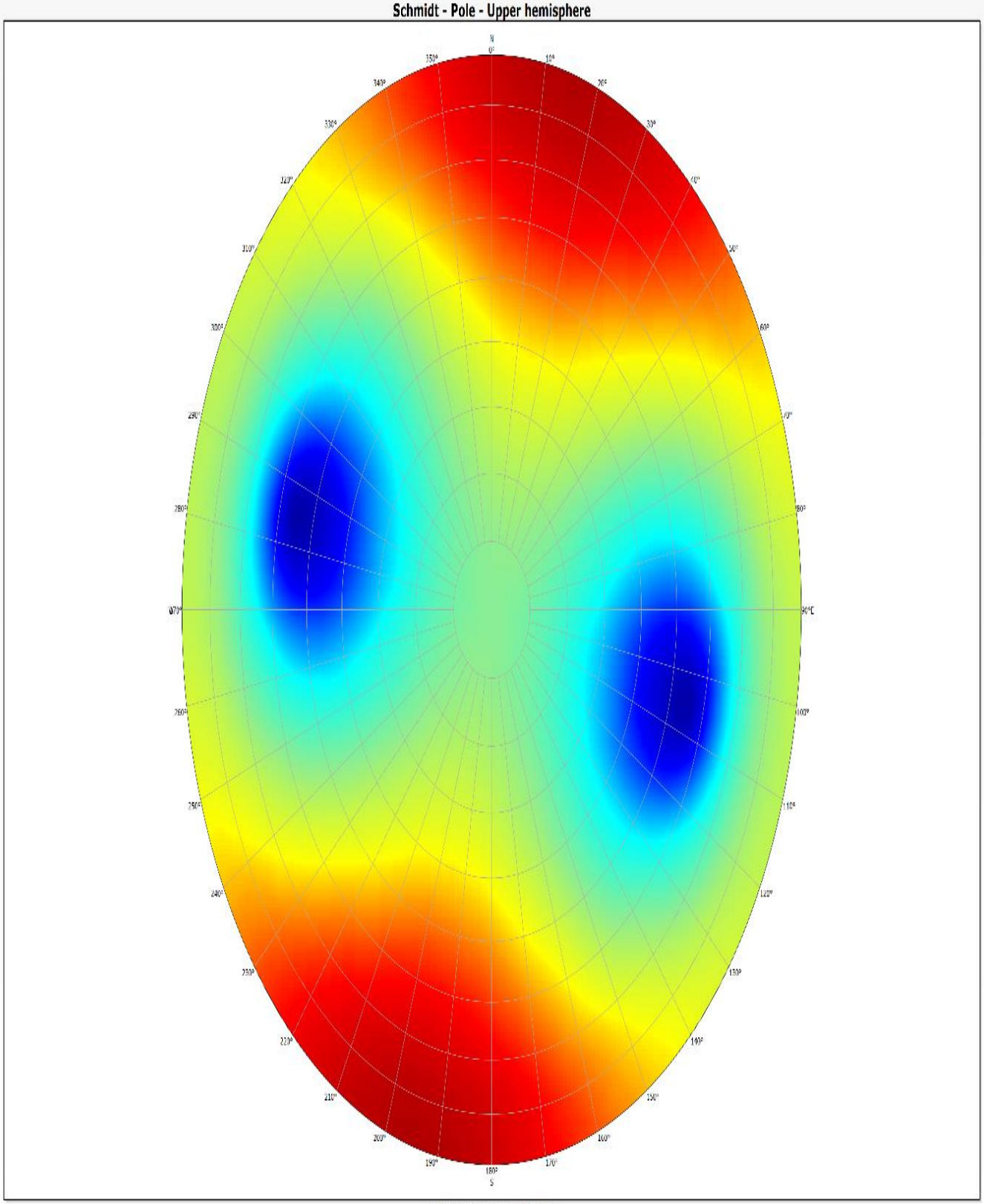

Deviation (dega) / Azimuth (dega)

6.6 Shear failure (ppg) 6.6 - 8 (Shear Failure) 8

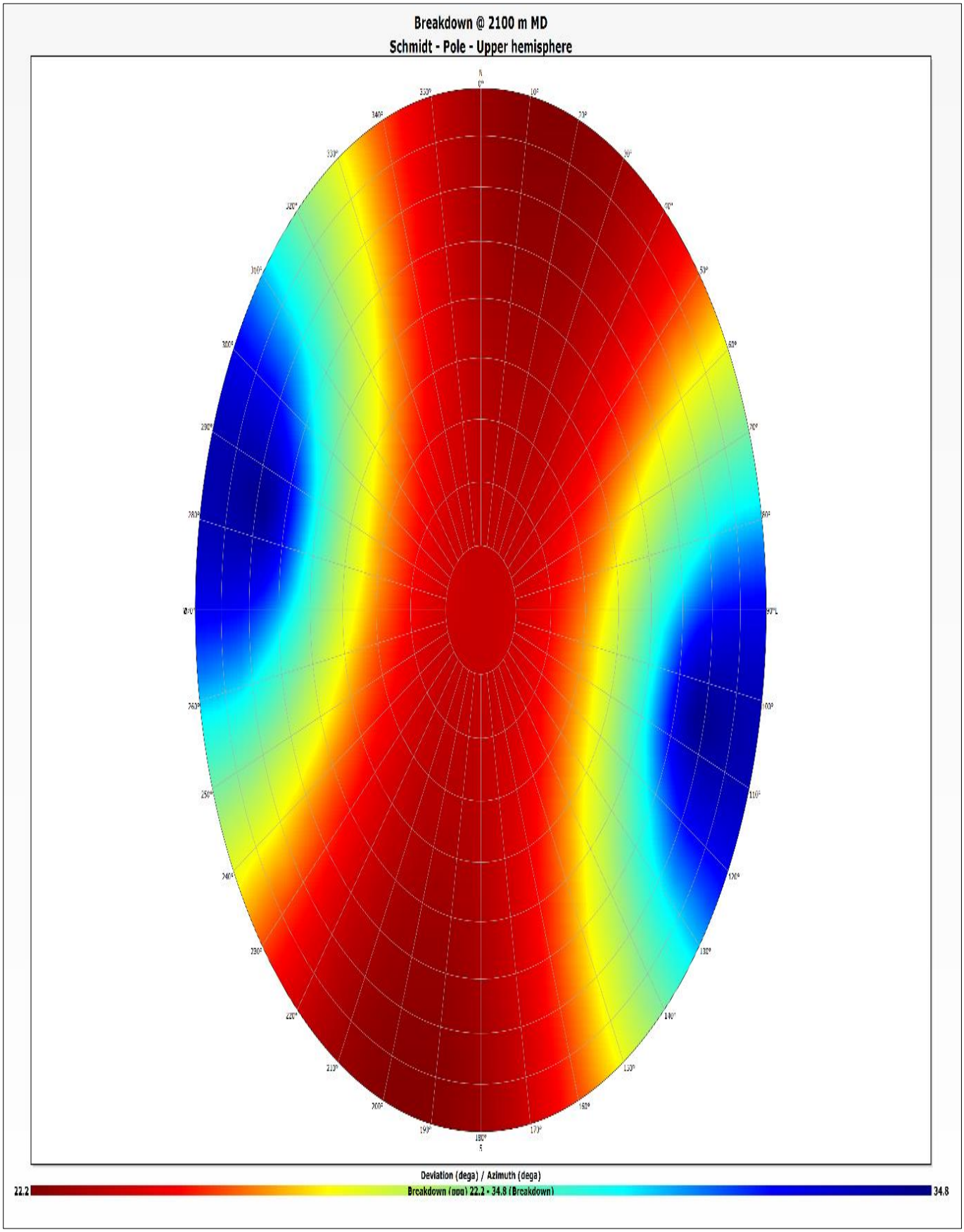
Breakdown @ 2100 m MD
Schmidt - Pole - Upper hemisphere
N
0°
10°
20°
30°
40°
50°
60°
70°
80°
90°
100°
110°
120°
130°
140°
150°
160°
170°
180°
190°
200°
210°
220°
230°
240°
250°
260°
270°
280°
290°
300°
310°
320°
330°
340°
350°
Deviation (dega) / Azimuth (dega)
22.2
Breakdown (ppg) 22.2 - 34.8 (Breakdown)
34.8

Fig. 6

Breakout @ 2440 m MD
Azimuth(Circular Angle) Deviation(0-Center, 90-Circumference)
Schmidt - Pole - Upper hemisphere

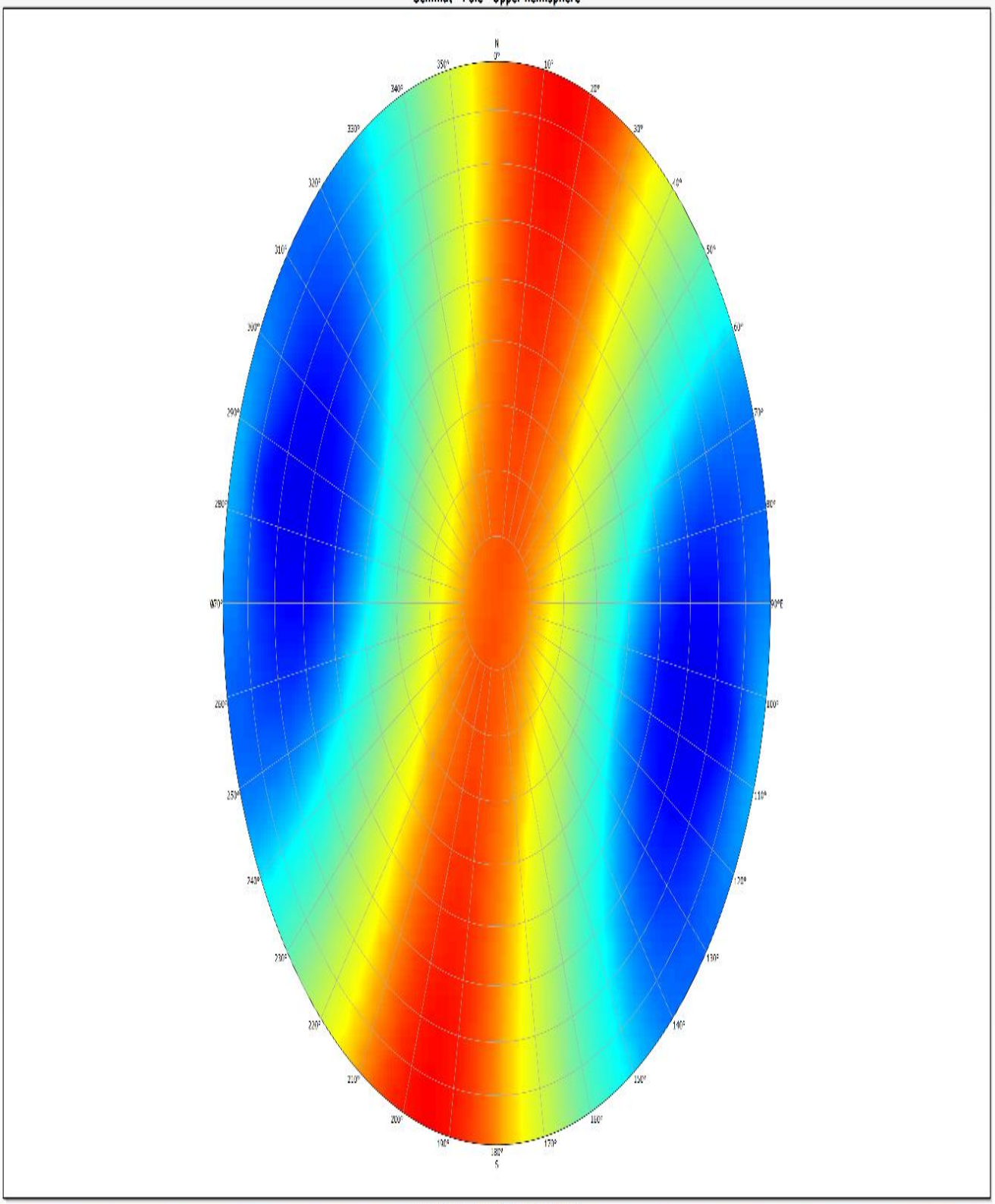

Deviation (dega) / Azimuth (dega)

4 Shear failure (ppg) 4 - 4.5 (Shear Failure) 4.5

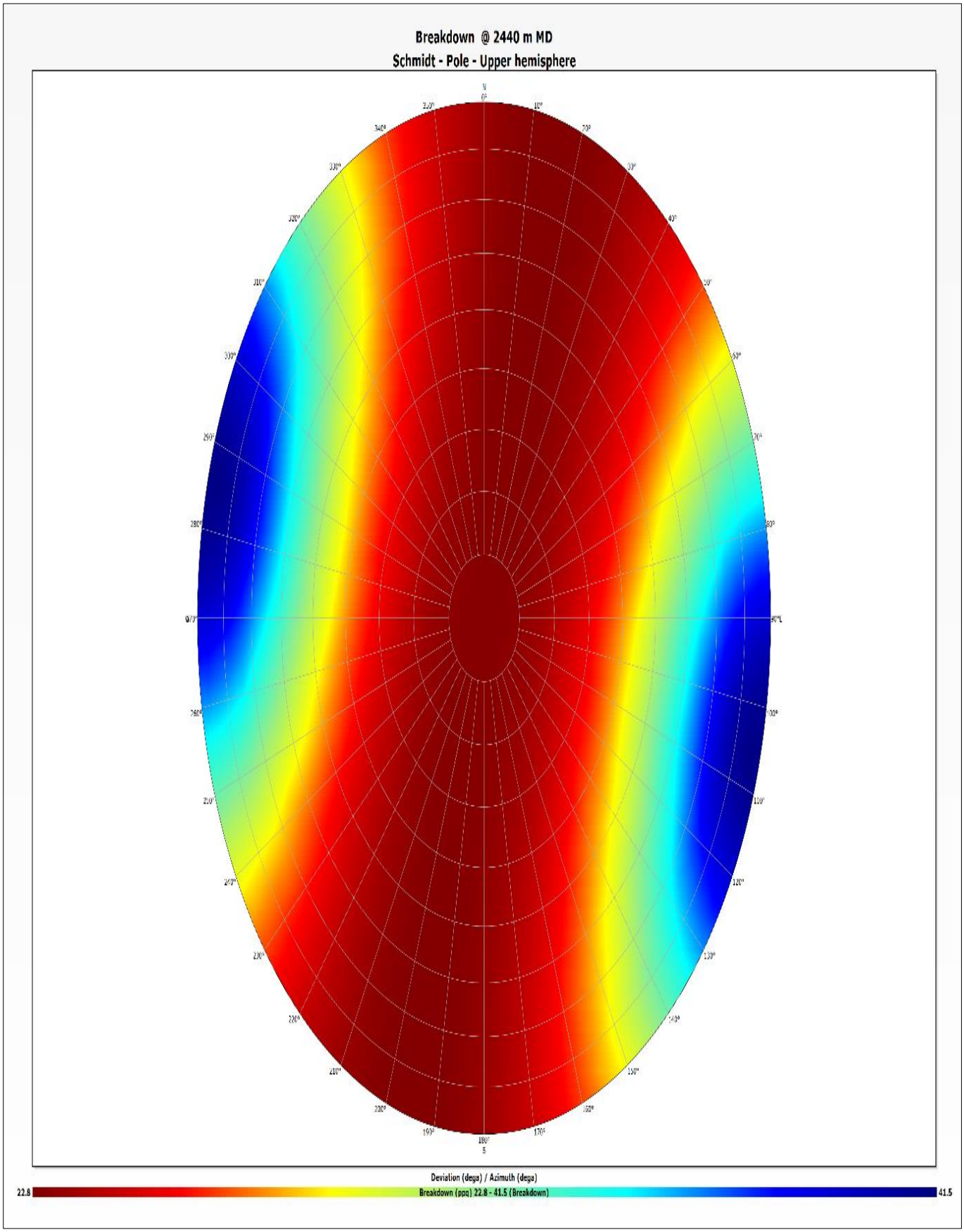
Breakdown @ 2440 m MD
Schmidt - Pole - Upper hemisphere
Deviation (deg) / Azimuth (deg)
22.8
Breakdown (ppg) 22.8 - 41.5 (Breakdown)
41.5

Fig. 7

Breakout @ 2900 m MD

Schmidt - Pole - Upper hemisphere

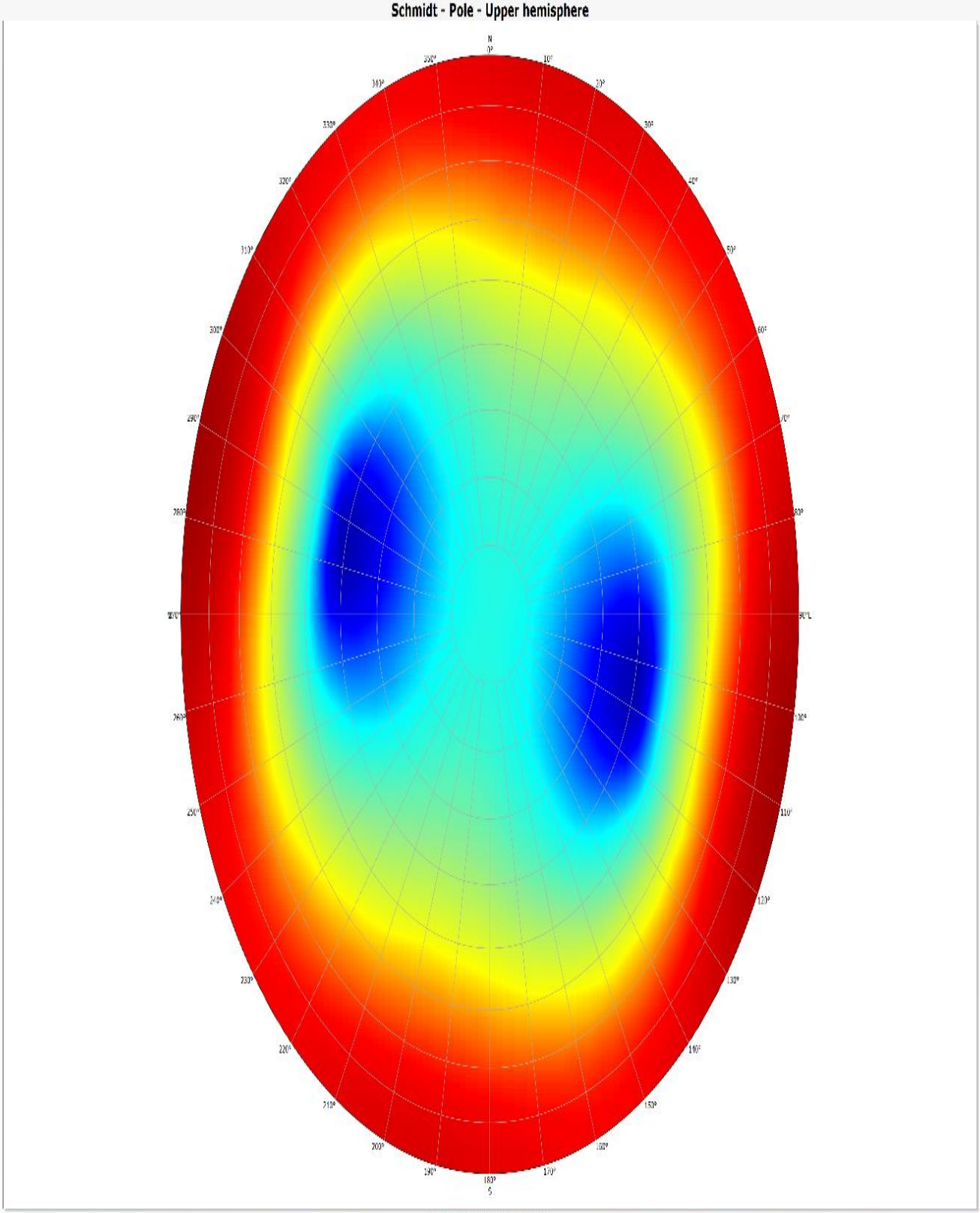

Deviation (deg) / Azimuth (deg)

3.7 Shear failure (ppg) 3.7 - 4.7 (Shear Failure) 4.7

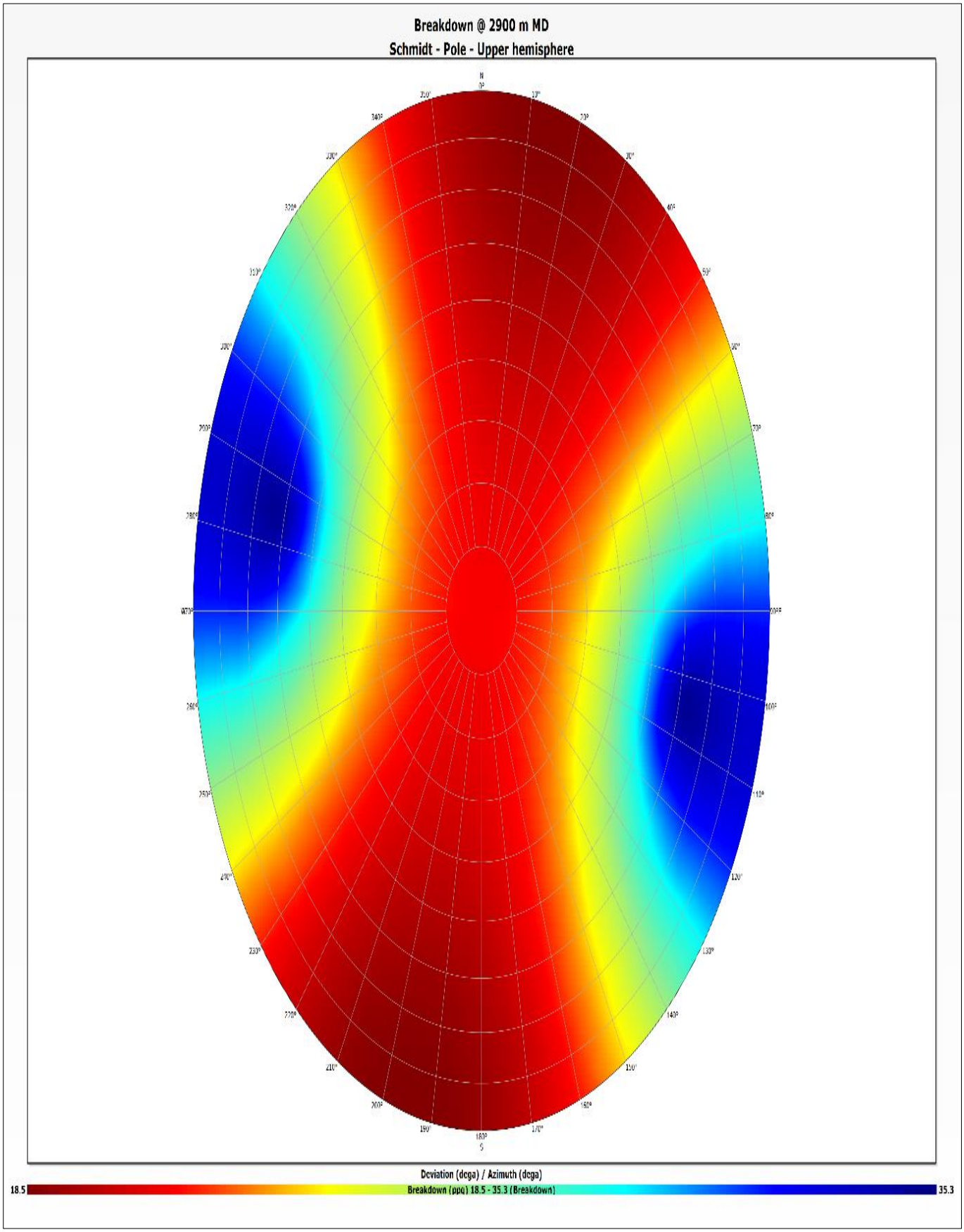
Breakdown @ 2900 m MD
Schmidt - Pole - Upper hemisphere
N
S
Deviation (degs) / Azimuth (degs)
18.5
Breakdown (ppg) 18.5 - 35.3 (Breakdown)
35.3

Fig. 8

Breakout @ 3580 m MD

Schmidt - Pole - Upper hemisphere

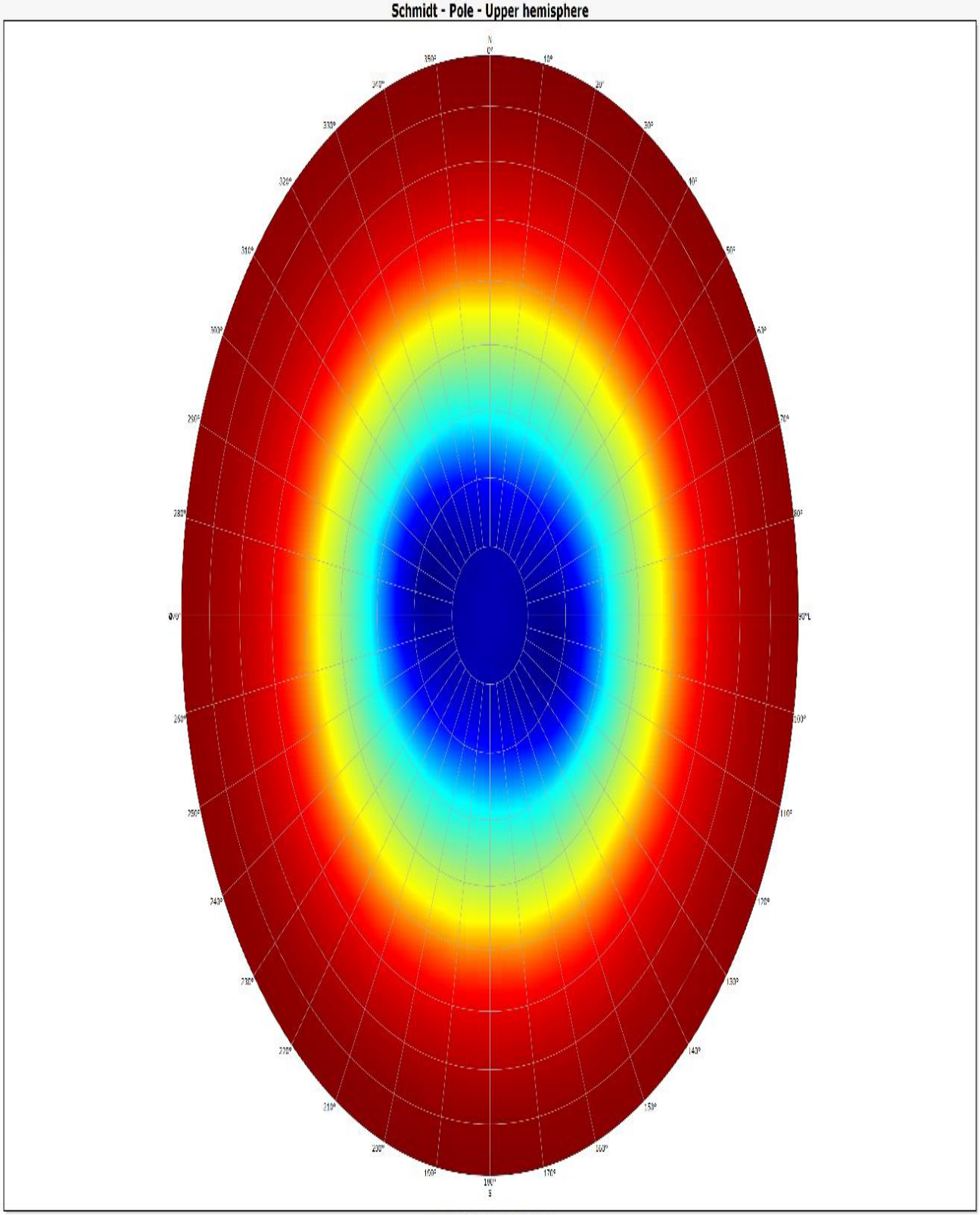

Deviation (dega) / Azimuth (dega)

10.3 Shear failure (ppg) 10.3 - 14.9 (Shear Failure) 14.9

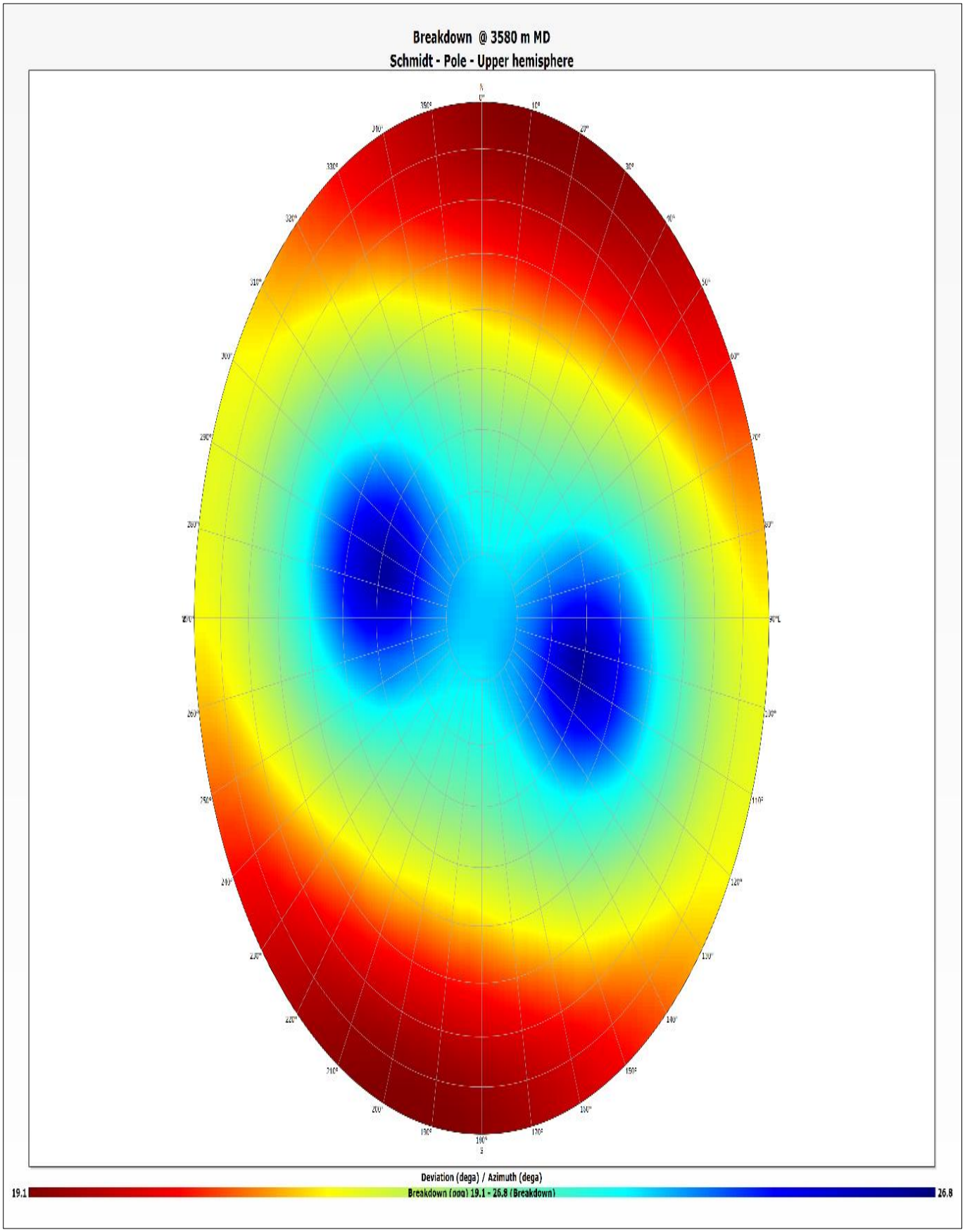
Breakdown @ 3580 m MD
Schmidt - Pole - Upper hemisphere
Deviation (dega) / Azimuth (dega)
19.1
Breakdown (pga) 19.1 - 26.8 (Breakdown)
26.8

Fig. 9

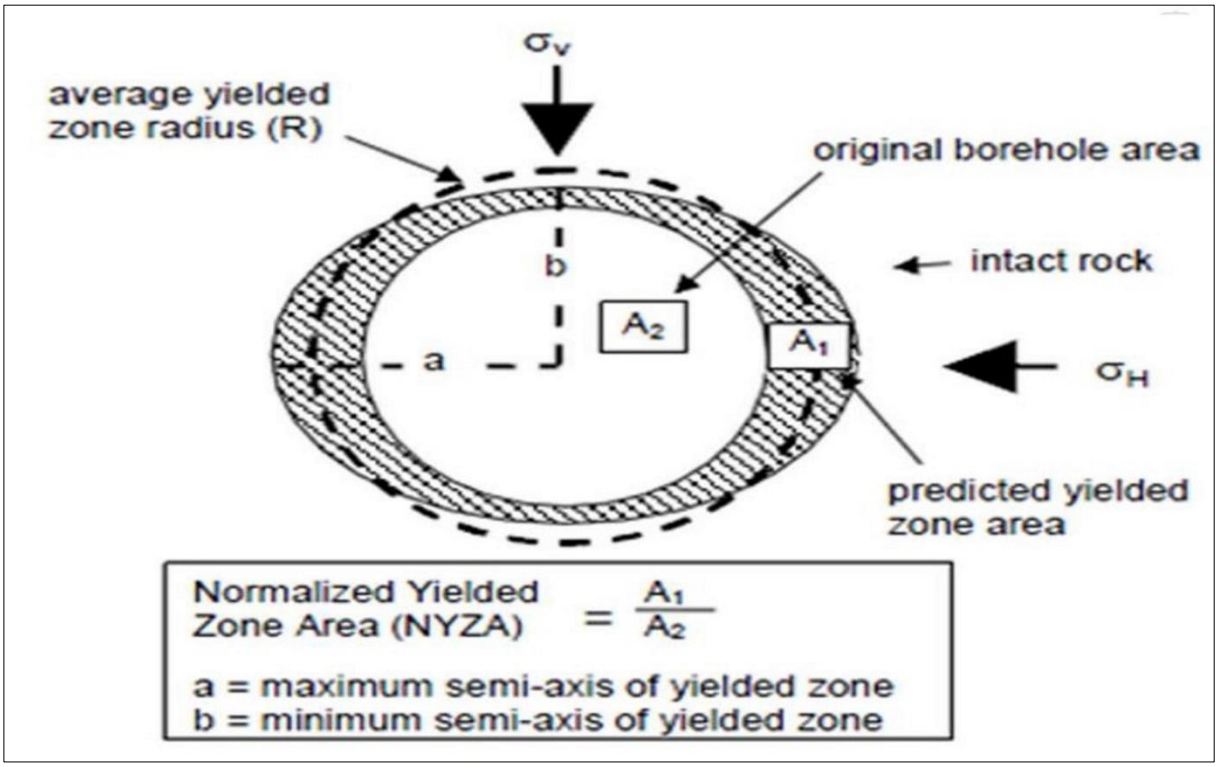
σv
average yielded zone radius (R)
original borehole area
intact rock
b
a
A2
A1
σH
predicted yielded zone area
Normalized Yielded Zone Area (NYZA) = A1/A2
a = maximum semi-axis of yielded zone
b = minimum semi-axis of yielded zone

Fig. 19

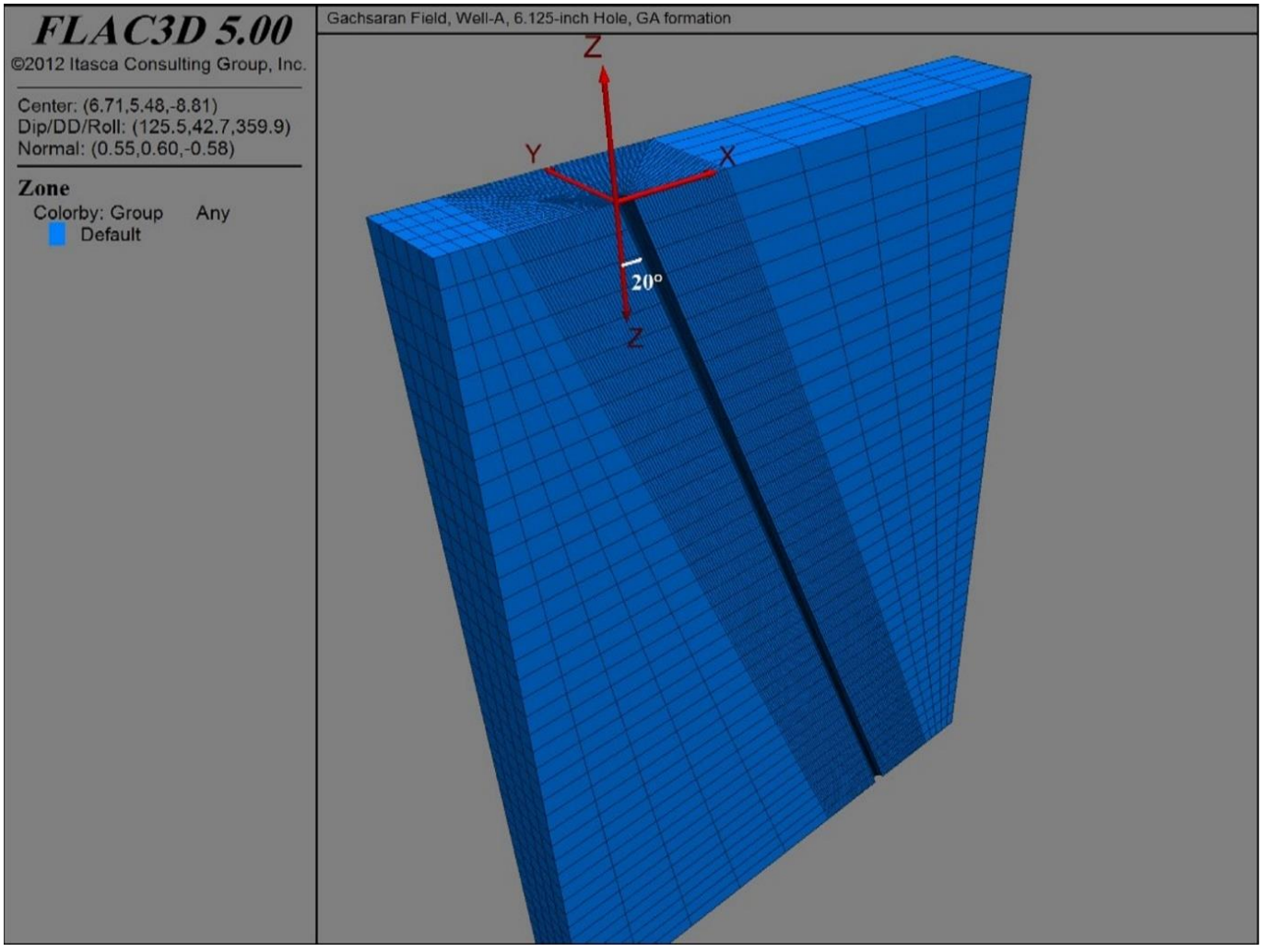
FLAC3D 5.00
©2012 Itasca Consulting Group, Inc.
Center: (6.71,5.48,-8.81)
Dip/DD/Roll: (125.5,42.7,359.9)
Normal: (0.55,0.60,-0.58)
Zone
Colorby: Group Any
Default
Gachsaran Field, Well-A, 6.125-inch Hole, GA formation
Z
Y
X
20°
Z

Fig. 10

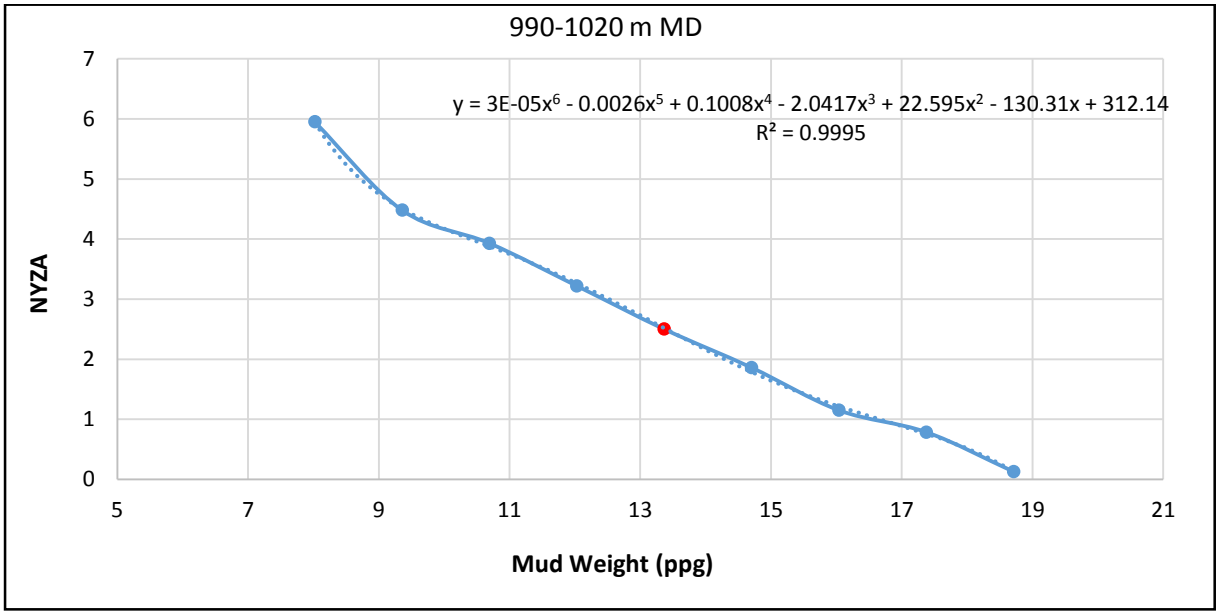
990-1020 m MD
y = 3E-05x⁶ - 0.0026x⁵ + 0.1008x⁴ - 2.0417x³ + 22.595x² - 130.31x + 312.14
R² = 0.9995
NYZA
Mud Weight (ppg)
0
1
2
3
4
5
6
7
5
7
9
11
13
15
17
19
21

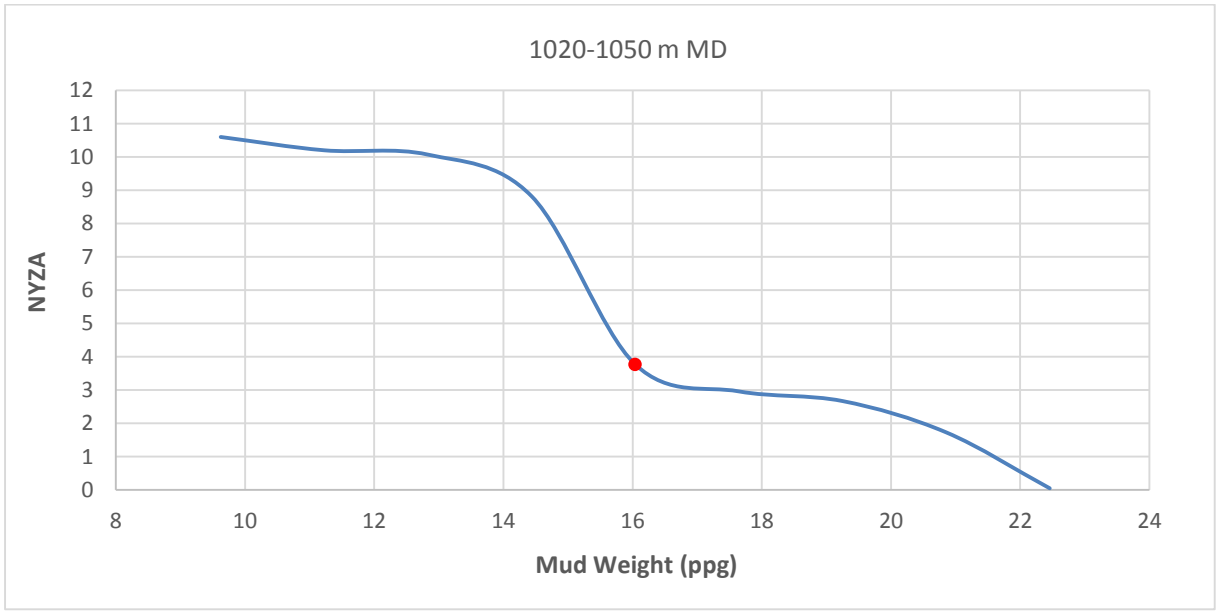
1020-1050 m MD
NYZA
Mud Weight (ppg)
0
1
2
3
4
5
6
7
8
9
10
11
12
8
10
12
14
16
18
20
22
24

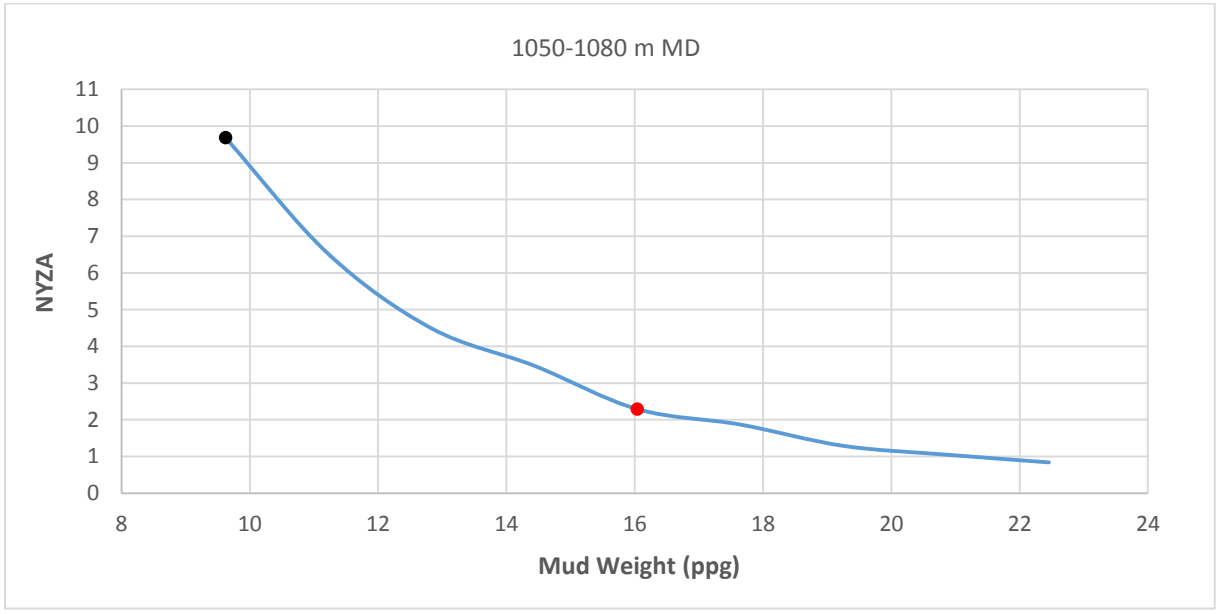
1050-1080 m MD
NYZA
Mud Weight (ppg)
0
1
2
3
4
5
6
7
8
9
10
11
8
10
12
14
16
18
20
22
24

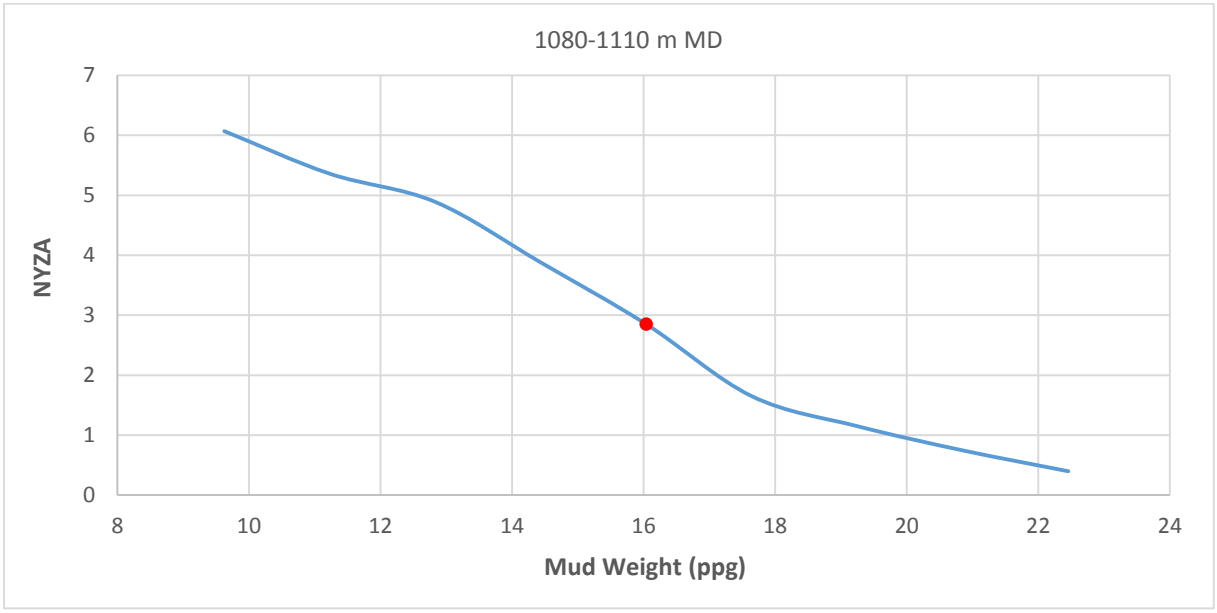
1080-1110 m MD
NYZA
Mud Weight (ppg)
0
1
2
3
4
5
6
7
8
10
12
14
16
18
20
22
24

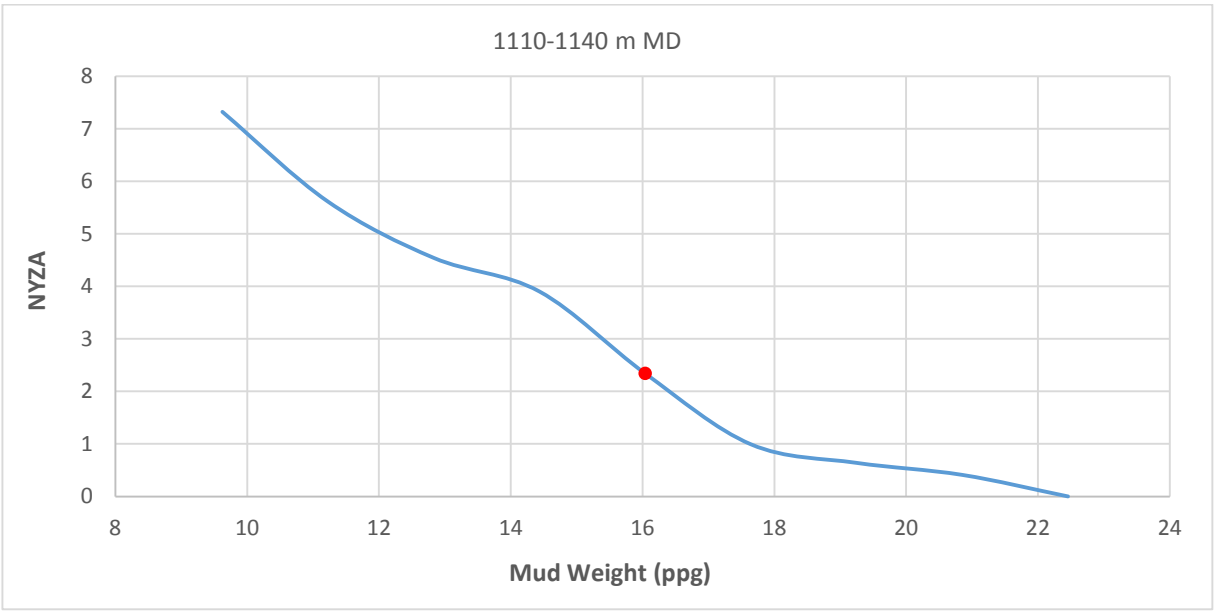
1110-1140 m MD
NYZA
Mud Weight (ppg)
0
1
2
3
4
5
6
7
8
10
12
14
16
18
20
22
24

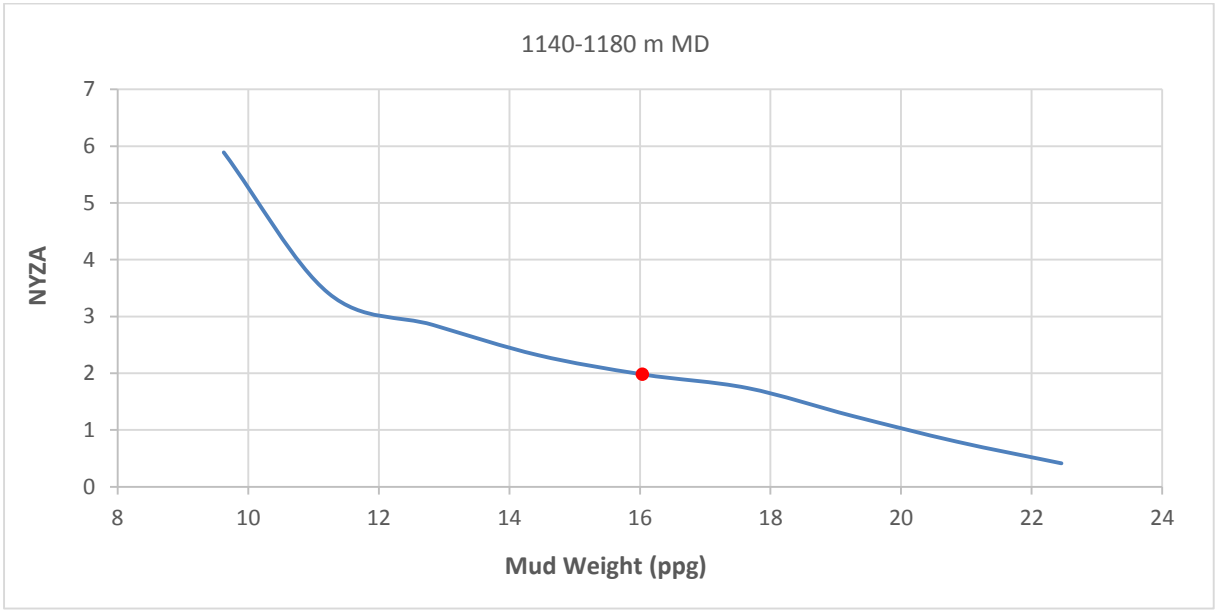
1140-1180 m MD
NYZA
Mud Weight (ppg)
0
1
2
3
4
5
6
7
8
10
12
14
16
18
20
22
24

Fig. 11

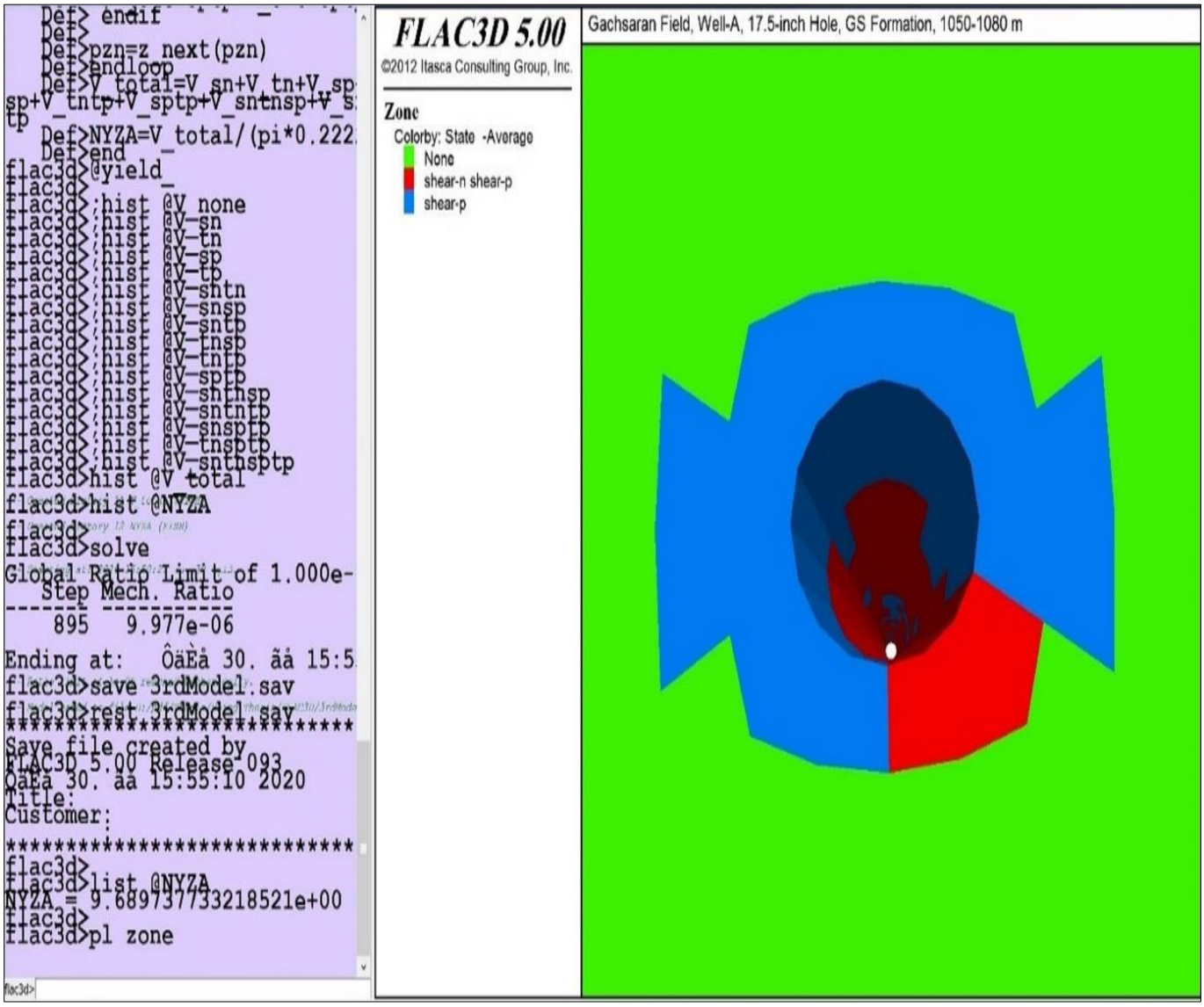
Def> endif
Def>
Def>pzn=z_next(pzn)
Def>endloop
Def>V_total=V_sn+V_tn+V_sp
sp+V_tntp+V_sptp+V_sntnsp+V_s
tp
Def>NYZA=V_total/(pi*0.222
Def>end
flac3d>@yield
flac3d>
flac3d>;hist @V_none
flac3d>;hist @V-sn
flac3d>;hist @V-tn
flac3d>;hist @V-sp
flac3d>;hist @V-tp
flac3d>;hist @V-shtn
flac3d>;hist @V-snsp
flac3d>;hist @V-sntp
flac3d>;hist @V-tnsp
flac3d>;hist @V-tntp
flac3d>;hist @V-sptp
flac3d>;hist @V-shtnsp
flac3d>;hist @V-sntntp
flac3d>;hist @V-snsptp
flac3d>;hist @V-tnsptp
flac3d>;hist @V-shtnsptp
flac3d>hist @V_total
flac3d>hist @NYZA
flac3d>
flac3d>solve
Global Ratio Limit of 1.000e-
Step Mech. Ratio
895 9.977e-06
Ending at: ÔäÈå 30. ãå 15:5
flac3d>save 3rdModel.sav
flac3d>rest 3rdModel.sav
Save file created by
FLAC3D 5.00 Release 093
ÔäÈå 30. ãå 15:55:10 2020
Title:
Customer:
flac3d>
flac3d>list @NYZA
NYZA = 9.689737733218521e+00
flac3d>
flac3d>pl zone
FLAC3D 5.00
©2012 Itasca Consulting Group, Inc.
Zone
Colorby: State -Average
None
shear-n shear-p
shear-p
Gachsaran Field, Well-A, 17.5-inch Hole, GS Formation, 1050-1080 m

Fig. 12

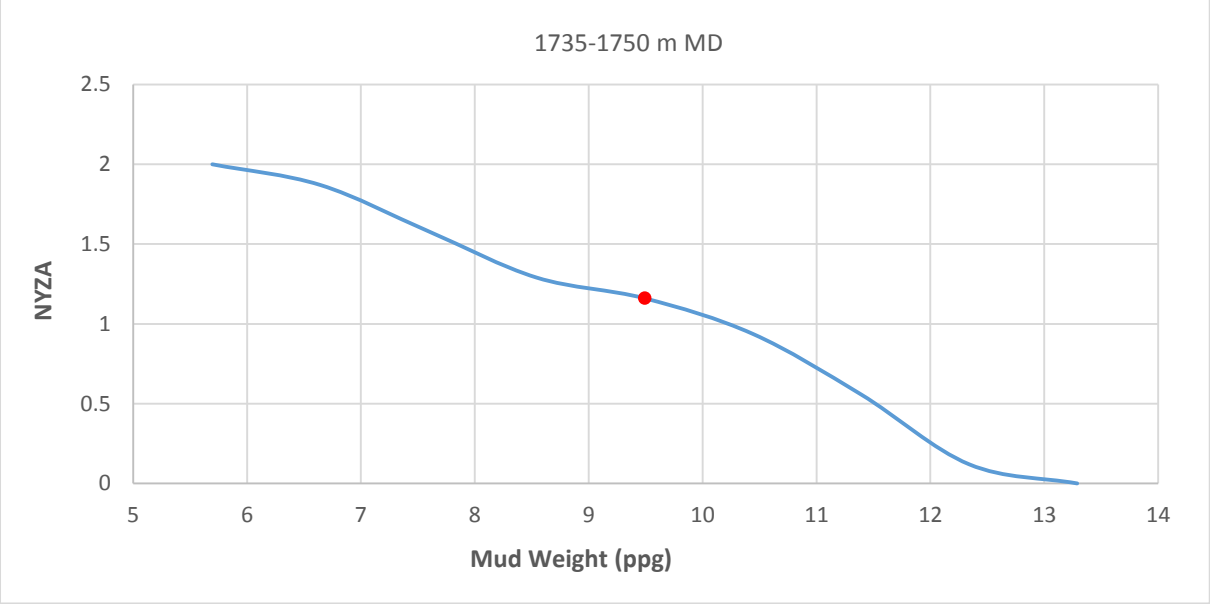
1735-1750 m MD
NYZA
2.5
2
1.5
1
0.5
0
5
6
7
8
9
10
11
12
13
14
Mud Weight (ppg)

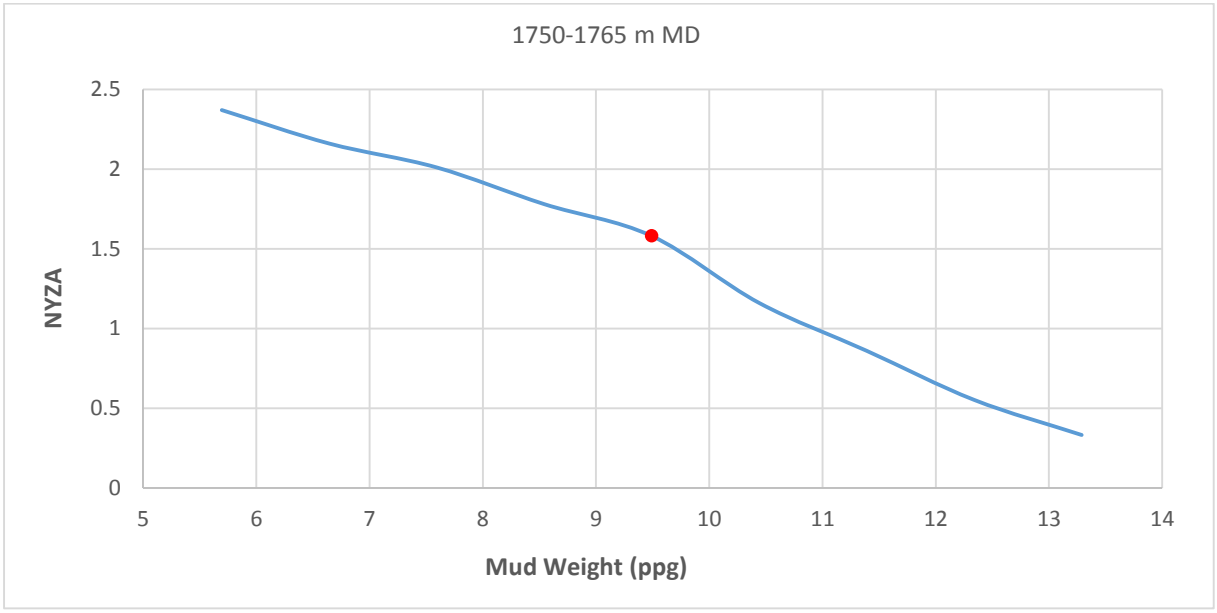
1750-1765 m MD
NYZA
2.5
2
1.5
1
0.5
0
5
6
7
8
9
10
11
12
13
14
Mud Weight (ppg)

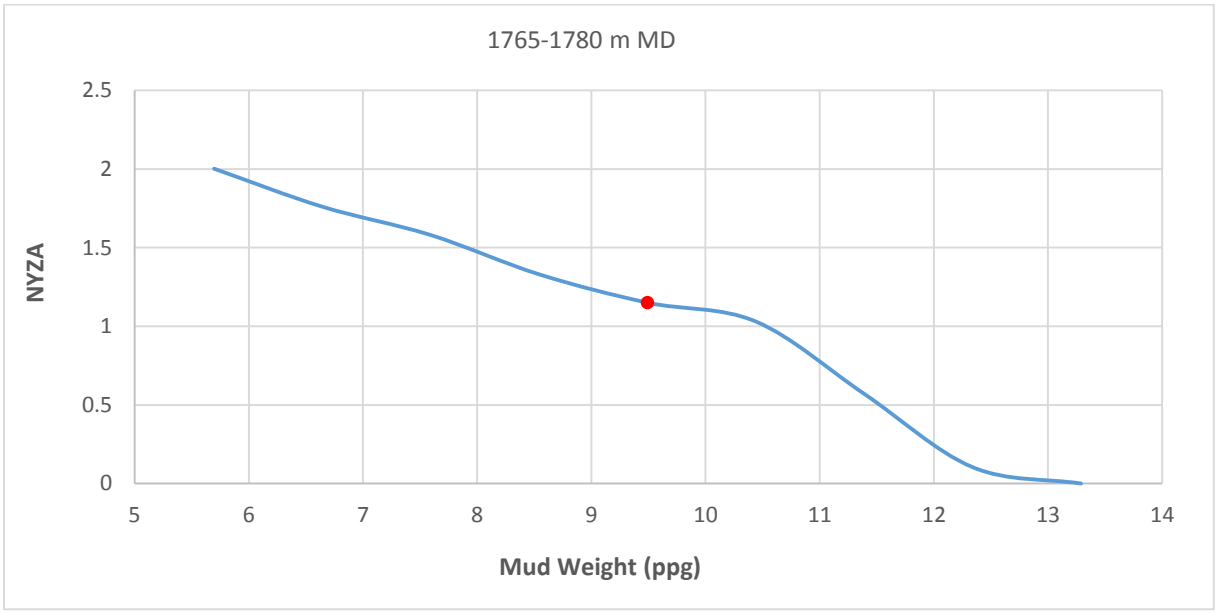
1765-1780 m MD
NYZA
2.5
2
1.5
1
0.5
0
5
6
7
8
9
10
11
12
13
14
Mud Weight (ppg)

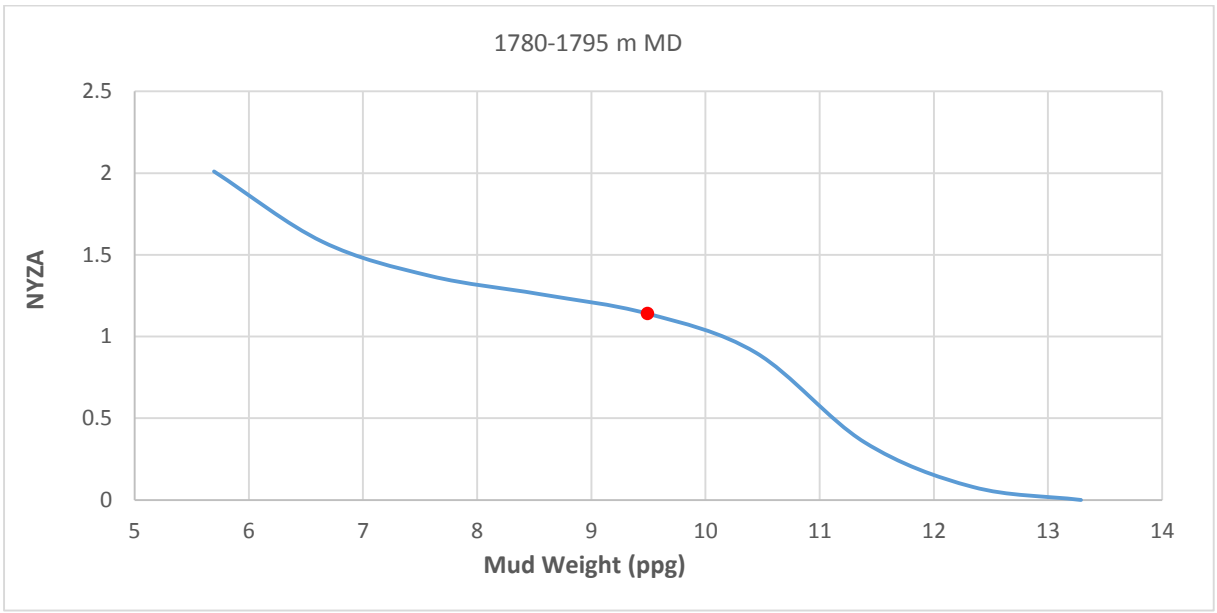
1780-1795 m MD
NYZA
2.5
2
1.5
1
0.5
0
5
6
7
8
9
10
11
12
13
14
Mud Weight (ppg)

Fig. 13

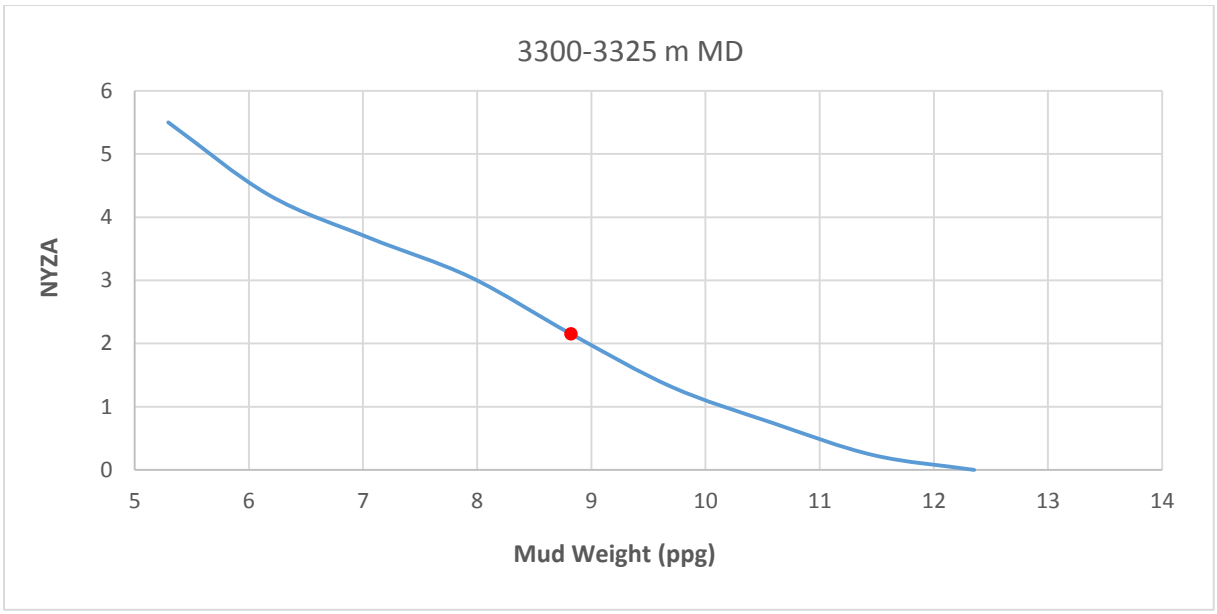
3300-3325 m MD
NYZA
0
1
2
3
4
5
6
5
6
7
8
9
10
11
12
13
14
Mud Weight (ppg)

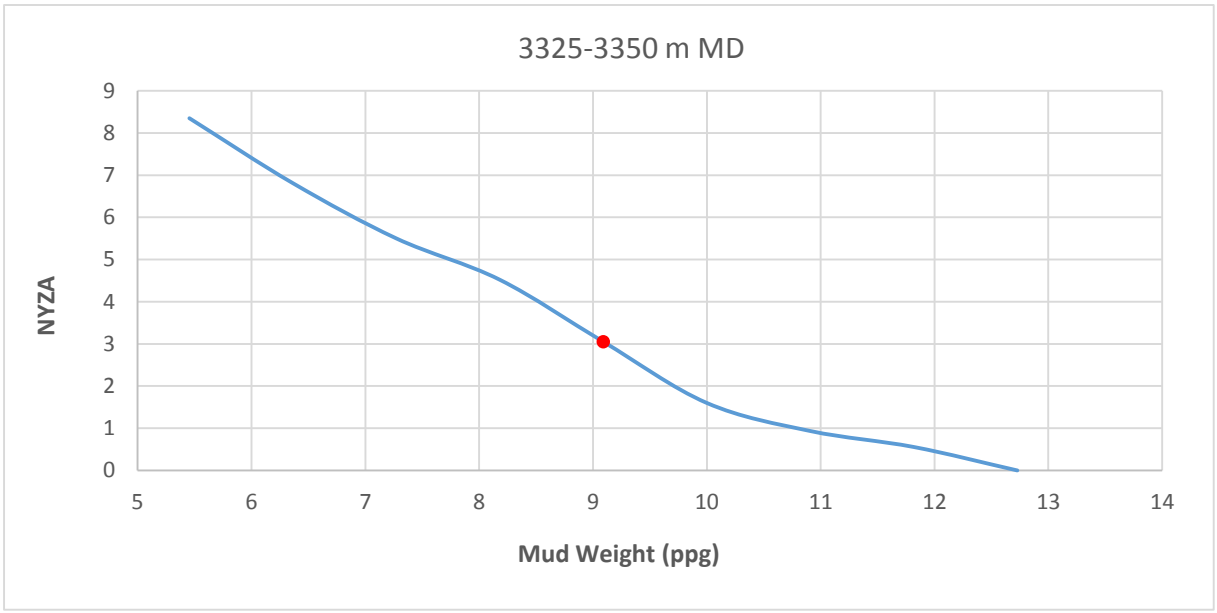
3325-3350 m MD
NYZA
0
1
2
3
4
5
6
7
8
9
5
6
7
8
9
10
11
12
13
14
Mud Weight (ppg)

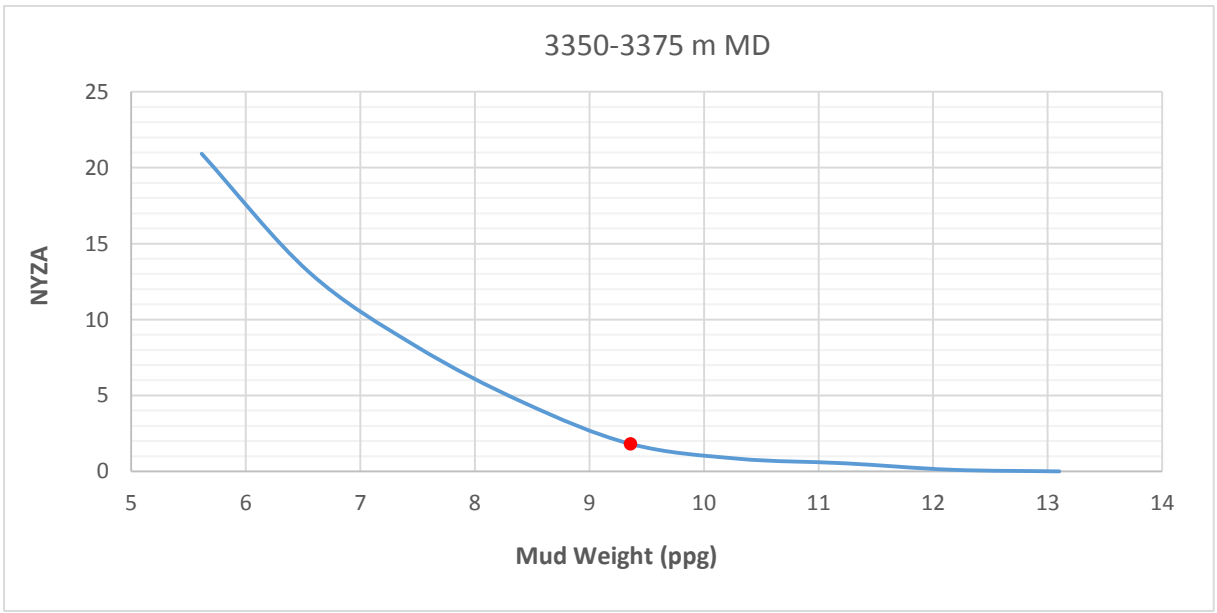
3350-3375 m MD
NYZA
0
5
10
15
20
25
5
6
7
8
9
10
11
12
13
14
Mud Weight (ppg)

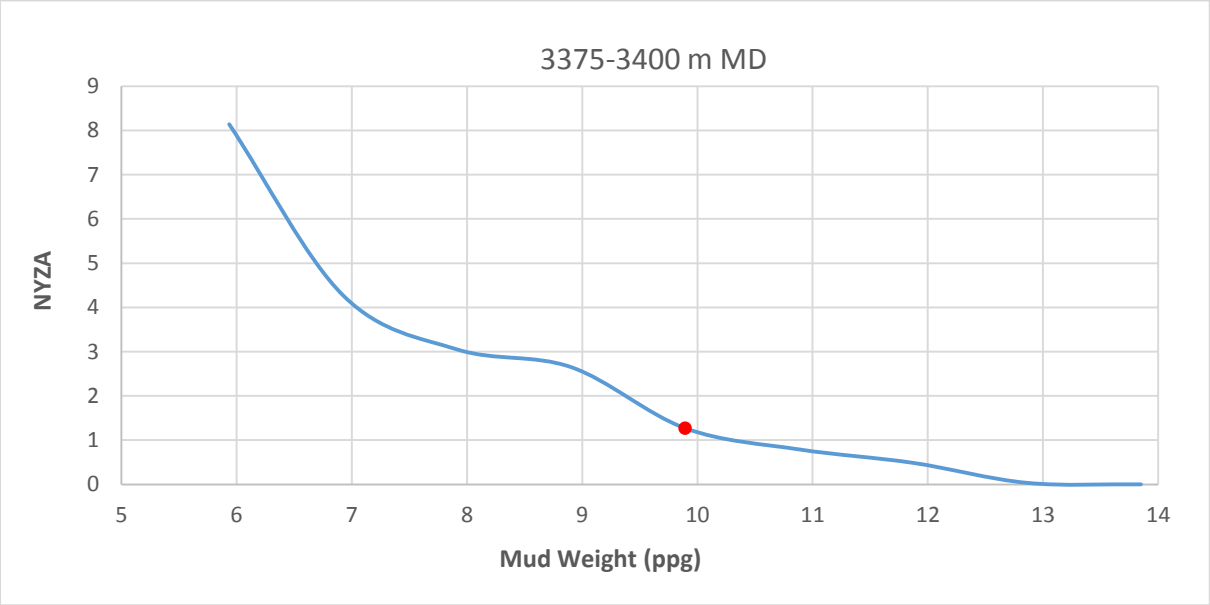
3375-3400 m MD
NYZA
9
8
7
6
5
4
3
2
1
0
5
6
7
8
9
10
11
12
13
14
Mud Weight (ppg)

Fig. 14

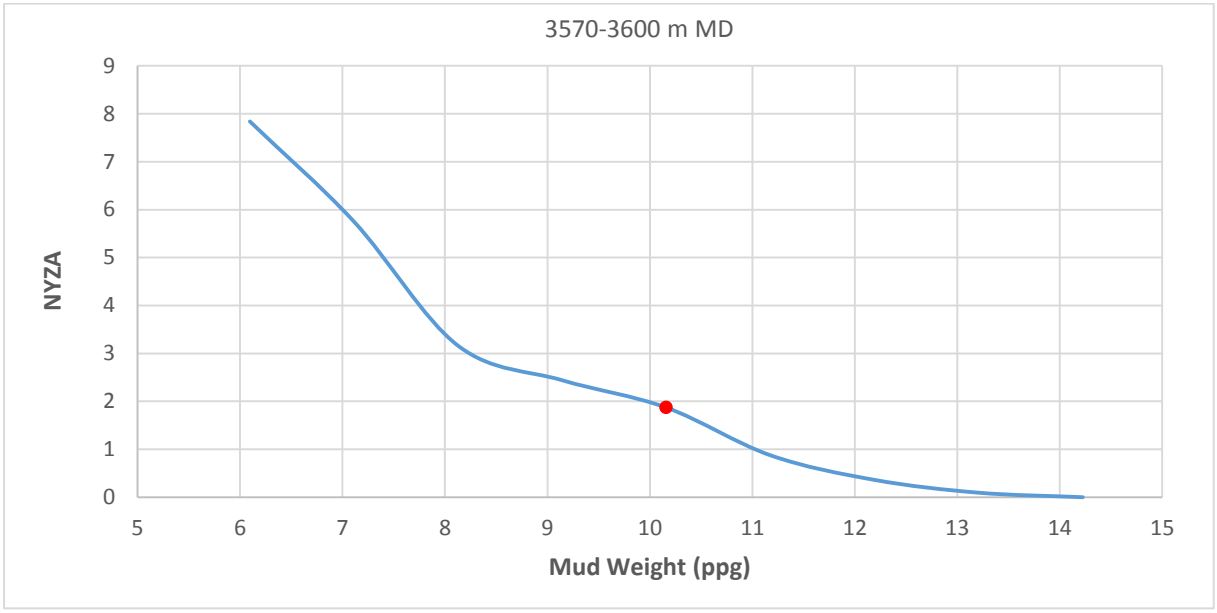
3570-3600 m MD
NYZA
Mud Weight (ppg)
0
1
2
3
4
5
6
7
8
9
5
6
7
8
9
10
11
12
13
14
15

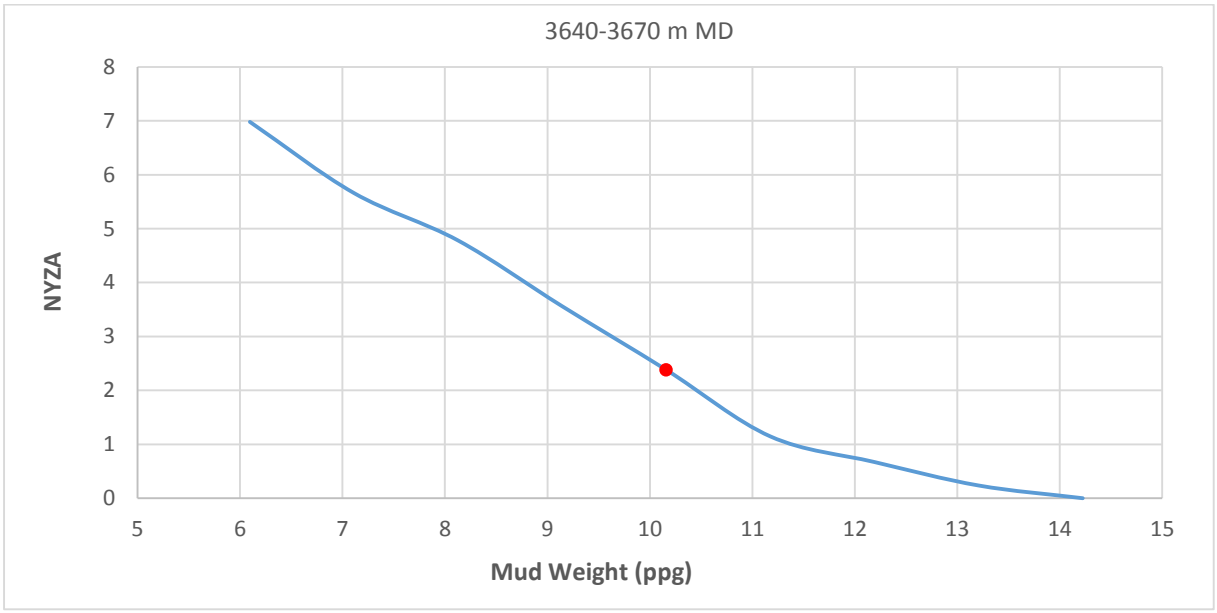
3640-3670 m MD
NYZA
Mud Weight (ppg)
0
1
2
3
4
5
6
7
8
5
6
7
8
9
10
11
12
13
14
15

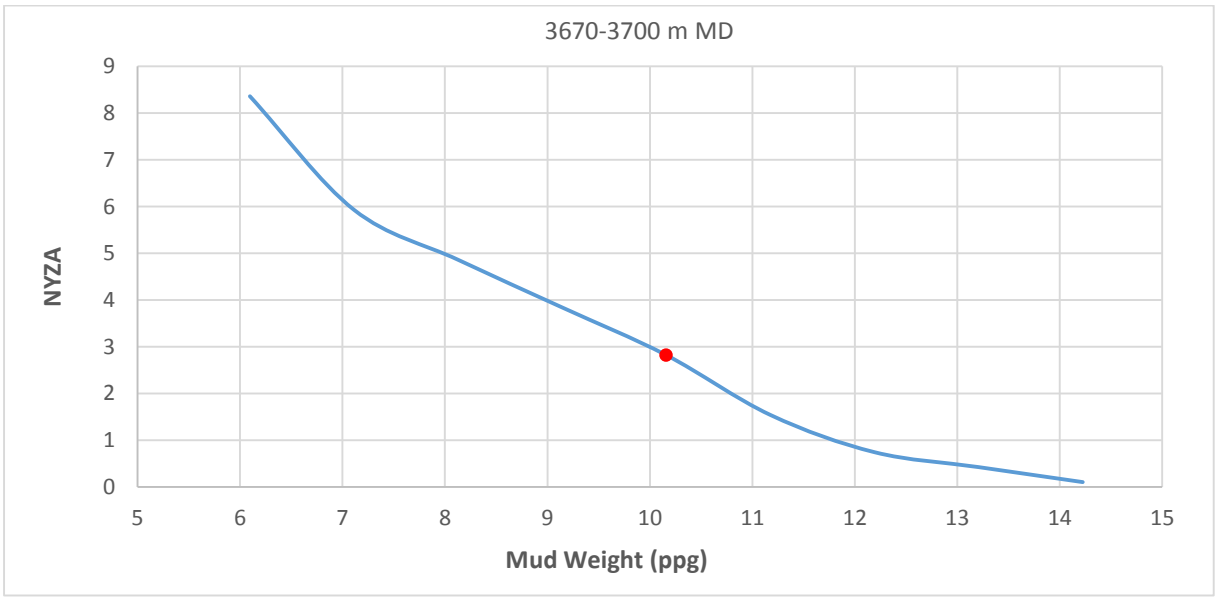
3670-3700 m MD
NYZA
Mud Weight (ppg)
0
1
2
3
4
5
6
7
8
9
5
6
7
8
9
10
11
12
13
14
15

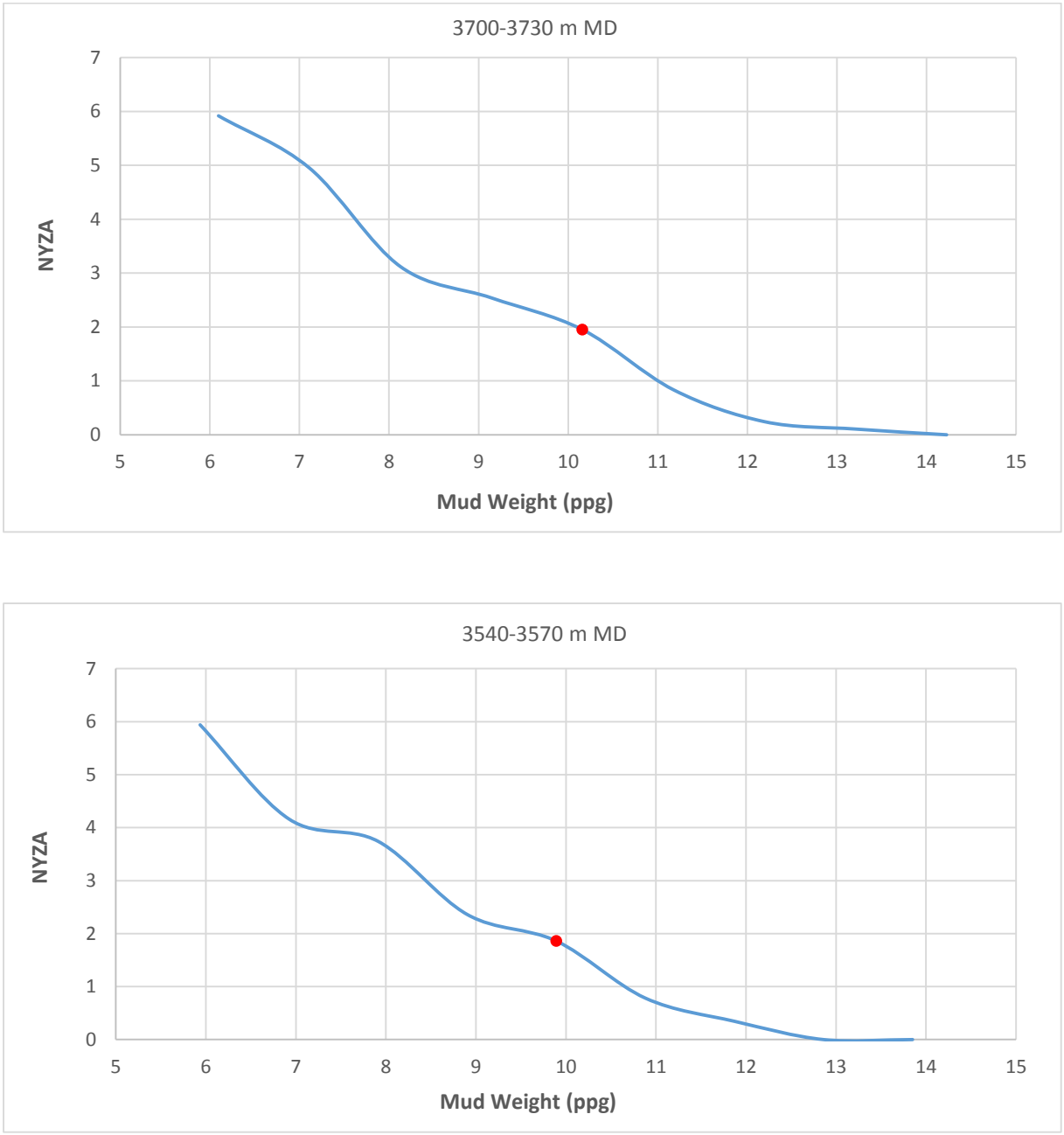
3700-3730 m MD
NYZA
Mud Weight (ppg)
3540-3570 m MD
NYZA
Mud Weight (ppg)

Fig. 15